

POLITECNICO DI TORINO

Master's Degree in Biomedical Engineering



Politecnico di Torino

Master's Degree Thesis

Towards closed-loop system for FES control

Supervisors

Prof. Danilo DEMARCHI

Ph.D. Fabio ROSSI

M.Sc. Andrea MONGARDI

Candidates

Adriana BIXIO

Sara RAFAIANI

July 2024

Abstract

Stroke is the second leading cause of death in Europe and often results in severe impairment. For individuals with Spinal Cord Injury (SCI), therapeutic techniques help in restoring lost motor functions, preventing muscle atrophy, improving blood circulation, managing pain, and enhancing autonomy. The rehabilitative treatment of the Functional Electrical Stimulation (FES) uses electrical pulses to stimulate muscles at the level of the neuromuscular junctions to recover their physiological activity. Since the efficacy of FES relies on the low-energy pulses injected into the patient, it is essential to monitor the patient's muscle activity during the FES to regulate stimulation energy. An open challenge in research seeks to automate the adjustment of stimulation patterns based on the subject's response within a closed-loop system.

The aim of this thesis project is to implement a closed-loop FES control system based on a biofeedback signal that provides details on muscle contractions and the movement they induce. The selected biofeedback signals included MechanoMyo-Gram (MMG), which monitors muscle activity by detecting mechanical vibrations during contraction, and Euler's angles to track articular movement. The wearable devices developed by the eLiONS Laboratory team have been used to collect these signals. These devices are embedded with an Inertial Measurement Unit (IMU), which records acceleration data from which MMG signals can be extracted, and a gyroscope that records angular velocity from which Euler's angles are obtained. The goal of the closed-loop system is to dynamically adjust the stimulation input in real-time based on feedback from the joint angle and muscle activity. The muscle studied in this project is the *biceps brachii* during elbow flexion. The synchronized operations between stimulation patterns and biofeedback signals were achieved by developing a real-time application using Object-Oriented Programming (OOP) in Python. This included creating a closed-loop system that effectively integrates and utilizes the combined data.

The developed closed-loop system drives the FES by adapting the stimulation pattern based on two factors: the muscle contractions detected from the MMG signal and the comparison between the angle achieved during movement and the subject's Active Range Of Motion (AROM). These parameters give two feedbacks that together produce an output related to the stimulation's effectiveness: a negative output causes the increase of the stimulation energy, whereas a positive output shows that the optimal stimulation energy has been identified. Moreover, ten healthy volunteers participated in a simulated clinical protocol focused on investigating the system's capability to distinguish between a purely stimulated contraction and one where the voluntary contribution from the subjects is present. This test revealed that the closed-loop system could also precisely detect voluntary contributions with an accuracy of 90 % when performing FES contraction with a weight corresponding to 30 % of the Maximal Voluntary Contraction (MVC). Furthermore, a study involving ten participants showed that an elastic band opposed to the movement, simulating a sick patient, detected with 88 % accuracy the voluntary contribution. Even though these preliminary findings are limited to a single muscle and movement, there is an opportunity for improvement. Nevertheless, this project demonstrated the potential for a closed-loop FES system driven by examining MMG and Euler's angle signals.

Acknowledgements

We are grateful to Prof. Danilo Demarchi for welcoming us into the eLiONS Laboratory and for providing the opportunity for us to collaborate on this thesis topic. We express our gratitude to Fabio Rossi and Andrea Mongardi, our supervisors, for their guidance and counseling throughout these months.

We want to express our gratitude to one another for our cooperation and support in finishing this project together. We would also like to thank our colleagues at the Hardware Laboratory for collaborating with us during these past several months as the project's test subjects and for enjoying great launch breaks together.

Ultimately, we owe an obligation of gratitude to our loved ones for their constant encouragement throughout our academic careers.

‘Desideriamo esprimere la nostra sincera gratitudine al Prof. Danilo Demarchi per averci offerto l’opportunità di lavorare a questo progetto e per averci accolto nel Laboratorio di ricerca eLiONS. Un sentito ringraziamento va anche ai nostri supervisori, Fabio Rossi e Andrea Mongardi, per la loro preziosa guida e i loro consigli durante tutto il percorso.

Inoltre, desideriamo ringraziarci a vicenda per la collaborazione e il supporto che ci hanno permesso di affrontare e completare insieme questo progetto di tesi. Un ringraziamento particolare va anche ai colleghi del Laboratorio Hardware per aver condiviso con noi questi mesi facendo da soggetti per le acquisizioni e divertenti pause pranzo.

Infine, desideriamo estendere la nostra più profonda gratitudine ai nostri cari per il loro sostegno costante e il loro incoraggiamento durante tutto il nostro percorso universitario.’

Adriana e Sara.

Table of Contents

List of Figures	X
List of Tables	XIII
Acronyms	XVI
1 Introduction	1
1.1 Functional Electrical Stimulation (FES)	1
1.1.1 FES functioning	2
1.1.2 Voluntary and electrical contraction	3
1.1.3 Open-loop and Closed-loop FES system	3
1.2 Skeletal Muscle	5
1.2.1 Muscle introduction	5
1.2.2 Muscle contraction	7
1.2.3 Changes due to muscle contraction	10
1.3 ElectroMyoGraphy (EMG)	12
1.3.1 EMG origin	13
1.3.2 sEMG electrodes	13
1.4 Average Threshold Crossing (ATC) technique	15
1.5 MechanoMyoGraphy (MMG)	17
1.5.1 MMG acquisition apparatus	17
1.6 Parameter extraction from MMG signals	21
1.7 Joint angles estimation	23
1.7.1 Imaging based techniques	25
1.7.2 Inertial Measurement Units (IMU)	26
2 State of Art	31
2.1 Open-loop for Functional Electrical Stimulation (FES) control	31
2.1.1 Average Threshold Crossing - Functional Electrical Stimulation (ATC-FES) system description	32
2.2 Closed-loop for FES control	36

2.2.1	Closed-loop with Surface ElectroMyoGraphy (sEMG)	38
2.2.2	Closed-loop with articular angles	41
2.2.3	Closed-loop with MechanoMyoGraphy (MMG)	44
3	System description	48
3.1	Apollux acquisition system	48
3.2	Electrical Stimulator	51
3.3	Closed-loop FES acquisition system	54
3.4	Software requirements	56
3.5	Software overview	57
4	MechanoMyoGraphy (MMG) signal detected by Apollux devices	60
4.1	MMG acquisition and signal processing	60
4.2	MMG signal characteristics	63
4.2.1	Time domain charateristics	63
4.2.2	Frequency domain charateristics	64
4.3	Comparing the Surface ElectroMyoGraphy (sEMG) and the MMG signals	66
4.3.1	sEMG and MMG processing operation	67
4.3.2	Results of comparing the sEMG and the MMG signals	67
4.4	MMG cross-effect	69
4.4.1	Cross-effect between <i>biceps brachii</i> , and <i>deltoid medius</i>	70
4.4.2	Cross-effect between <i>biceps brachii</i> , and <i>upper trapezius</i>	74
4.5	MMG during stimulated contractions	78
5	Software enhancement	80
5.1	Software connection	81
5.1.1	Software communication by queue	82
5.1.2	Data synchronisation	84
5.2	Main changes in the software	87
5.2.1	Inertial Measurement Unit (IMU) software main changes	87
5.2.2	Functional Electrical Stimulation (FES) software main changes	93
6	Software Testing on MechanoMyoGraphy (MMG) signals	100
6.1	Test Protocol Description	100
6.1.1	Details regarding subjects and acquisitions	101
6.1.2	Evaluation of MVC and AROM values	102
6.1.3	Experimental set-up	104
6.1.4	Research of optimal stimulation parameters	105
6.1.5	Comprehensive Testing: Integration of Voluntary and Stimulated Responses	105
6.1.6	Statistical Analysis	106

6.2	Results of Test	108
6.2.1	Results over parameters analysed	108
6.2.2	Statistical analysis result	115
7	Closed-loop software	117
7.1	Closed-loop communication with IMU and FES SW	117
7.1.1	System Closed-loop	118
7.1.2	Closed-loop object	119
7.2	Introduction of the closed-loop operations and explanation of the area of FES GUI dedicated to the closed-loop.	122
7.3	The FES calibration driven by closed-loop system	124
7.3.1	FES calibration aim and functioning	124
7.3.2	FES calibration outputs	127
7.4	The FES session driven by closed-loop system	130
7.4.1	FES session aim and functioning	130
7.4.2	FES session outputs	132
8	Experimental Protocols description	138
8.1	First Protocol	138
8.1.1	Experimental set-up for <i>biceps brachii</i> performing an <i>elbow flexion</i>	140
8.1.2	Experimental set-up for <i>quadriceps femoris</i> performing an <i>knee extension</i>	144
8.2	Second Protocol	148
8.2.1	Experimental set-up for <i>biceps brachii</i> performing an <i>elbow flexion</i> using an elastic band	149
9	Results and discussion of the results obtained from experimental protocols	153
9.1	First protocol	153
9.1.1	Results of <i>biceps brachii</i>	153
9.1.2	Results of <i>vastus medialis</i> and <i>rectus femoris</i>	155
9.1.3	Second Protocol	157
9.2	Discussion of the results obtained in this experimental protocol . . .	160
9.2.1	First protocol	160
9.2.2	Second protocol	164
10	Conclusion and future developments	167
10.1	Conclusion about the final closed-loop system developed	167
10.2	Future developments	169

A Appendix	171
A.1 Subject specific closed-loop accuracy	171
Bibliography	177

List of Figures

1.1	Functional Electrical Stimulation (FES)	5
1.2	Muscle Anatomy	6
1.3	Cross-bridge theory of contraction	7
1.4	Muscle: from synapses to contraction	9
1.5	Changes induced by muscle contraction	11
1.6	ElectroMyoGraphy (EMG) origin	13
1.7	Surface ElectroMyoGraphy (sEMG) electrode-skin model	15
1.8	Average Threshold Crossing (ATC)	16
1.9	MechanoMyoGraphy (MMG) and surface ElectroMyoGraphy (EMG) recordings	18
1.10	Force-amplitude relationship in MechanoMyoGraphy (MMG)	19
1.11	Wrist joint movements	24
1.12	Accelerometer model	27
1.13	Micro Electro Mechanical Systems (MEMS) gyroscope	28
1.14	Euler's angles	29
2.1	Average Threshold Crossing - Functional Electrical Stimulation (ATC-FES) system	33
2.2	Wireless Average Threshold Crossing (ATC) acquisition device	33
2.3	Analog Front-End (AFE) of the Average Threshold Crossing - Functional Electrical Stimulation (ATC-FES) system	34
2.4	Torque prediction by Polynomial Hammerstein Model (PHM) in ElectroMyoGraphy (EMG)	38
2.5	ElectroMyoGraphy (EMG) feedback: torque predictive control	39
2.6	Electromyography (EMG) stimulation artifact	40
2.7	Acquisition apparatus in closed-loop Functional Electrical Stimulation (FES) with articular angles	42
2.8	Predictive controller with articular angles	42
2.9	Acquisition apparatus in closed-loop Functional Electrical Stimulation (FES) with accelerometers	44

2.10	Acquisition apparatus in closed-loop Functional Electrical Stimulation (FES) with MechanoMyoGraphy (MMG)	46
3.1	Apollux devices circuitry	49
3.2	Packaging of the LSM6DSO32X iNEMO inertial module	50
3.3	Orientation of the acceleration axes (a) and Euler's Angles (b) given by the IMU LSM6DSO32X [89].	50
3.4	Electrical Stimulator: RehaStim2 by HASOMED®	51
3.5	Electrical Stimulation: biphasic pulses	52
3.6	Continuous Channel List Mode (CCLM) for Electrical Stimulation	53
3.7	Closed-loop Functional Electrical Stimulation (FES) acquisition system	55
3.8	Starting Softwares Architecture	58
3.9	New Softwares Architecture	59
4.1	MechanoMyoGraphy (MMG) Power Spectral Density (PSD) sampled at 208 Hz	61
4.2	MechanoMyoGraphy (MMG) signal filter	62
4.3	Filtering effect on MMG data	63
4.4	MechanoMyoGraphy (MMG) signal in time domain	64
4.5	Power Spectral Density (PSD) of the MechanoMyoGraphy (MMG) signal acquired from <i>biceps brachii</i>	65
4.6	Surface ElectroMyoGraphy (sEMG) Electrode	66
4.7	Comparison of Surface ElectroMyoGraphy (sEMG) and MechanoMyoGraphy (MMG) signals acquired from <i>biceps brachii</i>	68
4.8	Exercise 1: elbow flexion	69
4.9	Exercise 2: shoulder abduction	70
4.10	Power Spectral Density (PSD) comparison of Surface ElectroMyoGraphy (sEMG) and MechanoMyoGraphy (MMG) signals acquired from biceps brachii and deltoid medius	72
4.11	Power Spectral Density (PSD) comparison of Surface ElectroMyoGraphy (sEMG) and MechanoMyoGraphy (MMG) signals acquired from biceps brachii and deltoid medius	73
4.12	Power Spectral Density (PSD) comparison of Surface ElectroMyoGraphy (sEMG) and MechanoMyoGraphy(MMG) signals acquired from biceps brachii and upper trapezius	76
4.13	Power Spectral Density (PSD) comparison of Surface ElectroMyoGraphy (sEMG) and MechanoMyoGraphy (MMG) signals acquired from biceps brachii and upper trapezius	77
4.14	Median frequency (fmed) of the MechanoMyoGraphy (MMG) signal acquired from 4 muscle groups	79
5.1	Block Diagram of SW	81

5.2	Synchronisation of FES and IMU processes time	86
5.3	Previous GUI IMU	87
5.4	Actual GUI IMU	88
5.5	GUI IMU labels assigned to Apollux devices	89
5.6	Active Range Of Motion (AROM) evaluation: software pop-up. . .	89
5.7	GUI IMU evaluated AROM value	90
5.8	IMU GUI Example of Acquisition	91
5.9	Previous GUI FES	93
5.10	Actual GUI FES	94
5.11	Actual Input GUI FES	95
5.12	Input Actual GUI FES	97
6.1	Estimation of Maximal Voluntary Contraction (MVC)	103
6.2	Electrode placement and resting position of arm	104
6.3	Root Mean Square (RMS) comparison between various levels of contraction	110
6.4	Standard Deviation (STD) comparison between various levels of contraction	111
6.5	Sum of Power Spectral Density (Psum) comparison between various levels of contraction	112
6.6	Mean frequency of Power Spectral Density (fmean) comparison between various levels of contraction	113
6.7	Median frequency of Power Spectral Density (fmed) comparison between various levels of contraction	114
7.1	FES GUI area dedicated to the closed-loop	122
7.2	FES calibration starting stimulation profile	123
7.3	Example of MMG and angle outputs in FES calibration	130
7.4	Example of MMG and angle outputs in FES session	136
7.5	Real-time closed-loop software example	137
8.1	Estimation of Maximal Voluntary Contraction (MVC) of <i>biceps brachii</i>	140
8.2	Electrode placement and resting position of arm	141
8.3	Estimation of Maximal Voluntary Contraction (MVC) of <i>quadriceps femoris</i>	144
8.4	Electrode placement and resting position of arm	145
8.5	Electrode placement and resting position of arm using the elastic band	150

List of Tables

4.1	Table of muscle and number of subjects for the MechanoMyoGraphy (MMG) evaluation	79
6.1	Subjects data during the experimental protocol. The studied muscle is the <i>biceps brachii</i> during the <i>elbow flexion</i> . For each subject are indicated gender, age, side, MVC value in kg, and AROM value in °.	102
6.2	Each subject's stimulation parameters during the experimental protocol. The studied muscle is the <i>biceps brachii</i> during the <i>elbow flexion</i> . For each subject are shown Current (C) and Pulse Width (PW) at the Low Energy level and the High Energy level.	102
7.1	Look Up Table (LUT) of stimulation parameters for the <i>biceps brachii</i>	125
7.2	Look Up Table (LUT) of stimulation parameters for the <i>quadriceps femoris</i>	126
7.3	Combined output of a single repetition during the FES calibration .	129
7.4	Combined repetition output, FES session	135
7.5	Combined repetition output, FES session	135
8.1	Subject data during the first protocol using the elastic band	142
8.2	Optimal Energy level for the <i>biceps brachii</i>	143
8.3	Subjects data during the experimental protocol. The studied muscle is the <i>quadriceps femoris</i> during the <i>knee extension</i> . For each subject are indicated gender, age, side, MVC value in kg, and AROM value in °.	146
8.4	Optimal Energy level for the <i>quadriceps femoris</i>	147
8.5	Subject data during the second protocol using the elastic band . . .	151
8.6	Lower and Upper Energy limit for the <i>biceps brachii</i> with elastic band	152
9.1	Threshold specific accuracy of voluntary effort recognition	154
9.2	Subject specific accuracy of voluntary effort recognition for closed-loop	155
9.3	Threshold specific accuracy of voluntary effort recognition	156
9.4	Subject specific accuracy of voluntary effort recognition for closed-loop	156

9.5	MMG signal RMS and accuracy	157
9.6	Second protocol: injected energy	158
9.7	Second protocol accuracy in voluntary effort detection	158
9.8	Second protocol, reached angle	159
9.9	Second protocol, MMG values obtained	160
A.1	Subject specific accuracy of voluntary effort recognition for closed-loop	171
A.2	Subject specific accuracy of voluntary effort recognition for closed-loop	172
A.3	Subject specific accuracy of voluntary effort recognition for closed-loop	173
A.4	Subject specific accuracy of voluntary effort recognition for closed-loop	174
A.5	Subject specific accuracy of voluntary effort recognition for closed-loop	175
A.6	Subject specific accuracy of voluntary effort recognition for closed-loop	175
A.7	Subject specific accuracy of voluntary effort recognition for closed-loop	176
A.8	Subject specific accuracy of voluntary effort recognition for closed-loop	176

Acronyms

Ach

Acetylcholine

ADL

Activities of daily living

AROM

Active Range Of Motion

AFE

Analog Front End

ATP

Adenosine TriPhosphate

AP

Action Potential

ATC

Average Threshold Crossing

BLE

Bluetooth Low Energy

CaW

Cauchy Wavelet

CCLM

Continuous Channel List Mode

CL
Closed-Loop

CPU
Central Processing Unit

DAC
Digital-to-Analog Converter

EB
Elastic Band

EEG
ElectroEncefaloGraphy

EMG
ElectroMyoGraphy

ES
Electrical Stimulation

FES
Functional Electrical Stimulation

FMEAN
Mean Frequency

FMED
Median Frequency

GUI
Graphical User Interface

IMU
Inertial Measurement Unit

KAS
Knee Angle Set-point

LUT

LookUp Table

MCU

MicroController Unit

MEMS

Micro Electro Mechanical Systems

MMG

MechanoMyoGraphy

MU

Motor Unit

MUAP

Motor Unit Action Potential

MVC

Maximum Voluntary Contraction

NIRS

Near-Infrared Spectroscopy

NMES

Neuromuscular Electrical Stimulation

ODR

Output Data Rate

OOP

Object Oriented Programming

OSCLM

One Shot Channel List Mode

PHM

Polynomial Hammerstein Model

PKA

Paretic Knee Angle

PSD

Power Spectral Density

PSUM

Sum of Power Spectral Density

RMS

Root Mean Square

ROM

Range of Motion

SCI

Spinal Cord Injury

sEMG

surface ElectroMyoGraphy

SHE

Stimulation Higher Energy

SLE

Stimulation Lower Energy

SW

Software

SR

Sarcoplasmic Reticulum

STD

Standard Deviation

TC

quasi-digital Threshold Crossing

VC

Voluntary contraction

Chapter 1

Introduction

This dissertation project aims to implement Functional Electrical Stimulation (FES) in a closed-loop system. FES is a rehabilitation technique often used with patients with limited mobility of the upper and lower limbs. Electrical stimulation is applied to the paretic limb and is modulated by patient biofeedback. To address this problem, biofeedback must be found to monitor and evaluate the muscular response to the stimulation. The modulation of stimulation parameters is essential for increasing the accuracy of the rehabilitation, i.e., ensuring the right amount of stimulation to produce the desired movement (avoiding under-stimulation or over-stimulation), adapting to subject variability response to the stimulation given, preventing muscle fatigue and damage, and dynamically modifying the FES to respond to physiological changes.

This introductory chapter discusses the main points of the argument, beginning with an overview of FES. A description of the muscles and their contraction is given. ElectroMyoGraphy (EMG) is commonly used to study muscle activity, but in this case, this technique is not feasible due to electrical interference, as it will be discussed during Chapter 2 in Section 2.2.1. Therefore, a method using joint angle information, which indicates the range of motion of the limbs, combined with MechanoMyoGraphy (MMG), which measures muscle vibrations during contraction, was proposed to determine muscle activity.

1.1 Functional Electrical Stimulation (FES)

Stroke is the second cause of death in Europe and the fifth in the USA and leads subjects to serious disability [1–3]. Indeed, a large number of stroke victims experience partial or complete motor skill loss. As reported in [3], a stroke can be hemorrhagic or ischemic, but in most cases (87%), strokes are ischemic.

This pathology not only has effects on motor skills but also causes problems in behavior and communication. To solve motor disability, researchers looked for an alternative strategy that would enable patients to engage in some degree of exercise even in the event of complete paralysis. L. Mercier *et al.* in [4] study the impact of motor, cognitive, and perceptual disorders after a stroke. Paralysis is caused by damage to the nervous system, particularly the spinal cord (Spinal Cord Injury or SCI) or brain. This damage makes muscle contraction not possible in a voluntary way since the electrical nervous input from the spinal cord to the muscle is ruined. External electricity generates a muscle contraction for those completely or partially paralyzed by supplying a current to neurons[3].

Electrical Stimulation (ES) is a method that uses electricity to engage muscles directly. ES encompasses several approaches, including Neuromuscular Electrical Stimulation (NMES), Functional Electrical Stimulation (FES), and Transcutaneous Electrical Stimulation (TENS). The goal of NMES is to assist patients in using their muscles by electrically stimulating their remaining innervations while developing and performing a functional movement, which is the aim of FES for patients. Because of its several advantages, the FES approach is used frequently in rehabilitation nowadays. Indeed, thanks to FES, it is possible to maintain mass, prevent atrophy, and improve muscle strength. Besides, recent studies have demonstrated that neurological mechanisms are essential for movement recovery. FES, stimulating muscles and nerves, can help restore communication pathways between brain and muscle, so FES can improve neuroplasticity and create new neural connections [3, 5].

1.1.1 FES functioning

Luo *et al.* [5] writes a review of FES treatment in SCI. Peripheral nerves are the main target of FES and are stimulated by electrical impulses. By the way, it's also possible to indirectly promote the activation of spinal cord neurons through afferent feedback. Typically, an FES system consists of a stimulator that sends brief electrical pulses to the motor nerves, directly causing skeletal muscle contraction.

Pulse width, frequency, and amplitude are the three parameters that determine electrical pulses. The stimulus must be based on the specific physiological conditions of patients.

Square, peak, or sine wave patterns produce pulses; the typical pulse width is from 150 μ s to 600 μ s. Different effects on muscles can be created depending on the pulse width. For instance, low-frequency electrical stimulation with a longer pulse width can result in a reduced level of muscle weariness.

Alternatively, a reduced pulse width might increase the number of muscle fibers recruited and produce greater joint torques in the muscle fibers.

The stimulation frequency can be adjusted based on the treatment, from 20 Hz to 50 Hz. Low-frequency FES produces a smooth muscle contraction at a lower force level and is used to prevent muscle fatigue. Rather, high-frequency FES can achieve a tingling sensation and a smoother force response. Additionally, some FES stimulators allow the user to select whether to stimulate with a single, double, or triple train spaced out at larger intervals; different frequency trains can modify muscle fatigue.

The intensity of the FES input can be modified by adjusting the amplitude parameters; the peak input ranges from 0 mA to 100 mA. Stronger contraction by stimulation is correlated with higher amplitude [5].

1.1.2 Voluntary and electrical contraction

However, voluntary and electrical contractions are very different. Indeed, during voluntary contraction, the contraction starts from the spinal cord and travels in a network of neurons till it reaches the neuromuscular junction. In the muscle, this shifts the potential voltage across the cellular membrane that propagates throughout the fiber and makes the muscle contract. On the other hand, during FES contraction, the input is given directly to the neuro-muscular junction and the action potential travels in the opposite direction with respect to voluntary ones.

Moreover, in voluntary contraction, muscle fibers are recruited in order to optimize movement. In contrast, the recruited fibers in FES are usually inversed to the voluntary ones since it depends on the fiber size.

Indeed, voluntary contraction activates type I fibers first and has the capacity for asynchronous activation, which permits the motor unit to switch during contraction and has a faster recovery. Rather, fibers are recruited synchronously by electrical contraction, beginning with larger (type II) and closer to the stimulation's electrodes [6].

1.1.3 Open-loop and Closed-loop FES system

Since FES is often based on an open-loop system, stimulation features are defined in accordance with a standard parameter rather than being unique to each patient's response [7].

According to G. Alon [8], patients would need to be stimulated using a customized FES. As reported by G. Alon in [7], patients actually continue to utilize FES for months or years after using open-loop technologies because of their dependence on FES to perform certain movements. A solution to this problem could be a closed-loop system; creating a closed-loop system that can adjust stimulation to each patient and, if needed, to each muscle has been one of the challenges of the last years. Iterative algorithms, which process data in real-time and provide an output starting from these data, are the foundation of closed-loop systems.

As illustrated in Figure 1.1, the difference between an open-loop and a closed-loop system is the feedback that returns from patients to the control unit. These iterative algorithms typically use motion sensors and EMG to gather input data for closed-loop systems. Many restrictions are associated with extra hardware, cost, and battery life when using EMG to control a closed-loop system. Furthermore, because EMG is an electrical data source, it has limits; for example, it is affected by stimulation artifacts. These arguments are discussed during Chapter 2 in Section 2.2.1.

The Inertial Measurement Unit (IMU) is a motion sensor that may be utilized in closed-loop systems. Its tiny size, wireless connectivity, and low energy consumption are just a few of its many benefits. However, strategies adopted for the realization of the open-loop FES and closed-loop FES will be examined in Chapter 2.

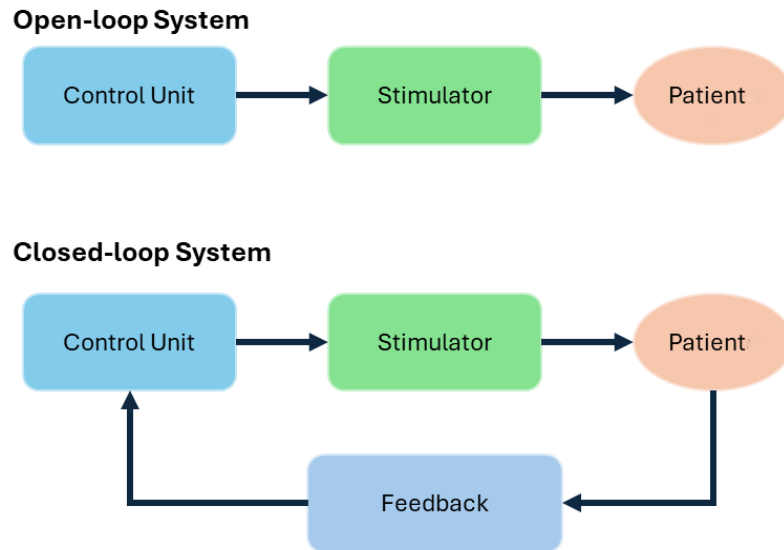


Figure 1.1: Logical descriptive scheme of difference between an open-loop and a closed-loop system adapted figure from [9]. Both systems comprise a control unit, a stimulator, and a patient. A closed-loop system also has feedback from patients after stimulation.

1.2 Skeletal Muscle

1.2.1 Muscle introduction

Skeletal muscle comprises fibers tied at their end with the bones by an elastic connective tissue called a tendon. Muscular fibers run all over the muscle, and their cellular membrane is called sarcolemma; it is surrounded by a layer of connective tissue named endomysium [10]. The cytoplasm of these cells (sarcoplasm) contains the contractile apparatus composed of cylindrical structures named myofibrils placed parallel to one another. Myofibrils are composed of two types of filaments: thick and thin; myofibrils are divided into functional units named sarcomeres by Z bands; muscle architecture is illustrated in Figure 1.2. Thick filaments are composed of the protein myosin and have a diameter two times bigger than the thin ones. They are made of actin, troponin, and tropomyosin proteins. Thick and thin filaments overlap each other during the contraction. Each myofibril is surrounded by the sarcoplasmic reticulum, which stores up Ca^{2+} ions and releases these ions during contraction; there are also other structures named T tubules. SR and T's tubules help transmit signals from the sarcolemma to myofibril.

Since there are different types of filaments when looking at a skeletal muscle under a microscope, three different regions (i.e., A, I, H) can be observed due to different refractive index [12]:

- I bands (light ones, isotope) are divided into two halves by the Z bands; in this region, the main components are thin filaments;
- A bands are located in the middle of a sarcomere (between two Z bands), and those regions are darker and with anisotropy properties;
- H bands are situated in the middle of an A band, and those areas are lighter than the A band. In the middle of them, there is a line M. In this region, thick filaments are mainly present.

Due to these different regions, when a muscle is relaxed, stripes can be observed on it, while in the muscle contraction, it is possible to notice only the A band and the M line. Thick filaments are created by thousands of myosin molecules tied together; each has two globular heads with two binding sites, one for the actine and the other for the Adenosine TriPhosphate (ATP). On the other hand, the thin filaments comprise two F-actin filaments wrapped in a double helix.

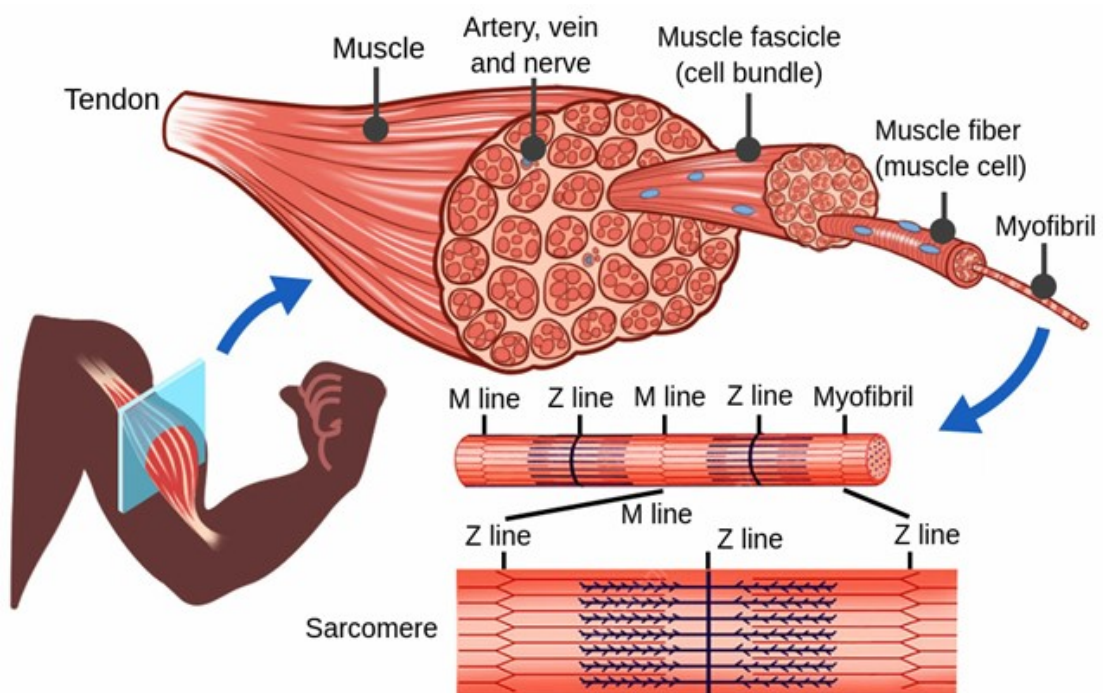


Figure 1.2: The architecture of a skeletal muscle [11].

Tied to it is the tropomyosin-troponin complex, which acts as a regulator of the sarcomeres contraction [12].

1.2.2 Muscle contraction

Cross-bridge cycle: force production in muscle

The muscle contraction mechanism is regulated by the interaction between the myosin heads and the actin, and it is called the theory of the ‘cross-bridge theory of contraction’. This phenomenon, described by Figure 1.3, was first introduced by Huxley in 1957 [13].

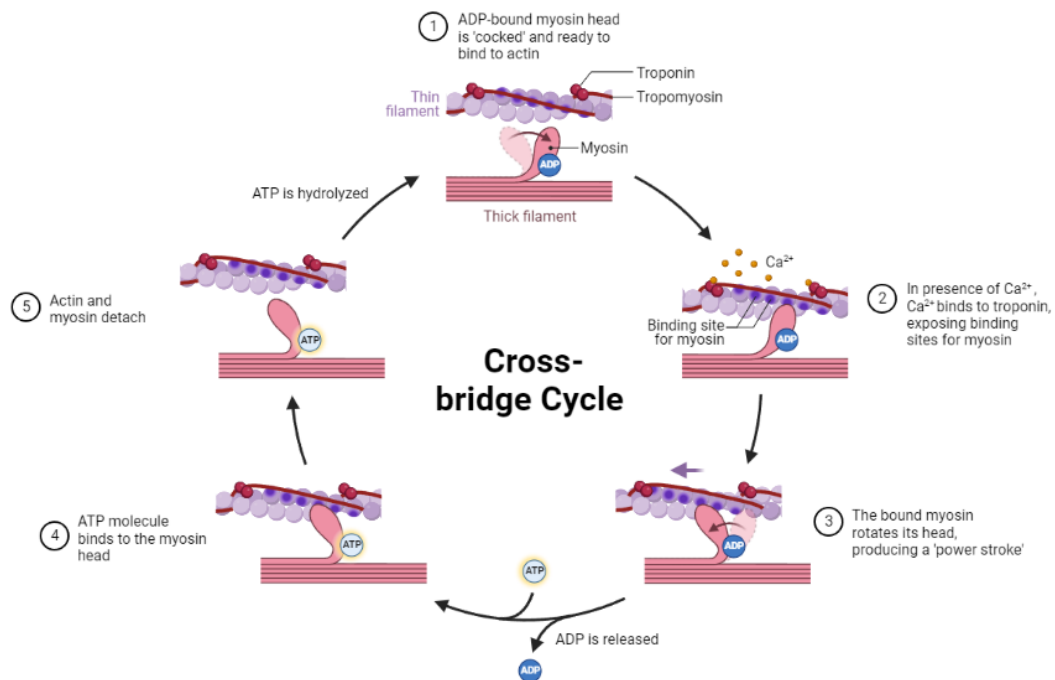


Figure 1.3: Phase of Cross-bridge theory of contraction [14].

In the first phase of this process, in which the muscle is relaxed, even though myosin is linked with Adenosine Diphosphate (ADP) and Phosphate (P_i), the troponin-tropomyosin complex covers the actine link sites on the myosin, so there is no coupling between them.

During the excitation-contraction (phase 2), the Calcium (Ca^{2+}) concentration in sarcoplasm rises considerably and links with the troponin (subunit C , TnC).

This link between Ca^{2+} and Troponin C (*TnC*) brings a structural change in the troponin molecule that distances the tropomyosin from the F-actin, and this links actin and myosin accessible. So, actin and myosin create a link between them and build up cross-bridges.

Lately, the complex actin-myosin loses the *Pi*, and the myosin heads' orientation changes from 90° (in phase 2) to 45° (phase 3) towards the M line. This is the power stroke phase that makes the motion of the thin filaments over the thick ones without shortening.

In the following rigor phase (phase 4), the actin-myosin complex loses the ADP but keeps generating force. Afterward, in phase 5, there is the detachment of the actin from the myosin due to the ATP link, and the cycle ends because the molecules recover in phase 1.

Besides, due to the high concentration of myosin molecules in the thick filaments, these cross-bridges are highly distributed over the sarcomere, so they cause the motion of the thin fibers towards the M line. Due to that, the I bands reduce their length till they disappear when all cross-bridges are formed.

The force generated by a muscle is controlled by the summation of the sarcomeres shortening since each sarcomere is connected in series with the adjacent one in a muscle. Muscle contraction is the mechanism through which muscular fibers shorten to respond to the nervous system. The contraction occurs because of some biochemical and physiological event in muscular cells, particularly inside sarcomeres [12].

Excitation-contraction coupling: activation of muscles

Muscle is constituted by the contractile apparatus that is made of proteins. The Action Potential (AP) takes place in the muscular tissue; AP allows the development of contraction and force. For this reason, muscular tissue needs high energy and follows the principle of cellular metabolism.

Acting as a link between the muscle cell and the motoneuron, the neuromuscular junction transmits AP and releases Acetylcholine (Ach), which permeates the membrane and enables membrane depolarization. As the AP travels along the entire sarcolemma, Ca^{2+} ions are released from the SR into the muscle cell when AP reaches the tubuli T. This is the cue to begin contracting muscle cells. This leads to the onset of a phenomenon known as calcium-induced calcium release, in which a portion of calcium binds to troponin that can change its shape, causing tropomyosin to migrate to its resting position and freeing up spaces on the actin filament for myosin. This mechanism is illustrated in Figure 1.4.

The cross-bridge cycle and sarcomeres contraction can begin after these modifications. When a neuron stops sending a signal, the sarcolemma stops producing AP, which leads to the ending of the contraction of muscle cells ends [10].

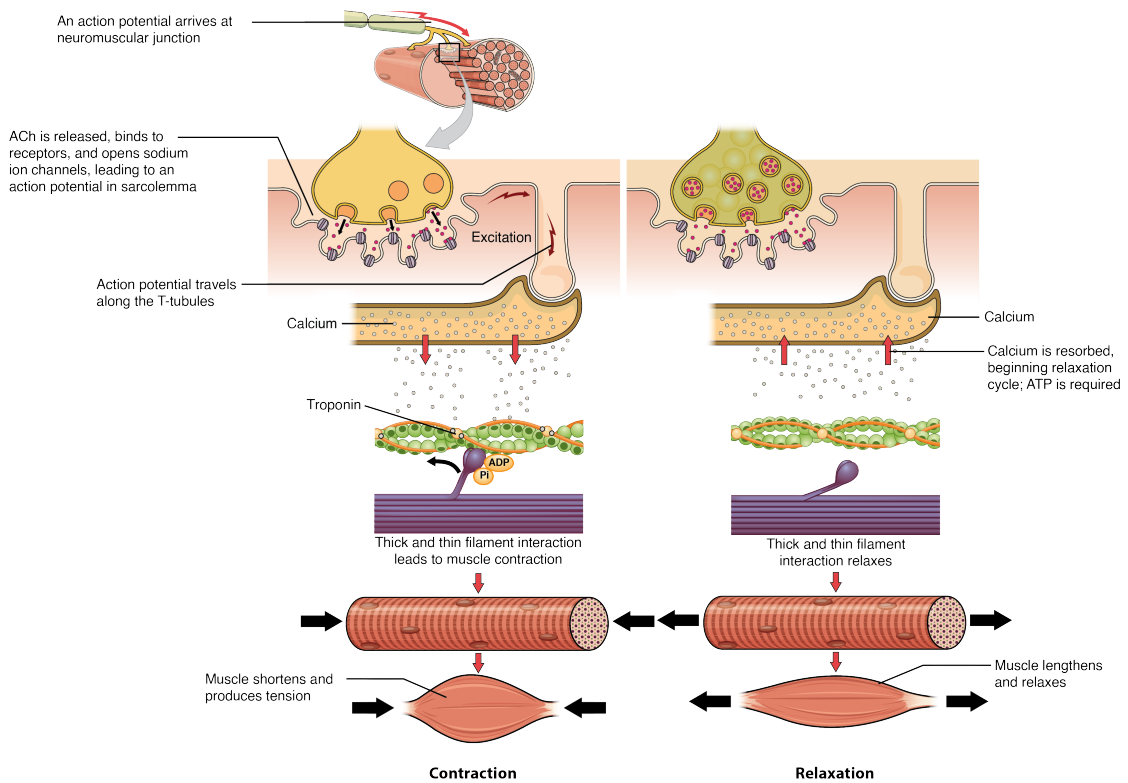


Figure 1.4: Muscle: from synapses to contraction. [15]

Mechanical reaction during muscle contraction

A single muscle cell's mechanical response is represented by a single twitch. Three phases make up this phenomenon: the latency period, contraction, and relaxation. The latency period is the few milliseconds that pass between the appearance of the AP and the start of the contraction. The contraction phase lasts between 10 and 100 ms and ends when the maximum voltage peak is attained. The concentration of calcium rises throughout this phase. The longest phase is the relaxation phase, which is represented by the interval between the contraction's finish and its maximum voltage peak. The number of cross-bridges also falls during this phase due to a drop in calcium concentration that is transported back to the SR, making the tropomyosin and actin link[10].

1.2.3 Changes due to muscle contraction

Muscle contraction brings different changes from the mechanical, chemical, and electrical points of view [16]; these changes are reported in Figure 1.5.

Biomechanical changes, illustrated in Figure 1.5A, arise from the link between actin and myosin head during contraction that changes the tension over the skin surface. Indeed, during the contraction, this alteration of the muscle fiber shape brings changes over the fiber length, overall muscle shape, vessel position, and surface tension that can be sensed on the skin surface in a non-invasive way by MechanoMyoGraphy (MMG).

On the other hand, the altered energy consumption of a working muscle leads to a modified amount of biochemical molecules in the blood, as described by Figure 1.5B. The request for oxygen during contraction increases and leads to a modification in the oxygen concentration in the blood, which can be detected through the changes induced in the hemoglobin and myoglobin. Depending on how those molecules are tied to oxygen or carbon dioxide, the molecules will react differently to near-infrared light and those interactions can be detected through Near-Infrared Spectroscopy (NIRS).

Moreover, bioelectrical alterations appear during contraction due to the polarization of the muscle fibers because of the action potentials propagating through the fiber; these alterations are reported in Figure 1.5C. The most common technique to detect those current changes is the ElectroMyoGraphy (EMG).

As a result, multiple techniques are used to disclose different changes caused by muscular contraction: MMG reveals biomechanical changes, NIRS reveals biochemical changes, and EMG reveals bioelectrical changes [16].

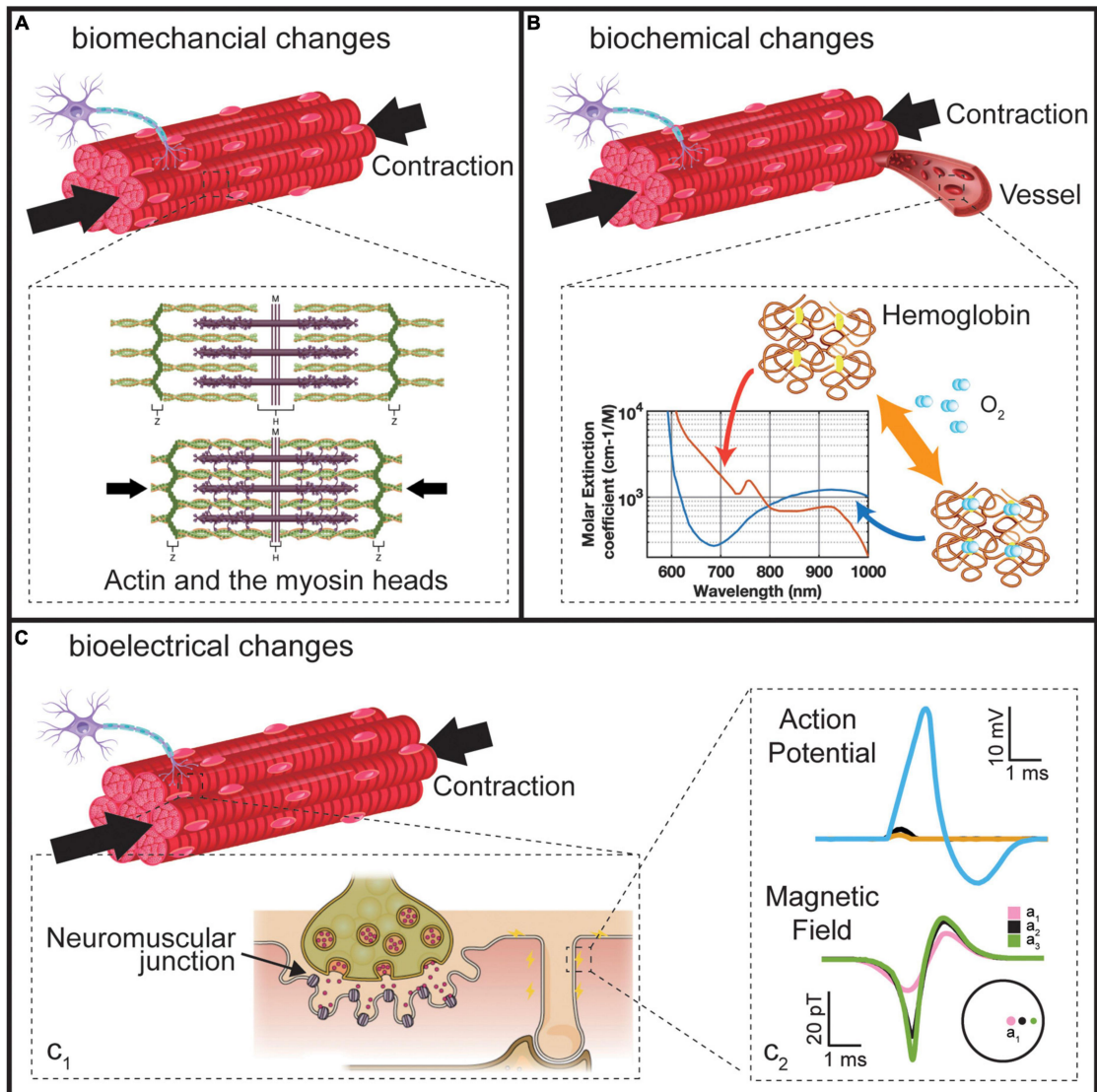


Figure 1.5: Overview of changes induced by muscle contraction [16].
 A. Biomechanical changes due to muscle contraction. B. Biochemical changes due to muscle contraction. C. Bioelectrical changes due to muscle contraction.

1.3 ElectroMyoGraphy (EMG)

ElectroMyoGraphy (EMG) is the technique used to investigate the electrical properties of contraction due to the propagation of the action potential through a muscle fiber [17, 18].

This technique produces an interferential signal (named electromyogram) that is the summation of the signal produced by each sarcomere of each excited Motor Unit (MU). This signal can be acquired either by inserting a needle electrode into the muscle, intramuscular EMG, or by placing electrodes on the skin above a muscle, Surface EMG (sEMG).

The first way of acquiring this signal is a more accurate way of investigating muscle activity since it allows the study of smaller muscle regions with high spatial resolution, so it is often used in neurological studies. However, this is an invasive technique that requires the insertion of a needle inside the skin, so this is uncomfortable for the patient and can possibly lead to collateral effects such as infection, bleeding, or hematoma formation [19].

On the other hand, for rehabilitation purposes, the general aim is to investigate the overall activity of a muscle in terms of force produced while contracting, so the required signal must contain information about a bigger muscle portion without the need for a high spatial resolution. To achieve this, the sEMG technique is usually used due to its non-invasiveness, ease, and faster application time and cost. The sEMG exhibits a peak-to-peak amplitude from 0 mV to 10 mV, and a frequency band from 0 Hz to 500 Hz, with the main power content from 20 Hz to 50 Hz [18, 20].

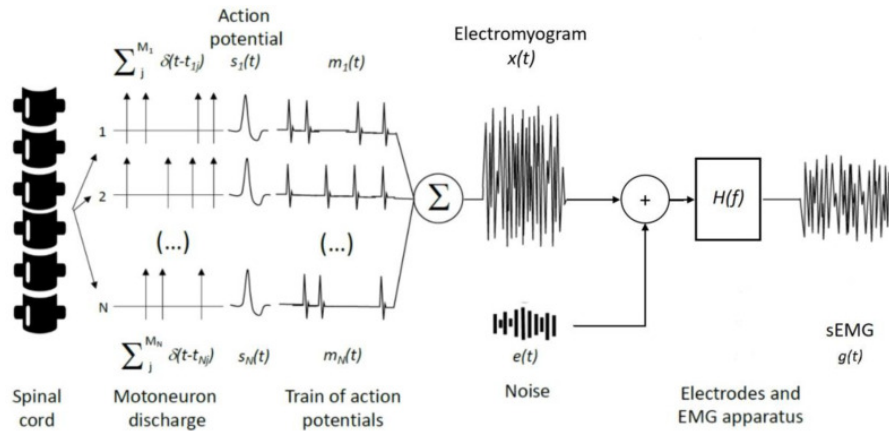


Figure 1.6: ElectroMyoGraphy (EMG) origins: various MUAPs are exited asynchronously by the spinal cord. The summation of the MUAPs is the recorded sEMG [17].

1.3.1 EMG origin

Muscle fiber contraction is regulated by the activity of a motoneuron that discharges and generates an action potential at its neuromuscular junctions that propagates through the muscle fiber. The summation of these action potentials is known as Motor Unit Action Potentials (MUAP) (Figure 1.6).

The muscle membrane's depolarization due to the MUAP propagation is electrically detectable by EMG recordings. The difference between the signal produced by intramuscular and surface recording stands in the feasibility of evaluating individual MUAP with the intramuscular technique. However, since MUAPs can be summed in time (depends on the firing rate of the motoneuron) and in space (number of MUs active), the lower selectivity of the sEMG technique results in an interferential signal [21].

1.3.2 sEMG electrodes

An sEMG electrode is identifiable as a transducer from the ions current, generated from the muscle membrane, to electrons current in the metal wires [18].

Electrodes can be divided into two categories based on the type of adhesion with the skin: they can either be dry or wet electrodes. Wet electrodes incorporate a layer of conductive gel that reduces the interface electrode-skin, but they often are self-adhesive and not reusable. On the other hand, dry electrodes are made of a noble metal (e.g., gold) or silver chloride, they are constituted only by the

conductive layer.

Moreover, they can be distinguished for their electrochemical behavior:

- Polarizable electrodes have a capacitive nature that creates a charge distribution at the electrode-electrolyte interface. Those electrodes possess a higher half-cell potential. Indeed, gold is a material that presents those properties.
- Non polarizable electrodes produce an ionic current at the electrode-skin interface when a voltage is applied, so their behavior is mainly representable as a resistive one. The most used non-polarizable electrodes are the Ag-AgCl.

The interface between skin and electrode can be described as a non-linear RC circuit that depends on current and frequency [18]. The whole model is also discriminated by an interface between the electrode and the electrolyte and another between the skin and the electrolyte.

Those two interfaces are modeled as in Figure 1.7: they are represented as an RC parallel (electrode-electrolyte) that contains the polarizability and the capacitive behavior in series with a DC voltage generator that models the half-cell potential and a resistor that represents the interface electrolyte-skin impedance. The impedance depends on various factors, such as electrode material and shape or gel composition. Besides, it is time-dependent and can change during long-term acquisition due to gel drying. The global impedance ranges from a few $k\Omega$ to $M\Omega$.

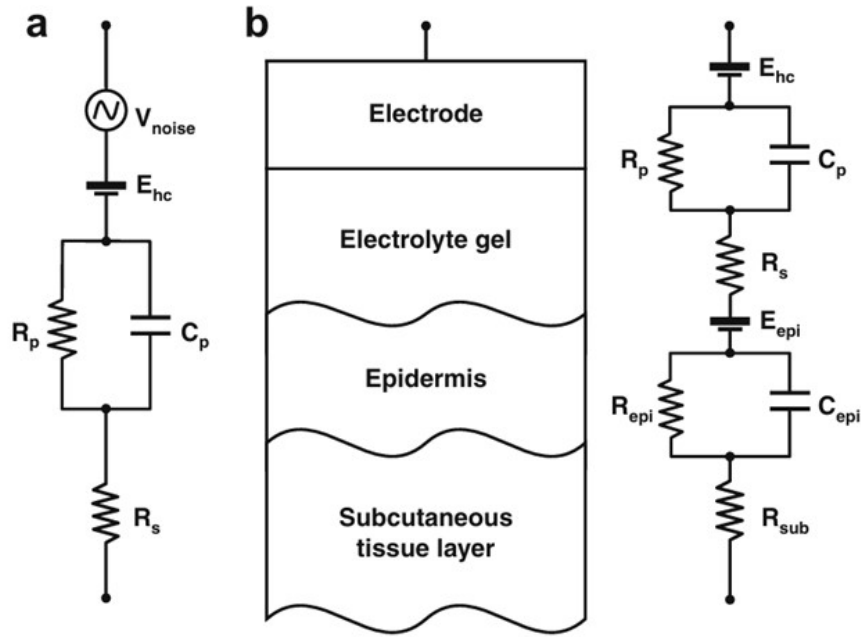


Figure 1.7: sEMG electrode-skin interface model [18]. In a, there is a global overview of the model: the double layer is represented by a parallel between a capacitor and a resistor while the gel is represented by a resistor. In b there is a graphical representation of the layer interposed between the electrode and the muscle and a more accurate electrical scheme that comprehends also the Epidermis and Subcutaneous model.

1.4 Average Threshold Crossing (ATC) technique

The Average Threshold Crossing (ATC) is an event-based method used on the sEMG signal to optimize the dimensions of the acquisition system, wireless transmission, and power consumption [22].

ATC is based on the imposition of a threshold (that can be static or dynamic) on the sEMG signal. The ATC parameter is defined as the number of Threshold Crossing (TC) events over an observing window length of 130 ms, which is proven to be a good compromise between spatial resolution and event counting. A TC event is generated every time the sEMG signal overcomes the threshold, producing a quasi-digital TC signal. Figure 1.8 represents how the TC signal is generated and how the ATC parameter is evaluated.

In [23], it is proven that this parameter is highly correlated to the muscle force

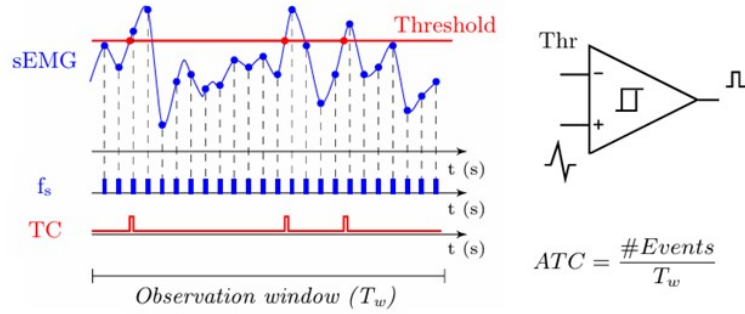


Figure 1.8: Average Threshold Crossing (ATC) technique: generation of TC signal starting from sEMG signal and evaluation of the ATC parameter [22].

(i.e., 95% ATC-force correlation). Due to the simple hardware requirements, this TC signal is directly implementable on board; indeed, F. Rossi *et al.*, in [22], computing of the ATC parameter directly at the microcontroller level and implemented its transmission via Bluetooth Low Energy (BLE).

This signal processing technique exploits the time dimension of a signal by the pulse generation rather than the amplitude one, so there is an sEMG morphological information loss that makes this technique nonapplicable in some diagnostic applications, such as fatigue analysis during contraction, or myopathies, or muscle spasms and tremors.

Moreover, the threshold imposition requires a first calibration phase for the threshold value selection. Indeed, this value must be as much as possible to the signal baseline; in this way, the environmental noise is considered, thus adjusting the threshold just above it and making the system detect also little muscular activations. If the threshold is too high or too low, neither enough nor too many TC events will be detected.

1.5 MechanoMyoGraphy (MMG)

The technique used for the study of the mechanical aspects of muscle contraction is called MechanoMyoGraphy (MMG). This technique produces an interferential signal derived from the activity of various sarcomeres and MU recruited during a contraction. It records vibrations generated (inside the muscle while it is contracting) that are detectable on the skin surface by contact microphones as sounds or as mechanical events with accelerometers.

In [24], they found a correspondence in the frequency of the muscle sound and the attachment-detachment of cross bridges. Indeed, the reaction time of the cross-bridges cycle is estimated as 50 ms, while the mean frequency content found in their study is about $25 \text{ Hz} \pm 2.5 \text{ Hz}$.

This signal represents the mechanical manifestation of the electrical activity measured by EMG [25]. In Figure 1.9, there is a comparison between MMG, EMG, and angle evaluated in the study [26]. Indeed, in this study, the activity of the first dorsal interosseus muscle and the index finger angle were analysed.

As reported in [27], muscle sounds have been deeply investigated since 1800 when they discovered that ‘muscle sound is related to muscle activity and its proprieties are related to the proprieties of the contraction’. However, only after 1980, thanks to technological improvements (such as piezoelectric transducers), the importance of this analysis grew.

1.5.1 MMG acquisition apparatus

In [27] describes the ideal configuration of the experimental setup for MMG recording. Firstly, its frequency response should have a cut-off low-frequency of around 2 Hz, and the upper one should be at 100 Hz. Moreover, it is important that the mass of the transducer does not modify the muscle shape, so its weight must be light.

Another important aspect of myographic techniques is the positioning of the sensors to find the place of a muscle, which gives a better result in signal accuracy.

This has been investigated in [28] with the study of sound propagation during a contraction. This research was done by changing the relative position of the sensor with respect to the muscle. The MMG sensor was moved along the muscle major axis, and the signal amplitude differences were evaluated. The results show that the maximum amplitude is recorded at the muscle belly, and when moving the transducer towards the tendon, it decreases.

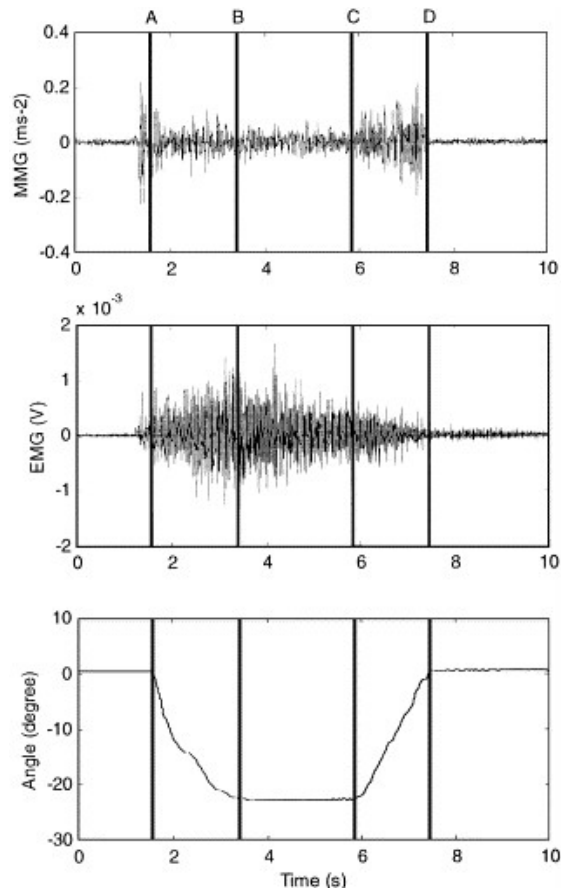


Figure 1.9: MMG (ms^{-2}) and EMG (V) activity from the first dorsal interosseus muscle, along with angular displacement ($^{\circ}$) of the index finger in the lateral–medial direction [26].

The signal analysis can be conducted in two ways: time domain (signal amplitude vs. force relationship) or frequency domain.

Time domain analysis

Starting from the signal amplitude analysis, it was found that the MMG amplitude increases with the increase in force. The force is measured in percentage of the Maximum Voluntary Contraction (% MVC) while the amplitude is evaluated as the Root Mean Square (RMS) of the MMG signal.

In Figure 1.10, it is possible to see the force-signal amplitude relationship over four muscles (*biceps brachii*, *quadriceps*, *erectores spinae*, and *adductor pollicis*) of the articles reviewed in [27].

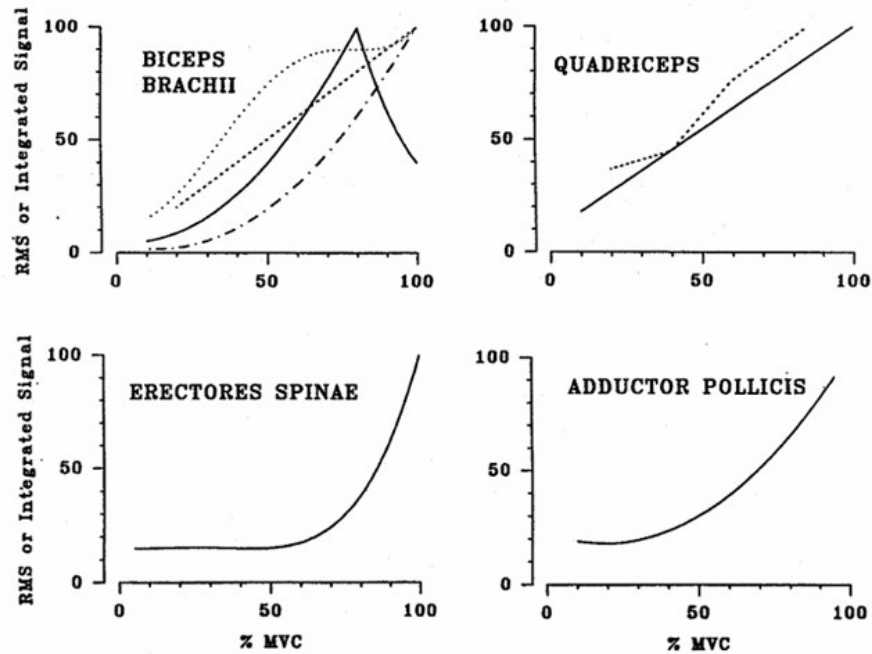


Figure 1.10: Force-amplitude relationship in MMG signal over four different muscles (Biceps Brachii, Quadriceps, Erectores Spinae, and Adductor Pollicis). On the x-axis, the force is expressed as % of the MVC, while on the y-axis, the RMS of the MMG signal is represented. [27].

It has emerged that the force-MMG amplitude relationship is different for the different muscles; it may be linear or quadratic due to the composition of muscle fibers. Indeed, for the *erectores spinae*, a quadratic relationship between MMG and Force was found in [29], while the amplitude increase in *adductor pollicis* was described in a curvilinear fashion [30]. On the other hand, in *quadriceps*, some studies reported a linear increase (solid line) [31], while others [32] found an increment decrease from 75 % to 100 % MVC (dotted line).

However, in *biceps brachii*, various relationships were found: the thin dotted line represents an S-shaped force-amplitude relationship found in [33]; solid line represents parabolic increase till 80 %MVC followed by a decrease till 100 %MVC [34], the dashed-dotted line shows a quadratic increase [35], and thick dotted line displays the linear relationship [36].

In biceps brachii, the steepest increase above 30 %MVC could be explained by the presence of fast-twitch fibers more superficially, which influences a lot the signal recorded on the skin surface [34]. Moreover, in [34], a decrease in MMG amplitude was found when there is an increase in the effort over 80 %MVC. This decrement could be related to the fact that for high firing rates, the fiber's shape is modified,

and the pressure waves on the skin surface are less intense. However, this is not present in the other muscles mainly because there could be an optimized management of MUs recruited and firing rate.

Frequency domain analysis

Regarding the frequency domain analysis, the first appreciable information is related to the signal band. The main power content of the signal is brought by frequencies under 100 Hz [16, 37, 38].

Moreover, in [27], various articles about the frequency that brings the main power content have been investigated. Even though the total signal band is represented from 2 Hz to 5 Hz to 100 Hz, various studies found the main frequency content below 20 Hz. In particular, in [39], it has been estimated that the main content frequency is $15 \text{ Hz} \pm 4.2 \text{ Hz}$ in *biceps brachii*. Moreover, in [40], the mean and median frequency increases from 11 Hz to 15 Hz when the effort increases. Other studies focus on differences between rest and contraction; indeed, in [41], during the rest, they locate two peaks at 10 Hz to 12 Hz, while during contraction, there is an increase in the power in the 1 Hz to 20 Hz band. Also, in another study [41] that considers the band till 49 Hz, the main power is brought by the 7 Hz to 14 Hz band (45 % of the total power brought from 1 Hz to 49 Hz).

Motion artifacts highly contaminate the MMG signal; they are usually removed with high pass filtering with a cut-off frequency that ranges from 0.1 Hz to 5 Hz. However, there are not any standards in the choice of cut-off frequency [42]. In [43], they evaluated the influence of motion artifacts in MMG signals. They have seen that even though the main components of the artifacts are centered at about 6 Hz, artifacts have a great influence till 15 Hz. However, since their influence is also present in the MMG signal band, a simple band-pass filter could not remove all of them. Moreover, they compared the artifact interference on signals recorded by microphones and accelerometers; they found out that MMG recorded with microphones is more robust to the influence of motion artifacts.

The choice to use mechanical vibration as mechanomyography was made due to the consistency of results regarding MMG signals that capture this biofeedback and because the Apollux device, developed by the eLiONS Laboratory and integrated with the Inertial Measurement Unit (IMU) (3, 3.1), will be used as part of the acquisition system in this project.

1.6 Parameter extraction from MMG signals

Several parameters are evaluated for each signal in the time or frequency domain to study MMG signals [44, 45].

Time domain parameters

Time domain parameters depend on signal amplitude, considering x_i a sample of MMG signal and a window length of N , the parameters evaluated are:

- **The Root Mean Square (RMS)** is evaluated as the square root of the mean of the squares of the quantity values over a specified time.

$$\text{RMS} = \sqrt{\frac{1}{N} \sum_{i=1}^N x_i^2} \quad (1.1)$$

- **The Standard Deviation (STD)** measures the dispersion or spread of data points from the mean value. It indicates how much individual data points in a dataset deviate from the mean of the dataset.

$$\sigma = \sqrt{\frac{1}{N} \sum_{i=1}^N (x_i - \mu)^2} \quad (1.2)$$

Frequency domain parameters

Frequency domain features are extracted from a signal's Power Spectral Density (PSD). PSD is evaluated over a range of frequencies that ranges from f_{\min} that is equal to 0 Hz, to f_{\max} that for the Nyquist theorem is equal to the sampling frequency of the signal divided by 2. PSD_f is the generic PSD value at a frequency f .

- **Sum of PSD (PSUM)** is the sum of the PSD for each f :

$$P_{sum} = \sum_{f_{\min}}^{f_{\max}} PSD_f \quad (1.3)$$

- **Mean Frequency (fmean)** is the frequency value that divides the PSD into two parts with equal area:

$$\text{fmean} = \frac{1}{N} \sum_{i=1}^N f_i \quad (1.4)$$

- **Median Frequency** (fmed) frequency value corresponding to the midpoint of the cumulative distribution:

$$\text{fmed} = \frac{\sum_{f_{\min}}^{f_{\max}} f \cdot \text{PSD}_f}{\sum_{f_{\min}}^{f_{\max}} \text{PSD}_f} \quad (1.5)$$

1.7 Joint angles estimation

Another way to study muscle activity for rehabilitation is by evaluating the joint motion while a muscle is contracting. For this purpose, an articular angle is evaluated as the angle formed between two body segments connected by a specific joint. In the human body, three types of joints are present: fibrous (not movable), cartilaginous (partially movable), and synovial (freely movable) [46]. The latter are the ones that provide movement between bones, and they are composed of a system of ligaments, muscles, tendons, cartilage, and synovial fluid that lubricates them [47]. Monitoring the mobility status of a joint is useful for monitoring musculoskeletal disorders that happen with aging or diseases and evaluating the effectiveness of a muscle contraction when a movement is performed. Different methods are present for evaluating joint movement. Usually, the angular changes between two reference axes or anatomical landmarks are measured. Techniques are distinguished by their purpose: joint angle, skeletal tracking, or joint motion.

Joint angle evaluation is based on studying a specific joint's Range Of Motion (ROM). It depends on subject-specific features (such as gender, age, or physical structure) and anthropometric limits (such as muscle length or bone structure). Several techniques are involved in this measurement, and they usually comprehend goniometers that use resistive potentiometers or strain gauges [47]. However, these techniques are highly affected by human error due to factors such as improper positioning, inconsistent force application, and subjective interpretation of data, all of which can compromise precision and reliability

Another technology used for this aim is the Inertial Measurement Unit (IMU), which has a minimal size and low cost and measures angles in three dimensions with high accuracy. IMUs minimize human error as they automatically collect data without requiring precise manual positioning, provide consistent measurements unaffected by subjective interpretation, and eliminate errors from inconsistent force application. These attributes make IMUs a more reliable and precise choice for measuring angles and movements.

On the other hand, joint motion studies the various movements that a joint can perform. An example of these movements in the case of the wrist is illustrated in Figure 1.11: they are flexion (bending), extension (straightening), adduction (moving towards the body's midline), abduction (moving away from the body's midline) and rotations (inward and outward motion) [48].

This technique focuses on both the study of the joint angle and the orientation and it is usually performed by imaging or video tracking [47].

Finally, in skeletal tracking, the main focus is the reconstruction of a skeletal

model to detect the position of body segments [47]. The main goal of these techniques is posture recognition, which evaluates physical impairment and the effectiveness of a rehabilitation process. Even though it uses the camera for joint monitoring, the main difference is in the more complex system that also comprehends artificial intelligence and depth of the imaging study due to the necessity of recreating a human model.

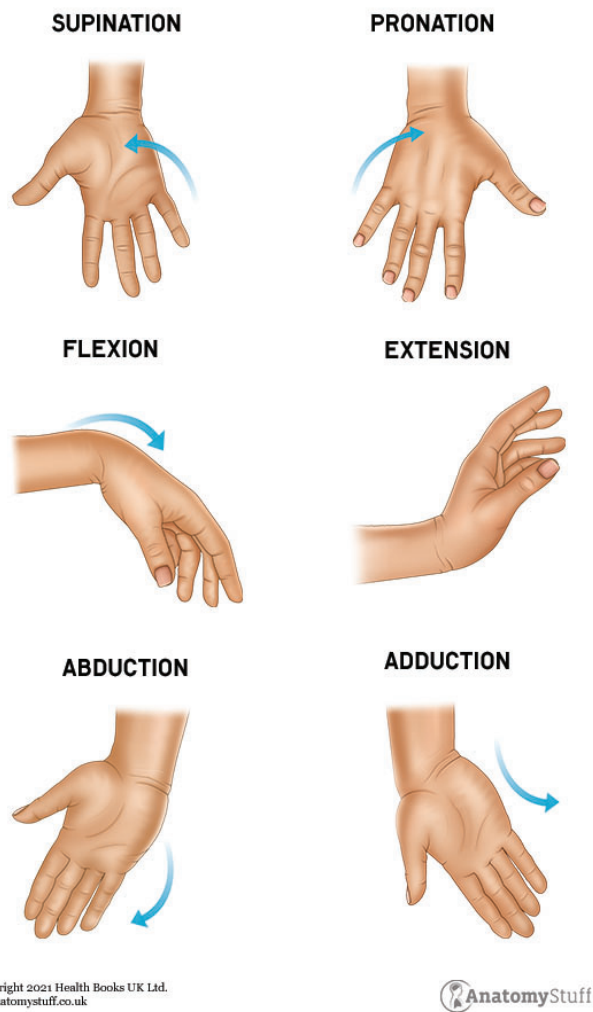


Figure 1.11: An example of several movements performed by the wrist articulation, from top: supination, pronation, flexion, extension, abduction, and adduction [49].

1.7.1 Imaging based techniques

The gold standard for joint estimation is using a set of cameras and acquiring images/video while the subject is performing a movement. Usually, the system comprises a network of cameras that simultaneously acquire data. Thanks to algorithms considering anthropometric constraints, reconstructing a 3D movement from 2D images is possible. Camera-based technologies can or may not require markers on the human body.

An example of a markerless technique is the Microsoft Kinect image sensor [50], which presents an RGB camera (R for red, G for green, and B for blue), a microphone, and a laser projector that can detect depth. Moreover, it is embedded with a skeletal tracking tool that can recognize various joint locations. This system is usually adopted in rehabilitation protocols because it does not require any wearable or controllable devices for the interaction patient-game, so it is highly usable during video games rehabilitation technique [51]. The main problem of this approach is due to the insufficient precision of movement tracking and the lack of customization to the patient's abilities.

A more accurate category of motion tracking is represented by marker-based motion capture systems. Markers are placed on the subject body in various locations, and the subject position and joint angles are estimated by the position of these markers [52]. The Vicon (Vicon Motion Systems Ltd, Oxford, UK) is the gold standard for marker-based technique. It uses infrared cameras that acquire data from reflective markers placed on the subject body following landmarks position directives reported in [53].

Imaging techniques are highly used in FES control to track the position and the joint angles the patient achieves during the stimulation session. Indeed, in [54], an FES system is validated thanks to motion capture over a population of 17 subjects and 6 movements performed. The FES system wants patients to reproduce the therapist's movement (detected by sEMG) and stimulate them in real-time using stimulation patterns directly from the therapist's muscle inputs. In this study, imaging was used to compare the trajectory of the patient and the subject; the results show that the similitude between the therapist's and the patient's movements is 97.39%.

1.7.2 Inertial Measurement Units (IMU)

Even though imaging is proven to be a highly reliable technique for joint estimation, its high cost, long preparation, high computational cost, and restrictiveness to a laboratory environment make it a difficult technique for rehabilitation.

Inertial Measurement Units (IMUs) are highly adopted to overcome those limitations due to their minimal dimension, low cost, and wearability with a small reduction in accuracy. Indeed, in [55], the authors compared the accuracy of hip angle and knee angle evaluated from an IMU wearable sensor with gold-standard motion capture, and the results show root mean square error of respectively 2.7° and 2.6° .

An IMU consists of three sensors: an accelerometer, a gyroscope, and a magnetometer. It measures three-dimensional acceleration, angular velocity, and the magnetic field vector. Each sensor has its coordinate system, but they are all aligned with each other to provide correlated and comprehensive measures of the sensor state [56]. Even though each sensor can work as an individual entity, i.e., evaluating acceleration from the accelerometer, the strength of this device is the feasibility of combining data via sensor fusion algorithm to estimate the device's orientation. IMU orientation can be expressed as quaternions or Euler's angle, it is evaluated by the combination of acceleration data and angular velocity to rectify the errors or drift that each sensor produces.

Accelerometer

An accelerometer is a sensor that detects acceleration (a). It is modeled in Figure 1.12 as a second-order spring-mass damper system with a mass (m) suspended by a spring with a spring constant (k) and a damping coefficient (b).

With Newton's second law, we obtain the equation:

$$\vec{F}_{\text{applied}} + \vec{F}_{\text{spring}} + \vec{F}_{\text{damping}} = m\ddot{\vec{x}} \quad (1.6)$$

$$m\ddot{\vec{x}} + b\dot{\vec{x}} + k\vec{x} = \vec{F}_{\text{applied}} = m\vec{a}_{\text{applied}} \quad (1.7)$$

The resulting transfer function is:

$$H(s) = \frac{X(s)}{a(s)} = \frac{1}{s^2 + \frac{b}{m}s + \frac{k}{m}} \quad (1.8)$$

To obtain a wide sensing bandwidth, a high resonant frequency is necessary. It can be done by decreasing the proof mass dimensions or increasing the spring constant. Sensitivity should be considered when doing this since it is evaluated as:

$$X_n = \frac{\text{Output Voltage generated (mV)}}{\text{Input acceleration along } n\text{-axis (g)}} \quad (1.9)$$

The unit of measurement for sensitivity is mV/g , and in a triaxial accelerometer, each axis has its sensitivity that is independent of the other axes. The term "Dynamic Range", which is measured in g , refers to the highest dynamic acceleration that an accelerometer can consistently measure.

Gyroscope

A gyroscope is a sensor that evaluates angular velocity; the observation principle is the conservation of the angular momentum. It is constituted by a spinning rotor that can rotate freely in three axes. Due to the conservation of angular momentum, when changes in angular velocity occur, the rotor tends to resist alterations and generates a measurable torque [58].

Many types of gyroscopes are used in different fields; however, for wearable devices, the Micro Electro Mechanical Systems (MEMS) gyroscope is the most used due to its small dimensions and high accuracy.

In the MEMS gyroscope, the sensing element is represented by a vibrating mechanical element rather than a rotating part due to its small dimension and manufacturability. The vibration is caused by the Coriolis acceleration a_c represented in Figure 1.13a), which is an apparent acceleration that occurs when there is a rotation in the reference frame .

In Figure 1.13b) there is the mass-spring model of a MEMS gyroscope; the mass can move along two axes (y and z), represented as two springs with respectively k_y and k_z stiffness. The resulting equations are:

$$\ddot{\vec{y}} = -k\vec{y} - b\dot{\vec{y}} + \vec{F}_{\text{Drive}} \quad (1.10)$$

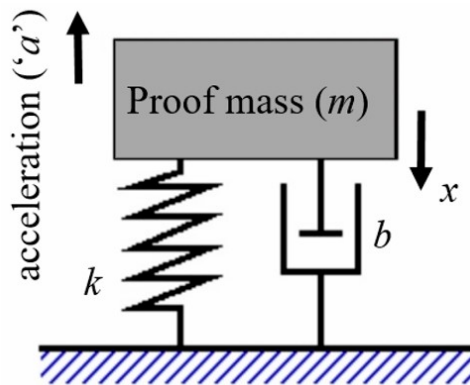


Figure 1.12: Accelerometer model: second-order spring-mass damper [57].

$$\ddot{\vec{z}} = -k\vec{z} - b\dot{\vec{z}} + \vec{F}_z \quad (1.11)$$

$$F_z = |2m\vec{\Omega} \times \vec{v}| \quad (1.12)$$

The force applied (F_{drive}) occurs on the y-axis, while the Coriolis Force F_z is on the x-sense axis.

The displacement along the z-axis can be evaluated as follows:

$$\Delta z = \frac{2\Omega_x F_z Q_y}{m\omega_y} \frac{1}{\sqrt{(\omega_y^2 + \omega_z^2)^2 + \left(\frac{\omega_y \omega_z}{Q_y}\right)^2}} \quad (1.13)$$

In Equation (1.13), Q_y is the quality factor, and ω_y are the resonance frequencies along n axis.

A gyroscope's sensitivity indicates how responsive it is to changes in rotational motion or angular velocity. It evaluates the efficiency with which the gyroscope produces an electrical or mechanical output signal based on angular velocity. Either matching the resonance frequencies or reducing friction can increase the sensitivity of the MEMS gyroscope.

Euler's angles

The positioning of a rigid body in the space can be determined with a set of three angles called Euler's angles [59].

Each Euler's angle represents the rotation along one axis of a three-axis reference frame (x,y,z).

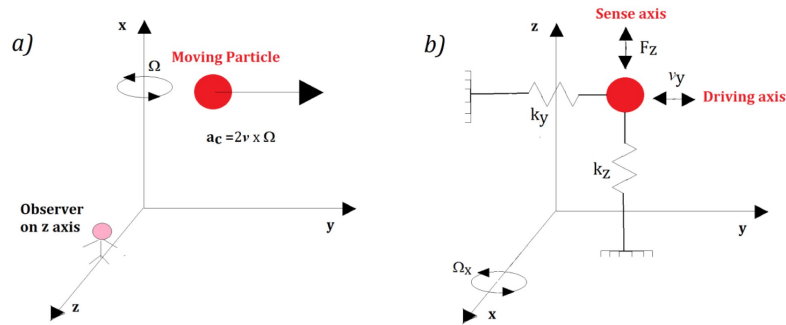


Figure 1.13: a) Coriolis acceleration (a_c) applied to a particle in motion. b) mass-spring model of a MEMS gyroscope [58].

They are represented in Figure 1.14; they refers to:

- roll (ϕ) rotation around the x-axis;
- pitch (θ) rotation around the y-axis;
- yaw (ψ) rotation around the z-axis.

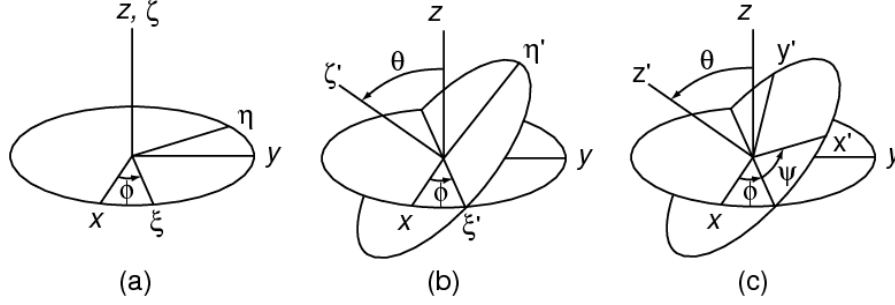


Figure 1.14: Representation of the Euler's angles on a 3D space (x,y,z) . ϕ is roll, θ is pitch and ψ is yaw [60].

The rotation matrix R (mathematical representation of the positioning or rotation of an object in the three-dimensional space) expressed in Euler's angles is equal to the product of the rotation matrices around the three axes:

$$R = R_z(\psi)R_y(\theta)R_x(\phi) \quad (1.14)$$

In Equation (1.14) $R_x(\phi)$, $R_y(\theta)$, and $R_z(\psi)$ are the rotation matrices around respectively the x-axis, the y-axis, and the z-axis. They are defined as:

$$R_x(\phi) = \begin{bmatrix} 1 & 0 & 0 \\ 0 & \cos(\phi) & \sin(\phi) \\ 0 & -\sin(\phi) & \cos(\phi) \end{bmatrix} \quad (1.15)$$

$$R_y(\theta) = \begin{bmatrix} \cos(\theta) & 0 & \sin(\theta) \\ 0 & 1 & 0 \\ -\sin(\theta) & 0 & \cos(\theta) \end{bmatrix} \quad (1.16)$$

$$R_z(\psi) = \begin{bmatrix} \cos(\psi) & -\sin(\psi) & 0 \\ \sin(\psi) & \cos(\psi) & 0 \\ 0 & 0 & 1 \end{bmatrix} \quad (1.17)$$

Euler's angles are defined as positive when they rotate counter-clockwise, and on the positive side of the axis, they are referred to [59].

They have different ranges, indeed roll and yaw range in 2π radians (usually considered as $[-\pi, \pi]$), while pitch covers a range of π radians (traditionally considered as $[0, \pi]$ or $[-\pi/2, \pi/2]$).

However, this angle representation suffers from gimbal lock; indeed, there is a degree of freedom loss due to an axis alignment. In this condition, two rotational axes are in a parallel configuration (when the pitch angle approaches $\pm\pi/2$ degrees), and the system degenerates into a two-dimensional space.

Magnetometer

A magnetometer is the final sensor found inside the IMU. The IMU typically contains three orthogonal magnetometers. Their function is to gauge the magnetic field's intensity in a particular direction to identify the north. After the magnetometer was inserted, the accelerometer and gyroscope measurements were complemented by the IMU. The magnetometer has an absolute reference to time and must correct the gyroscope's data to enhance the orientation's overall estimation because the gyroscope can drift in time. As an aside, the magnetometer is not without limitations; in fact, interference from adjacent magnetic objects may cause problems for it [61].

The navigation application is the primary benefit of integrating a magnetometer into the IMU. Because of this, the IMU of the devices that will be utilised in this thesis project only consists of the accelerometer and the gyroscope, despite the magnetometer's advantage.

Chapter 2

State of Art

An overview of the state of the art of Functional Electrical Stimulation (FES) technology will be provided in this chapter.

The chapter opens with a synopsis of the experimental setup employed in this project and a quick description of the actual stimulation devices. The current literature on FES open-loop and different closed-loop applications using surface ElectroMyoGraphy (EMG), joint angles, and MechanoMyoGraphy (MMG) is summarised below.

2.1 Open-loop for Functional Electrical Stimulation (FES) control

Functional Electrical Stimulation (FES) is a type of therapy used in rehabilitation to assist Spinal Cord Injury (SCI) patients by restoring loss of function or accomplishing daily life movements.

Usually, an FES stimulator uses non-invasive surface electrodes to provide current in brief bursts of $10\ \mu\text{s}$ to $500\ \mu\text{s}$. Current excites motor nerves and causes skeletal muscle contraction, while the central system can concurrently modulate neurons [62]. Improvements in the FES system are related to the stimulator and the stimulation's pattern choice.

Regarding the stimulator, the upgrades are towards the wearability of the device, so the advancements in hardware and software made it possible to pass from a stimulator not wearable that delivers current via wires, to a wearable FES system that sends current via wires but the stimulation pattern is sent via wireless from a

remote control. Examples of wireless FES stimulators are Compex Wireless from Compex [63] and NESS L300 from Bioness [64]. This improvement is useful when considering home therapy and in the daily life of a patient who could wear the stimulator directly under its clothes [62]. However, these stimulators are usually designed for a specific muscle movement and a specific FES rehabilitation, so their application is restricted to a specific set of patients.

On the other hand, the research tends toward optimizing the stimulation pattern since movements performed in rehabilitation are complex and require the synchronicity of the activation of various muscles, so it is necessary to find an activation pattern that suits the desired movement. This leads to a need for stimulation that is regulated actively rather than a passive stimulation pattern that is established *a priori*. A pattern determined by *a priori* can be used; for instance, a pattern based on the therapist's correct movement can be created as *a priori* and used to stimulate the subject. The problem is that the profile created is customised for the movement to do rather than for the subject.

Surface ElectroMyoGraphy (sEMG) is used in various studies to indicate a muscle activity level. A stimulation pattern (current amplitude, pulse width, and stimulation frequency) is obtained from this force data. sEMG could be detected either from a healthy subject (named therapist), from the healthy side of a hemiplegic patient, or from the patient's residual intention of movement. Indeed, in [65], the voluntary sEMG is the driving solution to estimate the stimulation parameters. The proposed algorithm aims to map the sEMG and muscle force using Gaussian mixture regression. Lately, thanks to polynomial fitting, stimulation amplitude, and pulse width are estimated from the force.

2.1.1 Average Threshold Crossing - Functional Electrical Stimulation (ATC-FES) system description

This thesis project starts from an Average Threshold Crossing - Functional Electrical Stimulation (ATC-FES) system that can define in real-time the stimulation patterns from the ATC parameter that is extracted from the sEMG of a healthy muscle [66]. Figure 2.1 describes the system division into three main units:

- Acquisition unit comprehends the wearable sensors that extract the ATC parameter from the sEMG acquisition. In the previous system versions, also articular goniometers were present in this part;
- Actuation unit is composed of an external stimulator with eight stimulation channels;
- Control Unit is a software environment that processes the data in input/output of the previous units. The communication between the sensors and the Control

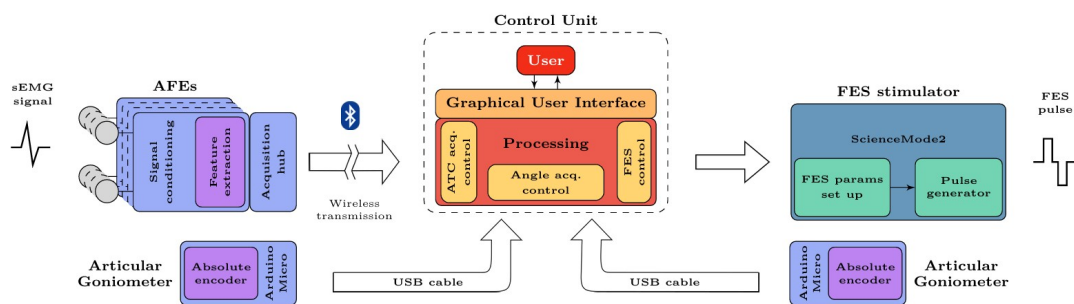


Figure 2.1: Average Threshold Crossing - Functional Electrical Stimulation (ATC-FES) system [66]. On the left, the Acquisition Unit detects the sEMG signal; on the right, the FES stimulator; and in the center, the Control Unit regulates the device connection and facilitates user interaction.

Unit is enabled with Bluetooth Low Energy (BLE), while the stimulator is connected through a USB interface.

Acquisition Unit

The sEMG is acquired and processed into the ATC parameter with a device developed by F. Rossi *et al.* [67], whose prototype is shown in Figure 2.2; it is composed of an Analog Front-End (AFE) constituted of a hardware part for sEMG signal processing; and a digital component with a microcontroller for the wireless data connection.

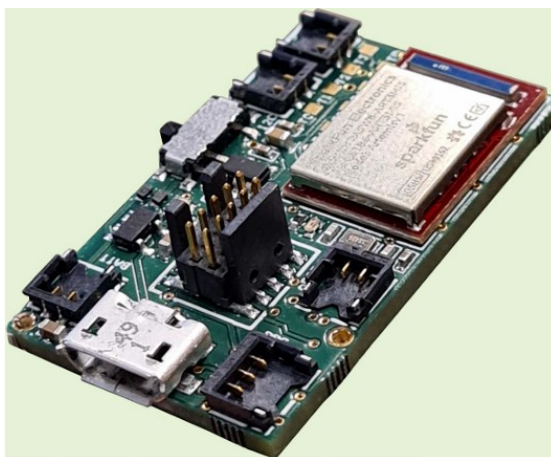


Figure 2.2: Wearable Average Threshold Crossing (ATC) acquisition device developed by F. Rossi *et al.* [67].

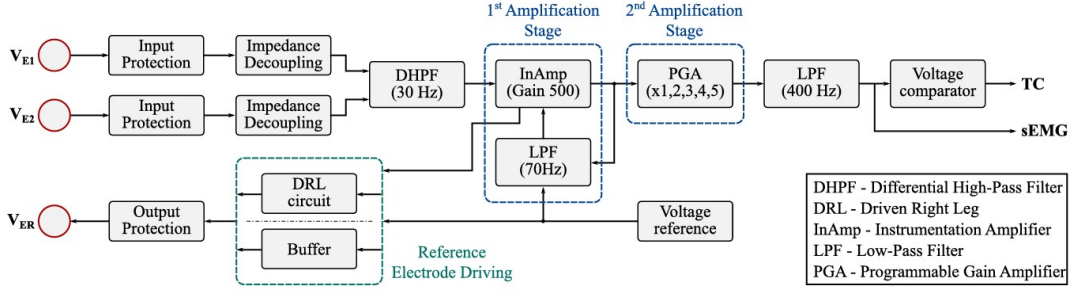


Figure 2.3: Analog Front-End (AFE) of the Average Threshold Crossing - Functional Electrical Stimulation (ATC-FES) system [67]. V_{E1} and V_{E2} are the sensing electrodes of the differential amplifier, while V_{ER} is the reference one; the detected signal passes through a series of filters and amplification stages before becoming the processed sEMG signal. This signal can also pass through a voltage comparator that extracts the ATC parameter.

The front-end scheme is represented in Figure 2.3; it acquires data with bipolar electrodes configuration (using two exploring electrodes V_{E1} and V_{E2}) and one to refer body potential (V_{ER}), which comprehend the Driven Right Leg (DRL) circuit that limits the effect of common-mode noise.

The device power voltage supply is equal to 1.8 V. Protection circuits are inserted after these electrodes to protect the circuitry from a possible higher voltage than power supply, i.e. when utilizing these devices during FES.

Moreover, the sensing channels (V_{E1} and V_{E2}) have a decoupling circuit constituted of a voltage follower that provides a good impedance to the amplifier inputs but also guarantees the sEMG integrity.

Before the amplification stage, a differential high-pass filter at 30 Hz covers the motion artifacts (induced by cable motion) that can bring the saturation of the consecutive electronic components. The amplification stage is divided into the following:

- 1st Amplification stage constituted of an instrumentation amplifier that subtracts the input channels (V_{E1} and V_{E2}) and amplifies the difference with a differential gain A_d equal to 500 V/V. Moreover, to improve the output's consistency and stability, there is negative feedback with a second-order Butterworth low-pass filter with a cutoff frequency of 70 Hz.
- 2nd Amplification stage made of a programmable gain amplifier that provides x2, x3, x4 and x5 additional amplification values.

After the amplification stage, there is a Sallen-Key low-pass filter with a cutoff frequency of 400 Hz.

After this chain, the sEMG is correctly acquired and could either be saved as sEMG or pass through a voltage comparator to extract the TC signal. The threshold of the comparator is generated by a Digital-to-Analog Converter (DAC) with a hysteresis of 30 mV.

The digital part is responsible for the processing stage used for the ATC parameter computation. This operation is done by a MicroController Unit (MCU) Apollo3Blue with an ARM Cortex[®]-M4F processor. A BLE 4.2 is implemented on Apollo3 MCU since it represents the best compromise between consumes and performances. Besides, it is a low-power communication for exchanging notifications like status, ATC, or sEMG.

Actuation Unit

The external stimulator is the RehaStim2, made by HASOMED[®] GmbH [68]. It is a portable device that generates biphasic rectangular pulses and can stimulate eight channels simultaneously [66]. The range of the current injected is 0 mA to 130 mA in amplitude, pulse-width range from 20 μ s to 500 μ s, the stimulation frequency f_s from 10 Hz to 50 Hz. The pulse amplitude is extracted from the ATC parameter evaluated from a healthy muscle (could be another subject or the contro-lateral segment in a hemiplegic patient).

A more detailed description of the electrical stimulator is provided in Chapter 3 during Section 3.2.

Control Unit

The control unit connects the user and the system with a Graphical User Interface (GUI) built in Python and connects the acquisition and actuation units.

It permits the synchronized control of the FES stimulator, the limb motion recordings, and the ATC acquisition [66].

A LookUp Table (LUT) ATC-Current defines the relationship between ATC and FES intensity. This is created after a calibration phase that evaluates the threshold suitable for the muscle just above the sEMG baseline and maximises the TC events with minimal muscle effort. After the calibration, each time a new ATC value is received, the median value between this new value and the previous three is evaluated, and the current value is associated with the table created in the calibration phase.

2.2 Closed-loop for FES control

Many FES studies focus on a control to define the stimulation input as time interval, and the stimulation pattern. Indeed in [69], the control is achieved with a brain-computer interface that analyses the ElectroEncephaloGraphy (EEG) of a subject to control a neuroprosthesis that stimulates Biceps Brachii, Triceps Brachii, anterior Deltoid and posterior Deltoid. This study extracted the EEG content in the beta frequency range (18 Hz to 28 Hz) recorded from a single channel (Fz). When the signal power decreases under a certain threshold, the stimulation is activated only with a 'brain-switch' that acts as an on/off mechanism that defines when the current should be injected. Still, it does not evaluate the intensity of it.

However, this system is considered as open-loop FES system since it controls only the input given but not the effect of the stimulation on the subject's body. The open challenge in the research field tends to control the subject reaction (in terms of muscle activity or movement performed) post-stimulation to adapt the stimulation input and give an optimized stimulation to the patient. The main difference between voluntary and stimulated contraction is due to the input given to the muscle; indeed, in voluntary contraction, the input comes from a central nervous system that modulates the Motor Unit (MU) and the firing rate to the exercise request. On the other hand, in FES contraction, the input is given from a current injected and is modulated by the intensity of the current given from the external world.

The problem lies in the fact that this leads to a rise in muscle fatigue, which is the reduction in a muscle's capacity to produce or sustain a specific amount of force when exercising. The nervous system adopts various methods to reduce it, such as changing the MU stimulated (giving them time to recover) and increasing/decreasing the firing rate of the MU [70]. However, this is not possible in stimulated contraction since the MU excited depends on a geometry factor, so the MU recruited are the same all the time. So, during FES stimulation, certain MUs overwork and are more affected by fatigue.

On the other hand, it should also be considered that FES is a solution adopted for SCI patients, and with paralysis, various changes occur, such as disuse atrophy that brings a transformation in the types of muscle fiber (from slow to fast twitch) [71]. Indeed, in [72], they tested the fatigability of paralyzed thenar muscle (and healthy patients considered as control) because they wanted to understand if delivering a varied or constant frequency could lower it. The outcome of this study is that in paralyzed muscles, the force reduction is associated with an increase in the half-relaxation time and a decrease in force-time

integral, independently of the stimulation frequency. Moreover, this fatigue effect was significantly increased in paralyzed muscles (with respect to the control ones), and the variation of the stimulation parameters did not affect the fatigue in both sets of subjects.

Another study [73] explored the possibility of applying random adjustment to the inter-pulse interval to modulate the pulse frequency randomly. They obtained promising results in increasing the time that the leg extensor could work (37%) when the frequency varied in a range of $\pm 12\%$. However, these results were obtained for a single subject. So, in [71], they tried to extend this discovery over a more amplitude set of subjects (nine) and varying pulse frequency, amplitude, and width because they wanted to check if the number of MUs recruited and their firing rate could change over time. Four modes were tested: randomized frequency (mean 40 Hz), randomized current amplitude, and constant stimulation, and randomized pulse width. However, they concluded that there was no significant evidence of improvements in induced fatigue since the rest time (10 min) between trials was not enough for the full recovery of a muscle.

So, there is growing research on the importance of different approaches based on the post-stimulation effect on the muscle rather than a random or controlled change of the stimulation parameters. The closed-loop feedback is aimed to control the stimulation parameters (current amplitude, stimulation frequency, pulse width) based on the muscle response after the stimulation, controlling fatigue induced, subject response (i.e., presence of residual muscle activity), or joint motion achieved during the stimulation period. The general requirements of a good feedback signal include the light weight of the sensor, wearability, no restriction to a laboratory environment, low computational cost to ensure a real-time application, and low cost.

This thesis project aims to add a closed-loop control to the ATC-FES system described in the previous section. The first step has been researching feasible sensors and techniques for evaluating muscle activity during FES treatment.

2.2.1 Closed-loop with Surface ElectroMyoGraphy (sEMG)

EMG signal is the gold standard for muscle activity investigation; from this data, it is feasible to evaluate several muscle parameters useful for investigating the dynamics of a contraction, fatigue, and force produced.

Some studies tried to investigate the possibility of using FES-evoked EMG as a control during the stimulation. For example, in [74], they used the EMG feedback to develop a torque control scheme that adapts to muscle time-variant responses (i.e., fatigue). Torque sensors are unadaptable to rehabilitation since they are restricted to a laboratory environment. However, this study focuses on estimating the force produced from the EMG signal. It started from a previous study [75] in which a torque prediction method was developed thanks to a Polynomial Hammerstein Model (PHM). A PHM model comprises a linear block (autoregressive structure with exogenous input) and a nonlinear block (polynomial basis function).

As shown in Figure 2.4, the system contains two PHM cascades illustrating the dynamics of contraction and muscle excitement. The input of the apparatus is the stimulation that enters the excitation model that predicts the EMG. The predicted EMG goes into the contraction model, which produces the torque estimation as an output.

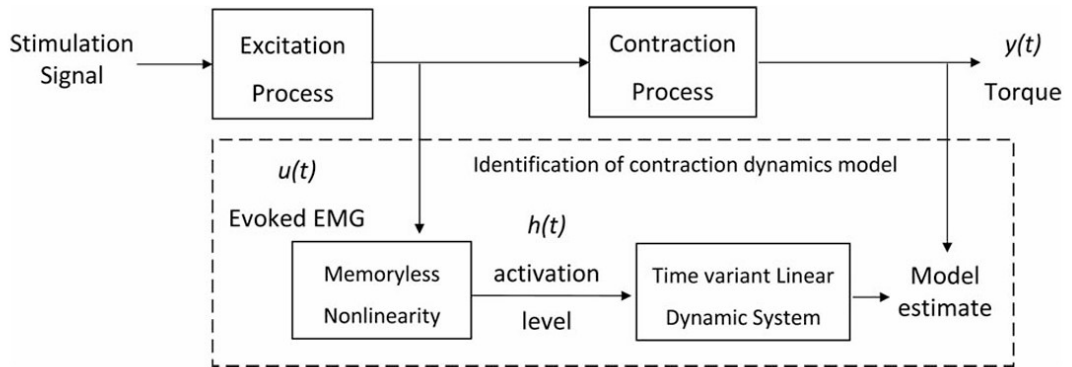


Figure 2.4: Polynomial Hammerstein Model(PHM) composed of a memoryless nonlinear block followed by a time-variant linear dynamic system [75], from the predicted evoked EMG a torque prediction can be evaluated.

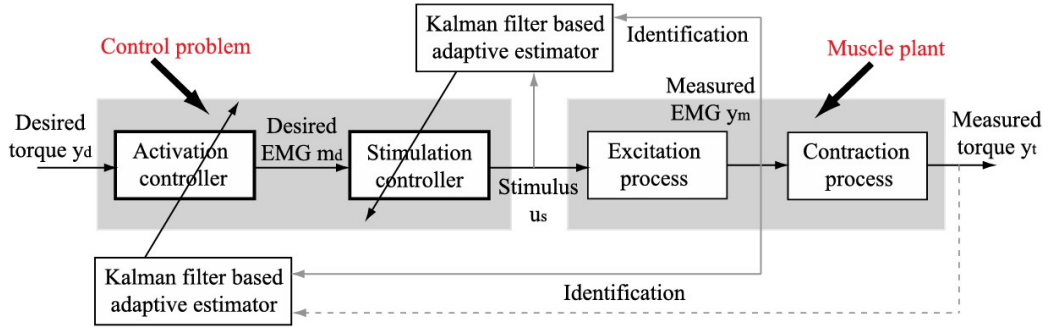


Figure 2.5: EMG-feedback predictive control [74]. The EMG (thanks to an activation controller) is evaluated from the desired torque, which passes into a stimulation controller step that evaluates the desired stimulation pattern. Then, this stimulation pattern is used in the excitation process, and from the apparatus in Figure (2.4), the real torque is estimated.

In [74], the aim was the development of an optimal stimulation signal that produces the desired joint torque from an EMG predictive control. The system in Figure 2.5 is divided into an activation controller and a stimulation controller (represented by a generic PHM model): the activation controller takes the desired torque as input and produces m_d in output that is the desired EMG, the EMG then passes through a stimulation controller that predicts the stimulus pattern. Then there is the stimulation with this founded pattern, and from the apparatus in Figure 2.4, the real torque is measured.

The results obtained in this study are promising since the RMS error of the torque is less than 4.5%, and EMG and stimulation mismatch was less than 10.5%.

However, one problem concerning the EMG feedback for a closed-loop regards the electrical contamination of the signal when there is an evoked contraction.

The interference of the injected current in the detected electrical signal is known as a 'stimulation artifact' as explained in Figure 2.6. It is constituted of 3 main components [77, 78]:

- Initial spike is subjected to an exponential decay and lasts around 2 ms to 3 ms. It depends on the stimulation parameters and unbalanced charges that accumulate after the stimulation;
- Conduction latency depends on the distance that exists between the innervation zone and the sensor positioning (detection site);
- M-wave is the sEMG resulting from the synchronicity of MUs stimulated.

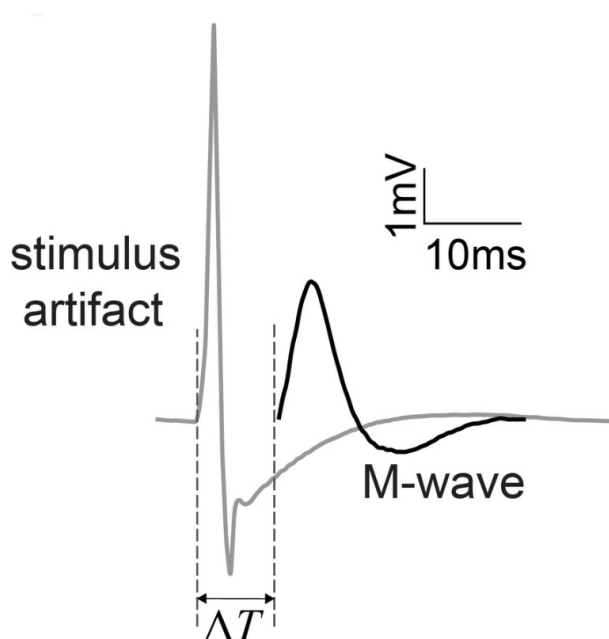


Figure 2.6: EMG stimulation artifact due to FES [76]. It can be divided into an initial stimulus spike affected by an exponential decay, followed by a period of conduction latency (ΔT) and M-wave.

So, when detecting FES-evoked sEMG, the stimulation artifact removal is necessary either to extract the volitional sEMG (residual voluntary muscle activity) or to remove the initial spike that can saturate the front-end of the sEMG sensor.

Techniques used to remove the effect of the initial spike comprehend the use of bipolar stimulation to reduce unbalanced charges and the detection front-end design that takes account of the saturation induced by the initial spike.

In [77], they proposed a detection front-end design that includes: 1. high-dynamic range of the amplifier; 2. fast recovery after each stimulation with a switch; 3. detection and stimulation site isolation; 4. blanking window with a switch that forces the output to zero after the stimulus for a predefined time window (7.6 ms).

On the other hand, various approaches are used to remove the M-wave (and extract the voluntary content of the signal). They can be divided into three categories:

- Filtering techniques that start from the hypothesis that M-wave produced by the same stimulation parameters are the same. Indeed, comb filters are the standard for this technique since they remove a specific frequency. In [79], they are using a Notch filter to remove the 60 Hz frequency;

- Template subtraction that considers the shape of an M-wave and removes it from the evoked sEMG signal. It may be achieved in various ways, i.e., with an adaptive matched filter optimized by genetic algorithms [80], or decorrelation and 6th order Gram-Schmidt algorithm [77];
- Decomposition techniques that decompose the EMG signal into uncorrelated components with algorithms like empirical mode decomposition [81] that divides the signal into Intrinsic Mode Functions, then there is a classification step to individuate the components affected by the artifact and remove them.

However, the sEMG feedback requires complex hardware and computationally expensive software. So, even though the EMG signal represents the gold standard for muscle activity analysis, other ways of extracting information are examined.

2.2.2 Closed-loop with articular angles

D. Andreu *et al.* [82] had developed a wearable wireless FES system utilised in both closed-loop and open-loop settings. The research team's objective is to create a tool that physiotherapists can use to assist patients with their rehabilitation and that patients can use in their daily lives. This can be achieved by a closed-loop, based on Inertial Measurement Units (IMUs) devices that control the stimulation given and its result. In this work, the angle generated by the knee during gait was estimated. Specifically, the difference between the reference angle during gait, defined as knee angle set-point (KAS) and paretic knee angle (PKA), was controlled.

As described in Figure 2.7, four sensors made up the system: two IMUs that provide direct quaternion estimation and two foot pressure sensors, communicating with two wearable Raspberry controllers over Bluetooth 4.0 BLE Protocol. The pressure sensor and IMU provide periodic data that the system gathers and analyses online.

The stimulated muscles are the hamstring and the quadriceps, FES is performed by electrodes placed in direct contact with the skin of the targeted muscle. Since the system is wireless, it also has a commercial USB power bank as a power source.

The paretic foot support (PFS) obtained from a pressure sensor is analysed to distinguish between the stance and swing gait phases. In order to compensate for the delayed muscle activation and anticipate the step, stimulation is applied shortly before the swing phase ends. The assessment of the difference between PKA and KAS controls the activation of both muscles during the stance period (Figure 2.8). The P controller will modify the stimulation parameters based on the error in pulse width evaluation between the two orientations.

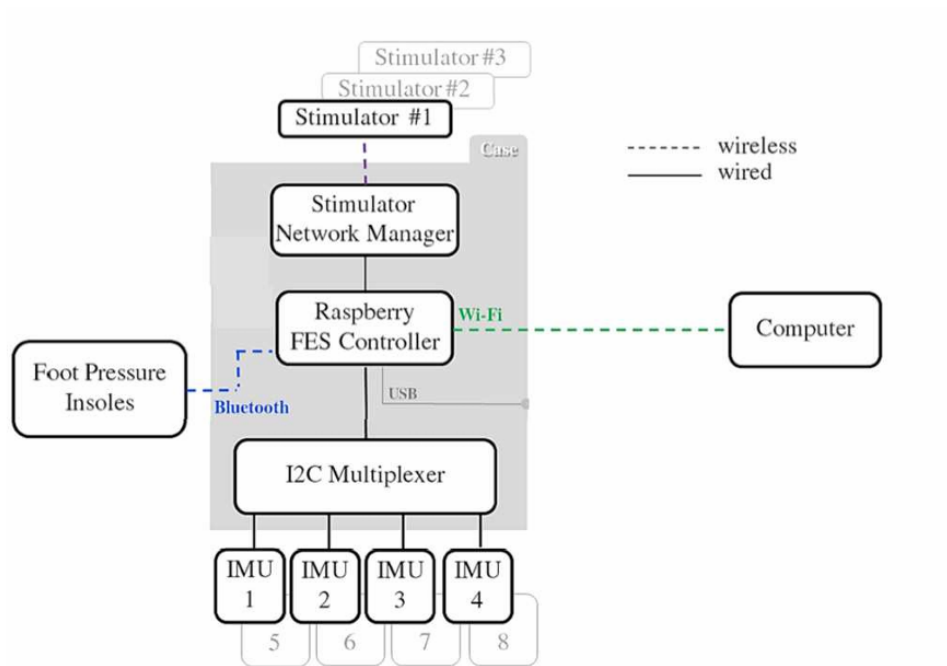


Figure 2.7: Architecture system scheme: input signals are sent to Raspberry FES Controller from foot pressure insole via Bluetooth and from IMU through wire. A computer is used to manage the start and stop of closed-loop via Wi-Fi. A stimulator Network Manager supervises stimulation via wireless [82].

Stimulation is applied to the hamstrings if PKA is greater than KAS and to the quadriceps if PKA is less than KAS.

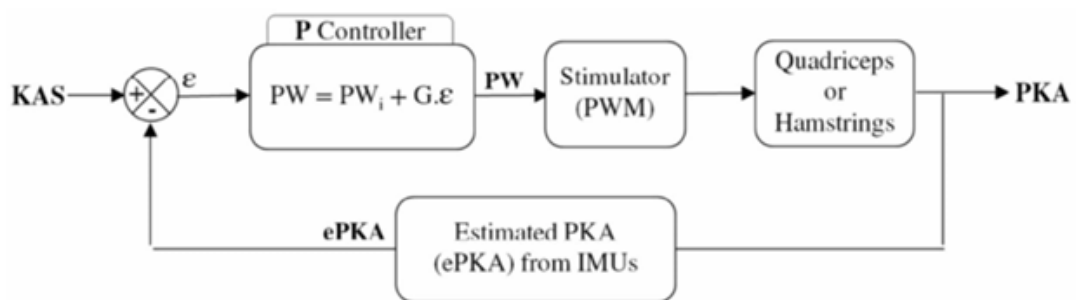


Figure 2.8: Explanation of how closed-loop works to control FES [82]: P Controller compares KAS and ePKAS and uses the error between two angles as input to manage stimulation on muscle of interest.

During this study, it was evaluated that it is possible to do this control in adequate time compared to stimulation time. Also, lost frames because of wireless transmission were considered, and it was reported that there isn't a critical cause of these samples.

Additionally, Man *et al.* [83] attempt to regulate a closed-loop system using angle to stimulate during FES. According to D. Andreu [82], they employ an alternative technique using an accelerometer to measure the angle and subsequently regulate stimulation. Providing stimulation control to patients was believed to improve their proprioceptive feedback and movement control [83].

In order to be included in this research [83], patients had to be able to extend their elbows at least 45° forward and extend their wrists, fingers, and elbows in response to stimulation.

The Odstock 2-channel Programmable Stimulator (O2PS) was utilised as the stimulator, allowing subjects to work independently and perform activities of daily living (ADL) independently. The arm movement was detected by a biaxial accelerometer and evaluated as the change in the angle between the accelerometer's axis and Earth's gravitational forces; this change caused the stimulation onset.

Stimulation was biphasic in the waveform, having currents ranging from 20 mA to 100 mA and pulse lengths with positive phases between $10\ \mu\text{s}$ to $350\ \mu\text{s}$. The stimulation frequency can be set as the last parameter, ranging from 20 Hz to 40 Hz.

The purpose of this research is to enable patients to fully extend their arms, grasp objects, and then release them. Therefore, stimulation of the elbow, wrist, and finger extensor muscles is applied based on the motor skills of the patients required to participate in the experiment. In Figure 2.9, there is the experimental setup; it is composed of PALS skin surface self-adhesive $5\ \text{cm}^2$ electrodes used to stimulate the extensor of the elbow, whereas $3.3\ \text{cm} \times 5.3\ \text{cm}$ electrodes are used to stimulate the extensor of the wrist and fingers. For extension of the elbow, the triceps brachii is the first channel to be activated.

To obtain a higher stimulation time, participants must initiate movement throughout this protocol, which is designed in accordance with a time-table stimulation. Two parameters computed before and after the experiment to track development are the Modified Ashworth Scale (MAS) and the Action Research Arm Test (ARAT). MAS measures the passive resistance of elbow, wrist, and finger flexors; while ARAT assesses the ability to perform specific functional tasks involving the arm and hand in everyday life.

Results show that the degree of disability, capacity, and standard of living significantly improved. The individuals' greater awareness of their hemiplegic arm, decreased muscle stiffness, increased movement, and one raised sensation were the key findings at the end of the study [83].

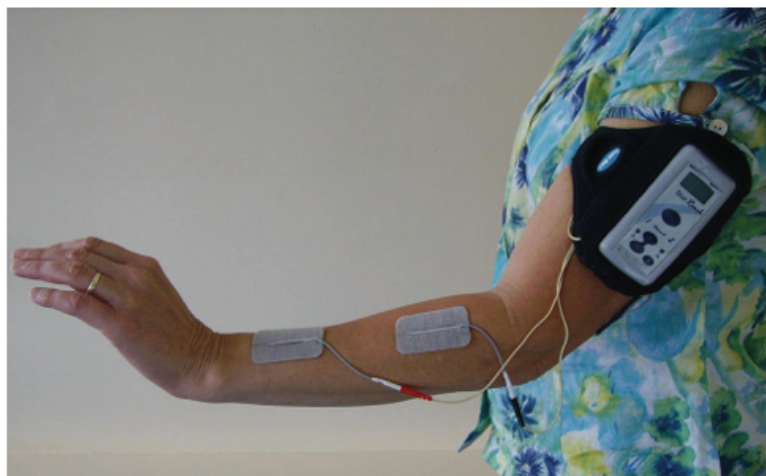


Figure 2.9: Experimental setup: Stimulator O2PS and PALS skin surface self-adhesive 2 cm² electrodes positioned to extension of wrist [83].

Except for two patients, everybody said this gadget has improved their hand function. None of the subjects had complaints regarding the feeling of electrical stimulation. This study demonstrated that electrical stimulation induced by an accelerometer can enhance the functional capacity and quality of life of people with upper limb hemiplegia.

2.2.3 Closed-loop with MechanoMyoGraphy (MMG)

In some papers [84, 85], E. Krueger *et al.* described how they employed MechanoMyoGraphy (MMG) as a tool to regulate a closed-loop FES system.

E. Krueger examined variations in the root mean square (RMS) and median frequency (MDF) of MMG signals in [86]. Because these signals are unaffected by electrical pulses, the research team in this work used triaxial accelerometers to evaluate oscillation in muscular contraction during FES sessions.

MMG sensors were situated precisely above the muscle bellies of the vastus lateralis and rectus femoralis during this trial. Additionally, they measured the movement angle's amplitude using an electrogoniometer.

The purpose of this work [86] is to observe the muscle oscillatory response during the application of FES using MMG. When fatigue of the muscles was monitored without FES using EMG and MMG, comparable results were found. MMG RMS and MDF magnitude plots tend to turn away from each other over time.

These findings suggest that muscle exhaustion and nerve cell adaptation may influence MMG RMS and MDF behavior. Thus, it can be said that in a closed-loop FES system, MMG MDF and RMS features extracted from MMG can be used as control methods.

Following up on this first research, E. Krueger kept looking into the possibilities of using MMG as a fatigue detector in a closed-loop FES system. Fatigue sets in quickly during a functional exercise session (FES) due to the electrical stimulation of muscle fibers [84]. As other studies have demonstrated [87, 88], during FES, there would be a drop in the MDF of power spectral density (PSD) and an increase in the amplitude of the RMS signal. In this investigation, E. Krueger used MMG to collect muscle activity during FES. The MMG technique was applied during the application of FES to individuals with spinal cord injuries in this trial. The primary aim of the study [84] was to analyze the fatigue characteristics of the quadriceps muscle in paraplegics patients while performing an FES-induced quasi-isometric contraction, utilising the Cauchy wavelet transform of MMG signals. Freescale MMA7260Q MEMS triaxial accelerometer was used as an MMG sensor, recording only the X-axis; through stimulation, subjects have to raise their leg from 30° to 5° . The experimental setup is described in Figure 2.10.

MMG signals were initially processed in 11 frequency bands using the Cauchy Wavelet (CaW) transform. In the end, RMS was calculated for each frequency band, and data were normalized using the first second of the first segment. The signals were first treated using a Butterworth pass-band filter in the range of 5 Hz to 100 Hz.

The study concluded that a rise in low-frequency energy was linked to tremors of exhaustion during isometric contractions and that individuals with spinal cord injuries experience muscular fatigue at a younger age. Thus, the frequency shift towards lower frequencies was unmistakably a sign of muscular exhaustion, as the results demonstrated [84]. This finding confirms that MMG can be applied as a kind of biofeedback or as a real-time indication of muscle exhaustion in a FES closed-loop system.

In subsequent work, [85], researchers used MMG to evaluate intrinsic alterations in SCI individuals during leg extension through FES. The research team is concentrating on analysing the frequency band produced from the CaW transform and trying to figure out how the FES fatigue induction methodology affects the muscle fibers' vibration pattern.

In healthy patients, the most significant MMG bands with submaximal contraction levels are those between 12 Hz and 38 Hz. According to the trial's findings, SCI participants could fall within this range.

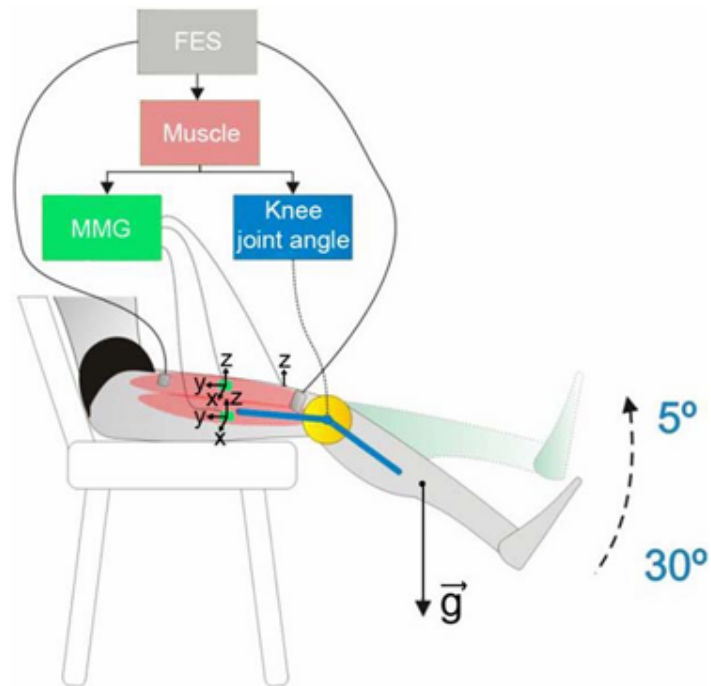


Figure 2.10: Experimental setup: FES electrodes are located over interest muscle, electrogoniometers are over knee to measure its angle, MMG sensors are positioned over bellies muscles [84].

The frequency band exhibiting the greatest significant decrease owing to fatigue is the 25 Hz range.

The results of this investigation [85] show that there is a robust linear correlation, indicating that the MMG signal can distinguish between different levels of muscle contraction and that the frequency bands of 20 Hz and 25 Hz are more responsive to the process of tiredness.

The MMG was selected to identify muscle activations following this state-of-the-art research, as it appears to recognize them when used during FES. The mechanical vibration of a muscle, which represents its contractions, can be studied using the MMG. Nevertheless, to confirm that the vibrations were muscle activations, it was also decided to track the subject's movement during the FES using Euler's angles to confirm that the vibrations were contractions carried out to accomplish the desired movement.

According to the literature, the processing that will be proposed will include an 8th order Butterworth high-pass filter with a cut-off frequency of 5 Hz. Additionally, it was determined that the roll angle should be considered solely. Chapter 4 Section 4.1 will cover every detail of signal processing.

Chapter 3

System description

This thesis project starts from the Average Threshold Crossing - Functional Electrical Stimulation (ATC-FES) system described in Chapter 2 Section 2.1.1. The study is focused on discovering a signal that works as a closed-loop mechanism to update the stimulation parameters during FES and can be used as biofeedback.

This chapter starts with a general overview of devices used and the software developed in the past by the eLiONS Laboratory. At the end, a general description of the implemented system will be provided in this chapter.

3.1 Apollux acquisition system

The acquisition devices used for the closed-loop biofeedback are called Apollux. They are an upgraded version of those described in Chapter 2 Section 2.1.1 and in [67] developed by F. Rossi *et al.* Their small dimension of 57.8 mm x 25.2 mm x 22.1 mm makes them easily wearable and data communication is achieved by using Bluetooth Low Energy (BLE) connection.

The improved version has an Inertial Measurement Unit (IMU) embedded, so it is capable of acquiring either Surface ElectroMyoGraphy (sEMG) signal (as described in Chapter 2) or kinematics data. The circuitry of the Apollux devices, and the IMU sensor, is displayed in Figure 3.1. In particular, in this thesis project, the chosen biofeedback signals are the MechanoMyoGram (MMG) data for the evaluation of the muscle activations, and the angle data of the distal segment for the movement performed. The former is obtained by acceleration data, while the latter is extracted from Euler's angles data acquired by the IMU sensor.

The embedded IMU sensor is the LSM6DSO32X iNEMO inertial module [89]. It

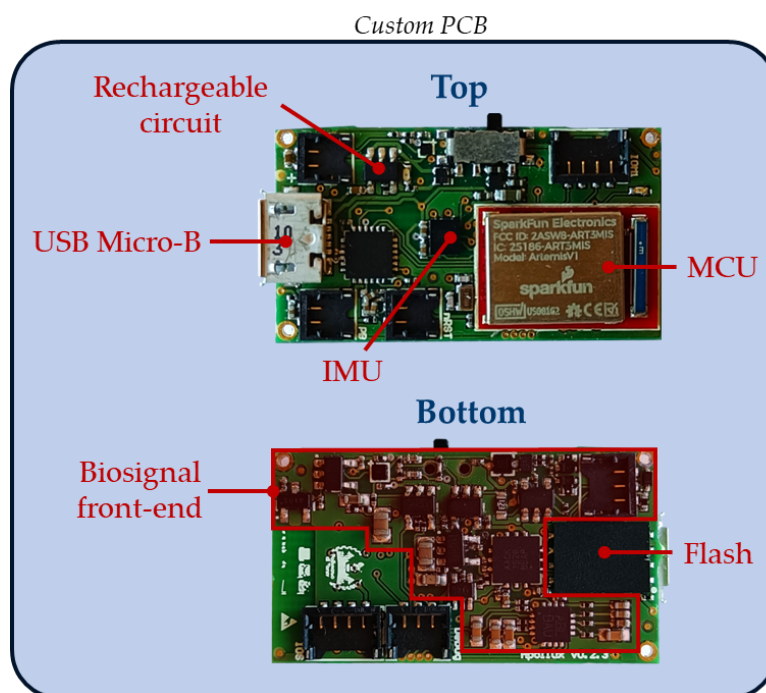


Figure 3.1: Apollux devices circuitry. In the top layer, it is possible to see the IMU sensor positioning, the Micro Controller Unit (MCU), the circuitry for the battery charge, and the USB connector. On the other side of the boards, the front-end for the sEMG detection is present as long as the flash memory.

is composed of a 3D accelerometer with ± 4 g, ± 8 g, ± 16 g and ± 32 g full-scale acceleration and a 3D gyroscope with an angular rate range of ± 125 $^{\circ}$ s $^{-1}$, ± 250 $^{\circ}$ s $^{-1}$, ± 500 $^{\circ}$ s $^{-1}$, $\pm 1,000$ $^{\circ}$ s $^{-1}$ and $\pm 2,000$ $^{\circ}$ s $^{-1}$.

The package has a dimension of 2.5 mm x 3 mm x 0.83 mm and is shown in Figure 3.2. It can operate in temperature ranges from -40 $^{\circ}$ C to 85 $^{\circ}$ C. The power consumption is low and equal to 0.55 mA; analog supply voltage ranges from 1.71 V to 3.6 V.

In Figure 3.3, there is an overview of the orientation axes for the acceleration and the Euler's angles estimated by the gyroscope. In the LSM6DSO32X, the accelerometer and gyroscope can be turned on/off independently of each other or work simultaneously. Moreover, they are allowed to have different Output Data Rate (ODR).

Apollux devices are able to send IMU data with a sampling frequency up to



Figure 3.2: Packaging of the LSM6DSO32X iNEMO inertial module [89].



(a) Orientation of the acceleration axes.

(b) Orientation of the Euler's angles.

Figure 3.3: Orientation of the acceleration axes (a) and Euler's Angles (b) given by the IMU LSM6DSO32X [89].

208 Hz, or sEMG with 1 kHz.

For this thesis project, these characteristics are essential since the sampling frequency of the kinematic data results is sufficient for respecting the Nyquist Theorem for the bandwidth of the MMG signal and the full-scale of the sensors is appropriate to the measures detected during muscle activations. In addition, the feasibility of being able to choose whether measurement to turn on makes the data transmission less computationally expensive.

3.2 Electrical Stimulator

The stimulation device used is the RehaStim2 by HASOMED® [90]; it is shown in Figure 3.4. RehaStim2 is an electrical stimulator that can produce impulses on 8 channels concurrently; the channels are divided into two electrode cables containing four stimulation channels each. It is a certified medical device (class IIa in accordance with EU regulations MDD 93/42/EWG) following the international standards EN 60601-1 and 60601-2-10 [91].

This device can be used for different tasks, including relaxation of muscle spasms, treatment against disuse atrophy, and enhancement of the range of motion and blood circulation.

RehaStim2 is a portable device with dimensions of 17 cm x 19 cm x 6 cm and weight of 0.950 kg. RehaStim2 has a maximum current output for each channel of 130 mA, and current is sent via biphasic rectangular impulses to balance electric charges. Between the negative and the positive phases, there is a fixed pause of 100 μ s to not compromise the action potential generated by the first positive pulse. The stimulation waveform is displayed in Figure 3.5.

The stimulation frequency ranges from 10 Hz to 50 Hz, while the pulse width

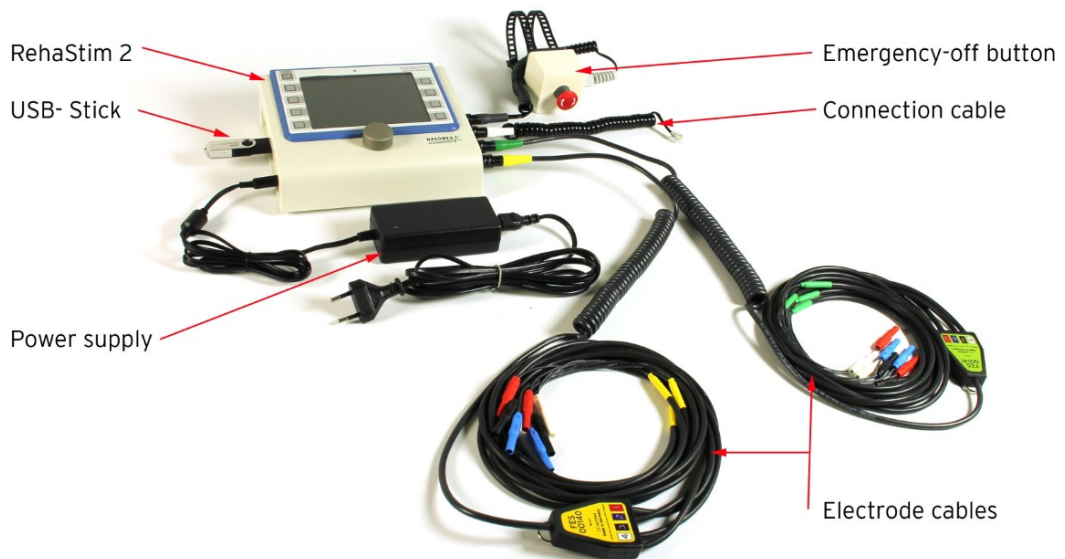


Figure 3.4: Electrical Stimulator: RehaStim2 by HASOMED® [92]. RehaStim2 has a USB port to connect to a computer, two electrode cables containing four stimulation channels each, an emergency stop button, and a power supply cable.

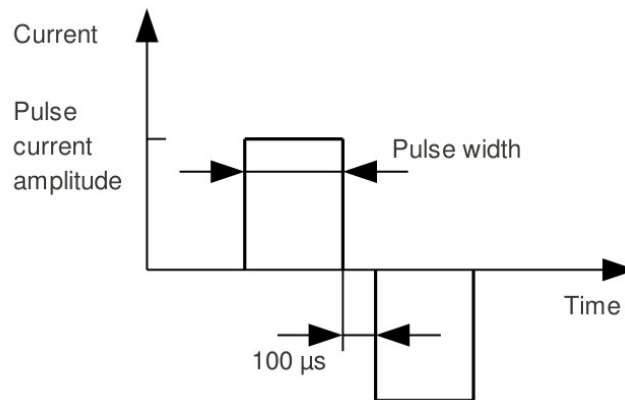


Figure 3.5: RehaStim2 biphasic pulses [93].

(duration of both positive and negative phases of the biphasic pulse) spans from $20\ \mu\text{s}$ to $500\ \mu\text{s}$ [91].

There are three ways of pulse generation available [93]:

- **Continuous Channel List Mode (CCLM):** generally used to create complex stimulation patterns. The sort of pulse that will be continuously generated for each stimulation channel must be chosen. Single, double, or triple pulses can be selected. Electrical pulses are repeatedly generated according to the main stimulation interval t_1 equal to $\frac{1}{\text{stimulation frequency}}$. Each stimulation channel has a selectable mode that can be single, double, or triplet. If the selected mode is single the biphasic pulse will be processed only once, while for the other two modes, the biphasic pulse will be sent respectively two or three times with an inter-pulse interval t_1 distance between the two pulses. An example is illustrated in Figure 3.6: Module A comprehends stimulation channels from 1 to 4, while Module B handles stimulation channels 5-8. The stimulation is stopped only when an appropriate command is sent to the stimulator.
- **One Shot Channel List Mode (OSCLM):** The channel list processing is not done repeatedly; indeed, it will be processed once the start/update command is sent. Moreover, the stimulation frequency is selectable by the user, while the inter-pulse interval is chosen by the stimulator.
- **Single Pulse:** On a single channel, the stimulator produces a single pulse.

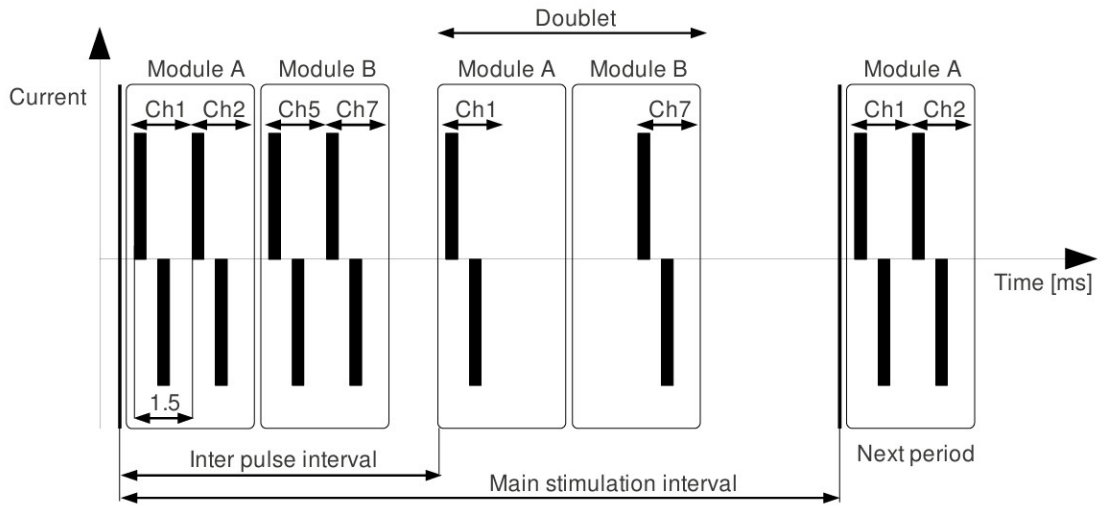


Figure 3.6: Continuous Channel List Mode (CCLM) for Electrical Stimulation [93]. Pulses are displayed by black bars; stimulation channels are 1 and 2 (Module A) and 5,7 (Module B). On channels 1 and 7, doublets are generated.

In the ATC-FES system, RehaStim2 is used in CCLM mode. The stimulator interfaces with a computer through a USB and ScienceMode2 serial communication protocol. This protocol handles the commands for all the operations that the RehaStim2 should perform, such as the initialisation of the device and the selected channels, checking the presence of possible errors during the device configuration and the stimulation (such as problems due to the cabled stimulation electrodes or the emergency stop button), and performs the disconnection of the device. During the stimulation, the sent commands regard start, update, or stop because the stimulation is performed continuously.

3.3 Closed-loop FES acquisition system

After describing the IMU sensors and the FES stimulator, the final acquisition system used in this thesis project will be explained.

The chosen biofeedbacks are two for closed-loop purposes: MechanoMyoGraphy (MMG) detected on the stimulated muscle belly and the articular angle produced during the contraction.

The data are acquired by the Apollux devices in IMU configuration described in Section 3.1. The one placed over the stimulated muscle belly acquires acceleration data, while the other one on the distal segment receives Euler's angles data.

For software development, the main movement studied is the elbow flexion. In this case, the stimulated muscle is the *biceps brachii*, and the distal segment is the forearm. Therefore, two Apollux devices are placed, one on the *biceps brachii* belly (MMG) and the other on the back of the forearm (Euler's angle). Devices are fixed on subjects using a bio-compatible tape.

Acceleration data are high-pass filtered at 5Hz. MMG is evaluated as total acceleration, defined in [94] as reported in Equation 3.1. In Chapter 4 there will be a discussion of the MMG signal in the time and frequency domain and various analyses of this signal. On the other hand, the roll angle is the one that changes the most between Euler's angle during elbow flexion.

$$ACC_{tot} = \sqrt{(ACC_X)^2 + (ACC_Y)^2 + (ACC_Z)^2} \quad (3.1)$$

The stimulation electrodes used to stimulate the *biceps brachii* have a size of 4 cm \times 6.4 cm large, as described in [95]. They are placed to guarantee the correct stimulation of the *biceps brachii*'s belly, following the directives reported in [95]. The Apollux device that acquires MMG data is placed between the two stimulation electrodes, as is illustrated in Figure 3.7.

Data acquired with Apollux devices is sent to a PC by Bluetooth Low Energy (BLE) thanks to the Nordic Semiconductors nRF52840 [96] USB dongle insert in the PC, while there is a USB connection between the RehaStim2 and the PC. IMU data and stimulation input given to the RehaSim2 are processed in Python[®] and Kivy Python framework [97] as it will be described in Section 3.5.

In Figure 3.7, there is an overview of the acquisition apparatus previously described.

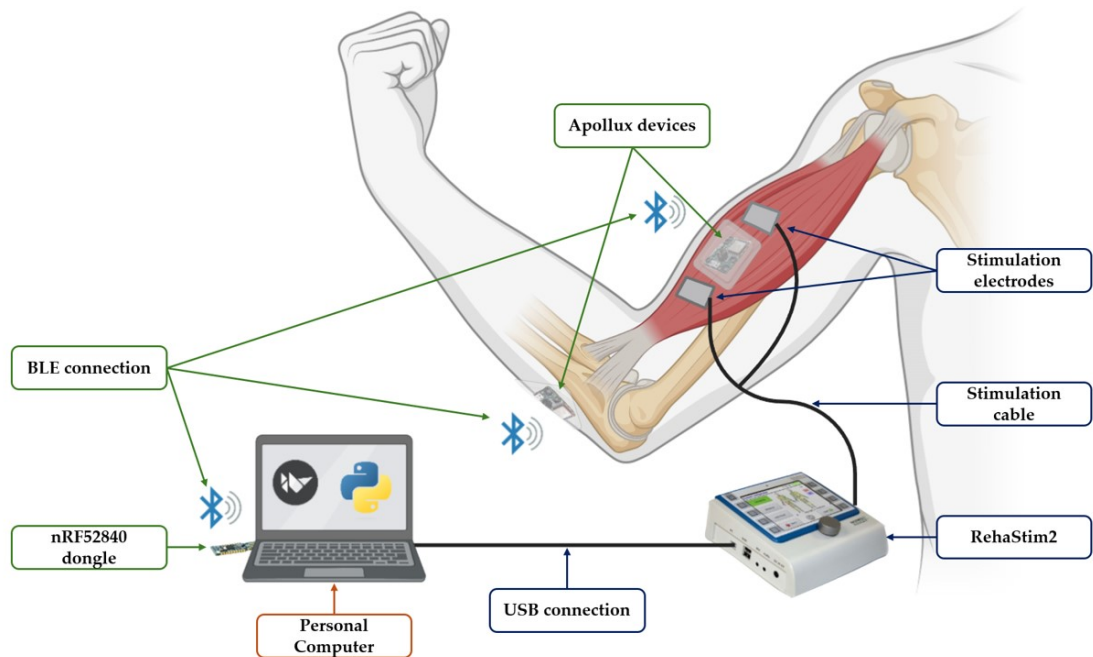


Figure 3.7: Closed-loop Functional Electrical Stimulation (FES) acquisition system: two Apollux devices are placed one over the stimulated muscle belly (in this example the *biceps brachii*), and the other on the distal segment (in this example on the back of the forearm). The former acquires MMG data, while the latter acquires Euler's angle data. They communicate via BLE to the PC, thanks to an nRF52840 USB dongle. RehaStim2 is connected by USB to the PC and by cables to the stimulation electrodes placed over the muscle skin. Data acquired and stimulation input are processed in Python and Kivy environments. Imagine adapted from [67], [98], [99], [100].

3.4 Software requirements

The starting point of this thesis project is to find a type of sensor that allows the monitoring of the muscular response to FES to create a closed-loop system.

For this reason, after choosing to use IMU devices to reach this objective, the first requirement is to have Software (SW) that can take both acceleration and Euler's angle signals from sensors.

Another requirement for the SW is to permit the user to generate the customized stimulation profile and handle the number of consecutive stimulations needed. Besides, the SW must also be able to define the time to stimulate the muscle. These are the first prerequisites required for the proper operation of Apollux and RehaStim2, the two primary components of the system, independently.

After the two parts function well apart, they must work together in a single SW or combine the two components' functions while maintaining their separation. In order to facilitate understanding of the description of the acquisition system, the SW responsible for managing Apollux will henceforth be referred to as *IMU SW* rather than the SW of the FES, *FES SW*.

Next, it is necessary to realize the closed-loop system, which can determine if there is or is not a voluntary contribution during the FES. To do this, it must understand how to discriminate a voluntary contraction from an only stimulated contraction.

To reach this goal, some first acquisitions of health subjects are done. In this phase, the IMU SW must be able to acquire only signals from Apollux devices for the voluntary case and also during the FES. Moreover, the FES SW must choose if it works alone or with IMU SW. From these first acquisitions, it was possible to establish that the standard deviation (STD) of the MMG signal during contraction can be the parameter used to discriminate voluntary from only stimulated cases. The setup and results of this first phase will be discussed in 6.

The last requirements are those related to the closed-loop system. After the STD is defined as the distinguishing parameter, it is necessary to realize a SW that links data from both SWs and supplies a response based on these data. Indeed, the Closed-Loop (CL) SW must take data from IMU SW, understand which type of contraction it is, and then communicate with FES SW to provide an output to the user and to change stimulation parameters on the basis of closed-loop analysis.

To be sure that movement and contraction done by the patient is desired, another parameter must also be used to certify that the wanted position is reached. This second control is done by monitoring the roll angle, so angle data are taken from IMU SW and then analysed from CL SW. Ultimately, stimulation parameters will be adjusted by FES SW based on CL SW's analysis.

Since the CL SW gives a response from two different analyses, it is necessary to join these two information in one only output.

3.5 Software overview

This thesis project is aimed at the development of Software (SW), which is able to self-regulate stimulation parameters based on the results of the stimulation. To achieve this, it was necessary to have a connection between the sensors used as biofeedback for the closed-loop (Apollux devices in IMU configuration, described in Section 3.1) and the electric stimulator (RehaStim2, described in Section 3.2).

However, even though the connection between the stimulation and acquisition devices has been developed through this project, both RehaStim2 and Apollux devices were already provided by the eLiONS Laboratory with their respective software. Both SWs are designed in Python[®] following the Object Oriented Programming (OOP) paradigm. In Figure 3.8, there is an overview of the starting point of the SW development:

- IMU software: it is divided into three layers. The top layer is the Graphical User Interface (GUI) coupled with the frontend built in Kivy Python framework [97]. GUI manages user interactions, visual presentation, and input handling. The middle layer is a system layer, which makes communication between the GUI and the bottom layer possible. Moreover, it contains data processing and resource management. The last layer contains the objects Apollux and BLE, which respectively manage the control of IMU sensors (Apollux) and Bluetooth Low Energy.
- FES software: it contains two layers. GUI and System layer are combined in one layer, which handles user operations, and connection with the electric stimulator. The bottom layer is the RehaStim2 object, which implements the Application Programming Interface (API) with the serial stimulator device.

The SW developed in this thesis project intended to integrate the functionality of the previous SW with the connection between the two SWs. The aim is to combine the information given by IMU devices and electrical stimulator to study the effectiveness of the stimulation and to adapt the stimulation parameters.

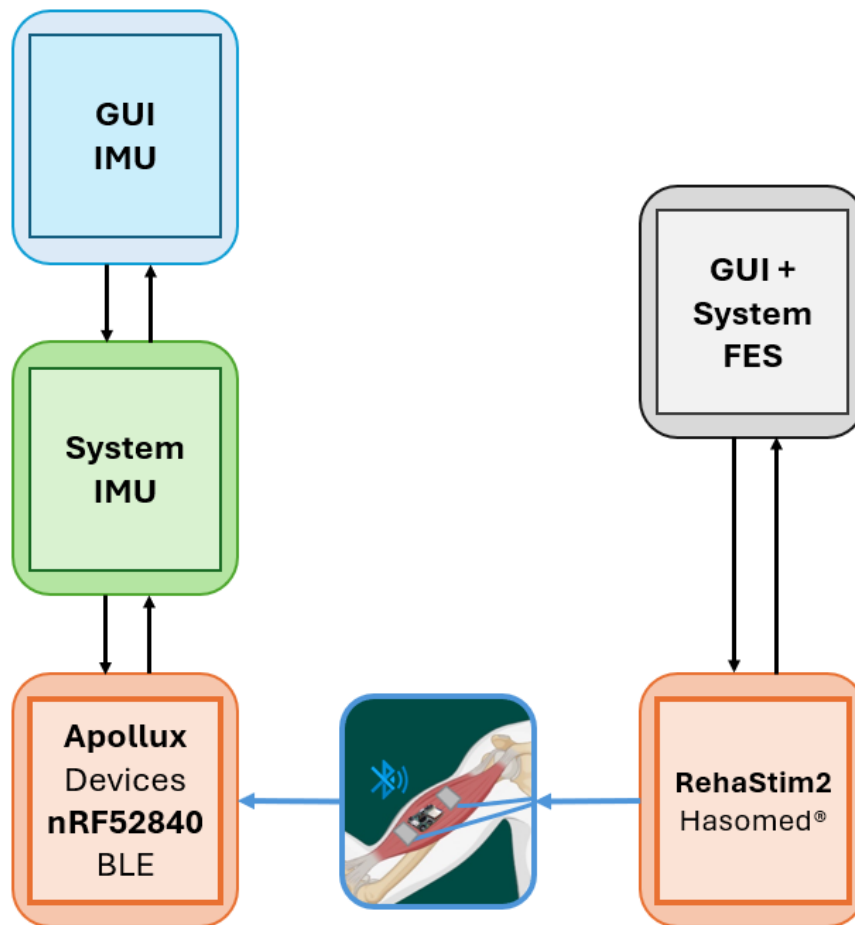


Figure 3.8: Starting Softwares Architecture.

In Figure 3.9 there is an overview of the developed softwares. It can operate in three configurations. The first configuration is the *voluntary* one, which allows the use of only Apollux devices to acquire IMU data when the FES SW is not running; the second configuration is the *stimulation* one, which allows to stimulate subject and acquire IMU data when FES SW is open but closed-loop SW is not active; the last is the *closed-loop stimulation* configuration that allows using of the closed-loop to control FES.

In particular, the final SW contains three levels:

- Top layer: The GUI layer is the one through which the user can easily interface with the IMU sensors and the FES stimulator. It presents two Kivy windows, one for the Apollux devices and one for the RehaStim2.
- Middle layer: The System layer is composed of three system objects: one for the

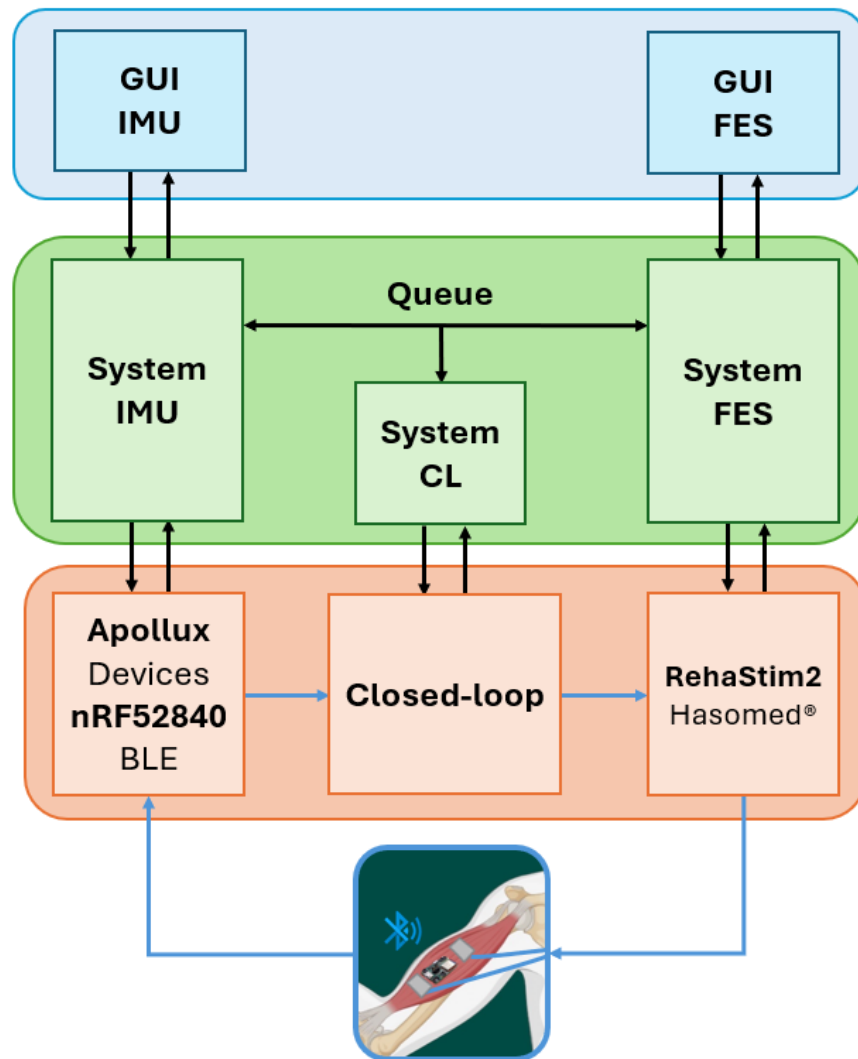


Figure 3.9: New Softwares Architecture. There are three main layers: GUI, System, and Object layer.

Apollux management, one for the RehaStim2, and the last one for the closed-loop administration. Data queues allow for asynchronous communication between the three system elements.

- Bottom layer: contains the objects that connect the hardware devices and the PC (BLE, Apollux, and RehaStim2 as seen in the previous software) and a closed-loop object that handles the operations needed to update parameters during FES.

Chapter 4

MechanoMyoGraphy (MMG) signal detected by Apollux devices

This Chapter will conduct a preliminary analysis of MechanoMyoGraphy (MMG) using acceleration data detected from Apollux devices.

Moreover, a comparison with the gold standard for muscle activations analysis, Surface ElectroMyoGraphy (sEMG), will be provided. Then, the MMG signal was analysed in terms of cross-effect between two muscles.

This Chapter ends with the analysis of the MMG during Functional Electrical Stimulation (FES).

4.1 MMG acquisition and signal processing

As anticipated during Chapter 3 in Section 3.3, MechanoMyoGraphy (MMG) signals are acquired from Apollux devices. In the case of voluntary contractions, devices are placed over the muscle belly to increase the signal amplitude. In contrast, the sensor is placed between the two stimulation electrodes as close as possible to the muscle belly for the stimulated contractions.

The accelerometer present in the Inertial Measurement Unit (IMU) of the Apollux acquires data in three dimensions (x, y, z). A sampling frequency of 104 Hz is used to sample acceleration data to ensure proper signal bandwidth and good SW performances. Indeed, in Chapter 1 Section 1.5.1, it has been said that the MMG

signal band ranges from 5 Hz to 100 Hz.

So, for the Nyquist Theorem, the ideal cut-off signal must be at least equal to two times the higher frequency in the bandwidth (at least 200 Hz). However, SW could not guarantee good performances in real-time with a sampling frequency of 208 Hz and multiple Apollux devices acquisition. Moreover, also in Chapter 1 Section 1.5.1, it has been determined that the main frequency content of the MMG signal is in the bandwidth 5 Hz to 20 Hz.

Indeed, in Figure 4.1, an experimental analysis of the Power Spectral Density (PSD) of the MMG signal of the *biceps brachii* acquired with 208 Hz sampling frequency from the Apollux devices is reported. It emerged that the main power content (frequency band from 10 Hz to 20 Hz) of the experimental data follows the bandwidth expressed in the literature.

PSD - MMG of Biceps Brachii. Sampling frequency = 208 Hz.

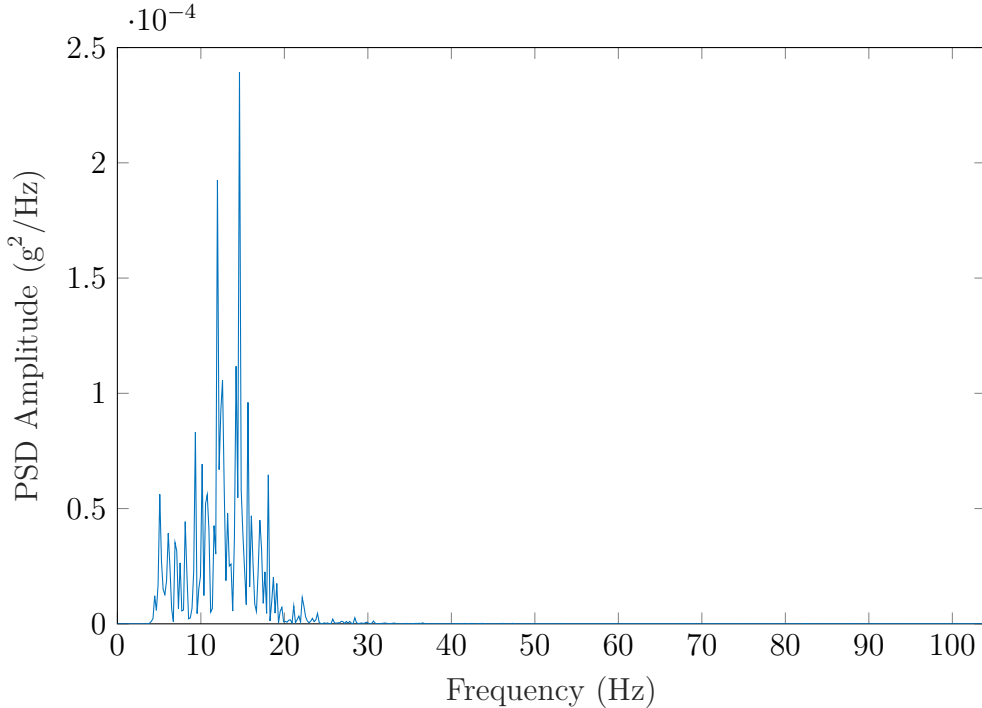


Figure 4.1: MechanoMyoGraphy (MMG) Power Spectral Density (PSD) sampled at 208 Hz. Signal is extracted from voluntary contractions at 70%MVC from *biceps brachii*.

Therefore, a signal sampling frequency of 104 Hz represents a good compromise between SW performances and the main content of the signal spectral domain.

Acceleration data are high-pass filtered with an 8th order Butterworth with a cut-off frequency of 5 Hz. The cut-off frequency is chosen thanks to directives reported in Chapter 1 Section 1.5.1, due to movement artifact reduction. The frequency response of the filter used is reported in Figure 4.2.

Frequency Response of the 8th order high-pass Butterworth Filter

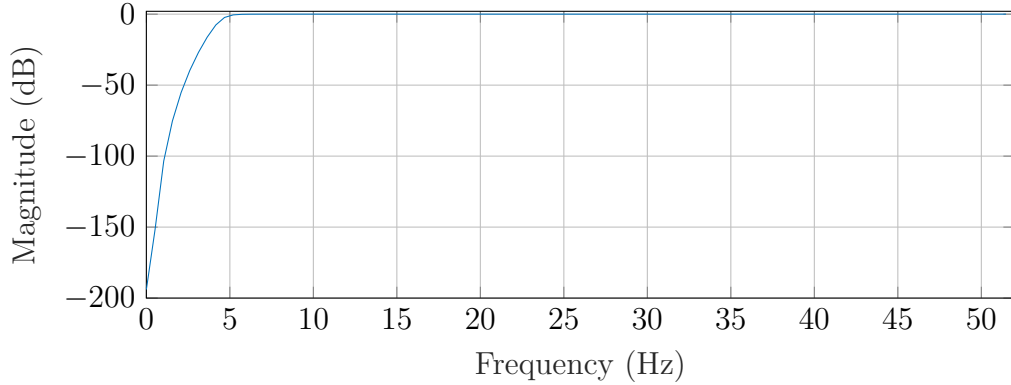


Figure 4.2: Complex frequency response of the digital filter used on MechanoMyoGraphy (MMG) signal. It represents an 8th order high-pass Butterworth filter with a cut-off frequency of 5 Hz.

The filter is applied directly on the MMG signal, which is evaluated as total acceleration defined in [94] as reported in Equation 4.1:

$$ACC_{tot} = \sqrt{(ACC_X)^2 + (ACC_Y)^2 + (ACC_Z)^2} \quad (4.1)$$

In Figure 4.3 the effect of the filter is purposed. In particular, the upper plot has the raw acquired signal from the *Biceps Brachii* during the elbow flexion of 90°. On the other hand, the lower plot has the filtered signal. It is possible to see that slow frequency oscillations, due to the movement of the arm while performing an exercise, are attenuated.

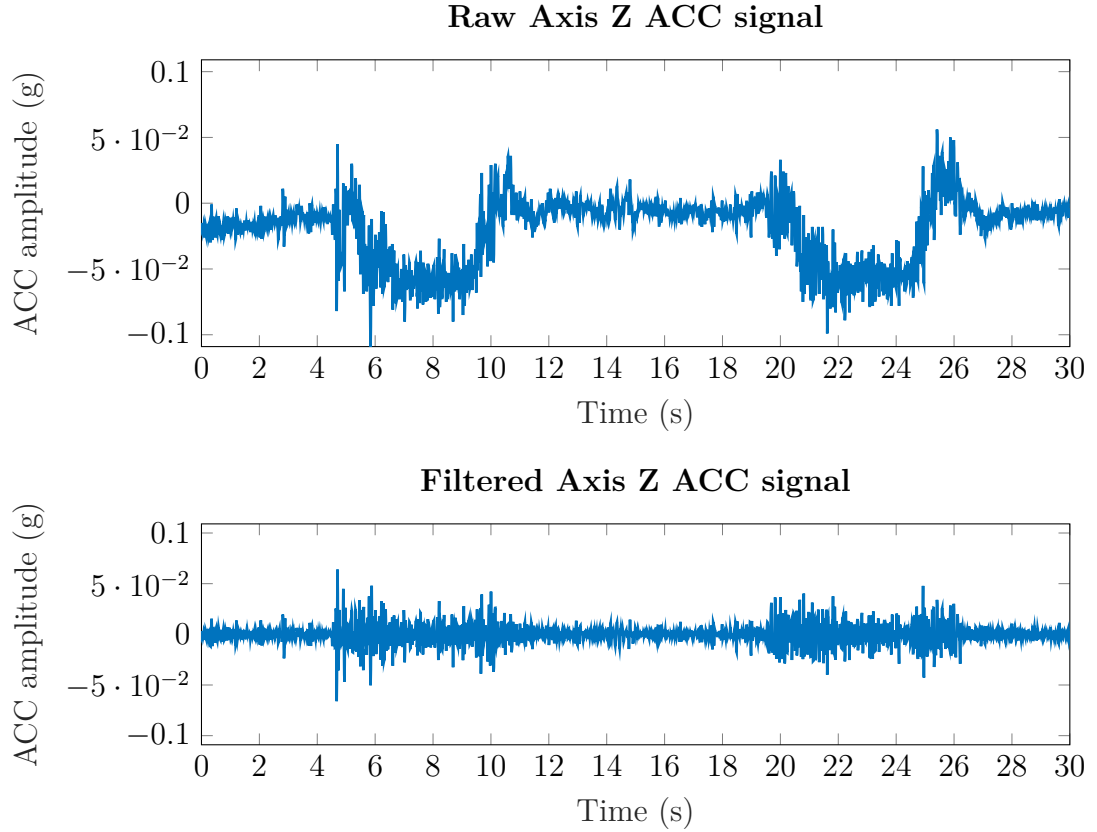


Figure 4.3: Filtering effect on MMG data. The muscle is the *Biceps Brachii*, and the movement performed is the elbow flexion of 90° .

4.2 MMG signal characteristics

Regarding the property of the MMG signal obtained with Apollux data, the differences in the time domain and in the frequency domain are exploited.

4.2.1 Time domain characteristics

As stated in the literature (Chapter 1, Section 1.5.1), the signal amplitude increases with the increase in effort. Indeed, in Figure 4.4, there is a comparison of the MMG amplitude during *biceps brachii* contractions while performing a 90° elbow flexion. In the plot, two visible contractions are observed: the first one ranges from 5 s to 11 s, while the second one ranges from 19 s to 27 s. The blue plot represents the signal amplitude during the 0% MVC contraction (motion without any effort), while the green plot represents the 70% MVC contraction.

It can be noticed that with the increase of the effort (from 0% MVC to 70% MVC), there is a visible increase in signal amplitude, measured in g.

MMG signal example, voluntary *biceps brachii* contractions.

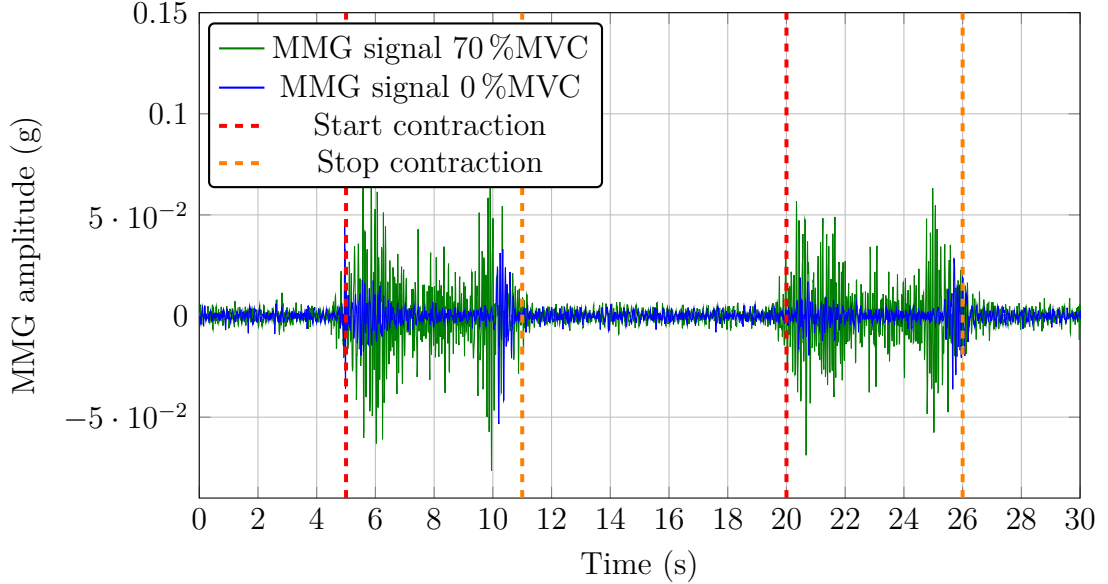


Figure 4.4: MechanoMyoGraphy (MMG) in time domain. Comparison between the MMG signal evaluated during *biceps brachii* in 2 voluntary contractions. The movement performed is 90° elbow flexion. The blue signal is performed at 0%MVC, while the green one at 70%MVC. The red dotted lines represent the instant of the start contraction, while the orange dotted one the end of the contraction.

4.2.2 Frequency domain characteristics

As reported in Section 4.1, the MMG signal is sampled at 104Hz. For the Nyquist Theorem, the upper frequency of the PSD detectable is equal to 52Hz. However, the signal bandwidth ranges till frequencies of 100 Hz, with the main power content in the range from 5 Hz to 25 Hz.

A PSD analysis has been performed in order to understand if the MMG detected with the Apollux devices was in agreement with literature studies (Chapter 1, Section 1.5.1).

In Figure 4.5, there is an example of the PSD evaluated over voluntary contractions at 70%MVC of *biceps brachii*. The signal analysed is constituted over ten repetitions of the movement. Each repetition’s MMG is concatenated with the

previous ones.

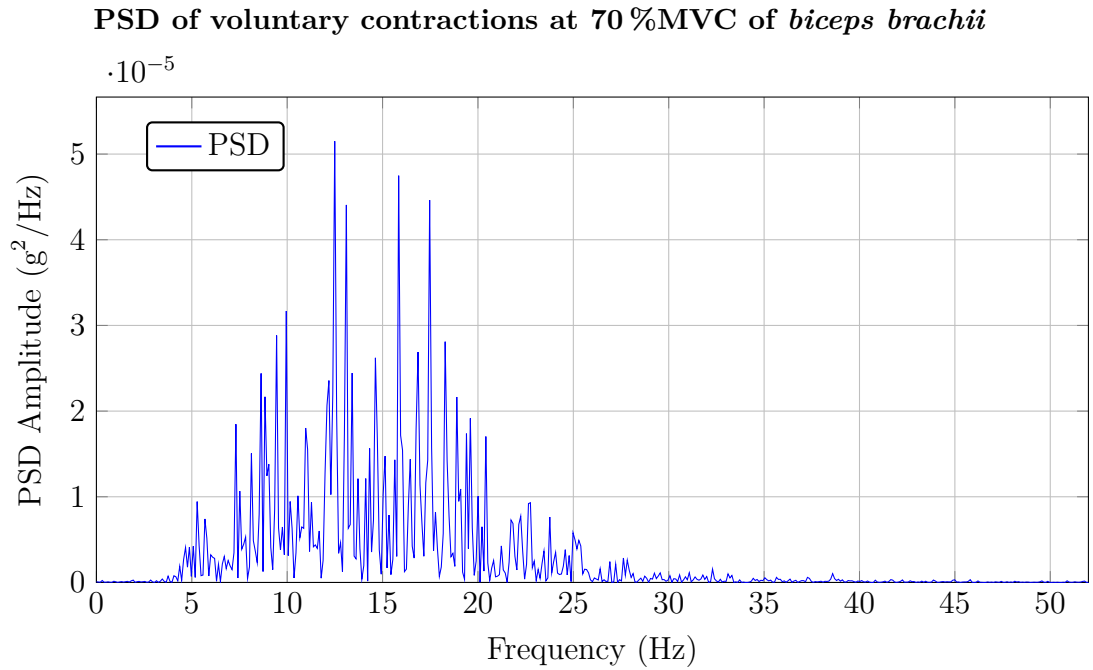


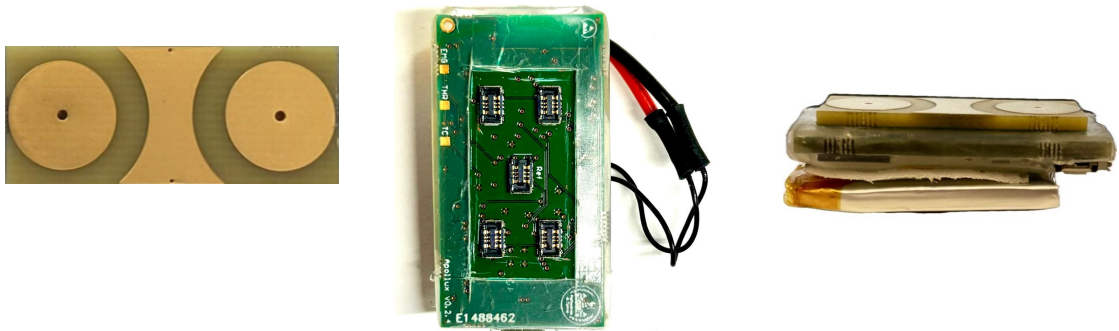
Figure 4.5: Power Spectral Density (PSD) of the MMG signal acquired from *biceps brachii*.

The results of the obtained signal confirm findings from literature studies, showing that the predominant content in the Power Spectral Density (PSD) ranges from 5 Hz to 25 Hz.

4.3 Comparing the Surface ElectroMyoGraphy (sEMG) and the MMG signals

After a primary analysis of the MMG signal, the sEMG, and the MMG signals are compared to understand if muscular activity detected from MMG is the same as that from the sEMG.

The sEMG signal is acquired with an Apollux device. Indeed, F. Rossi and his research team use the Apollux device with some gold-plated electrodes to acquire sEMG signals. In particular, this type of configuration was tested by L. Cantore in her master thesis project [101]. These types of electrodes are applied on the back of the Apollux device; in [101], L. Cantore tested different configurations of electrodes, and based on results obtained for this thesis project, the circle configuration with InterElectrode Distance (IED) equal to 2.0 cm it was chosen. Figure 4.6 illustrates the type of electrode used during the preliminary test to compare sEMG and MMG signals (Figure 4.6a), the back of the Apollux device where there are pins to connect electrodes (Figure 4.6b), and the complete device that includes the battery, Apollux device, and gold electrodes (Figure 4.6c).



(a) Circular configuration of gold-plated electrodes with InterElectrode Distance (IED) of 2.0 cm

(b) Bottom view of Apollux device, pin to connect electrode are represented in this image.

(c) Overall view of Apollux device connected to the electrode.

Figure 4.6: Surface ElectroMyoGraphy (sEMG) Electrode: in figure (a) gold electrodes are illustrated; in figure (b) bottom view of Apollux device is illustrated; in figure (c) profile view of Apollux device connected to gold-plated electrodes is illustrated.

4.3.1 sEMG and MMG processing operation

The first processing operations are done only for the MMG signal. MMG signals are filtered with a high-pass filter with a cut frequency equal to 5 Hz, then the MMG signals are oversampled through a resample from 104 Hz (sample frequency of IMU) to 1 kHz (sample frequency of sEMG). Processing sEMG signals extracted from Apollux devices is unnecessary before comparing them with MMG signals. After both signals have the same sampling frequency, it is possible to realign them. After the two signals are realigned, to compare the signals to understand if they are detecting the same activations, they are rectified separately, and then the envelopes are extracted filtering using a 5 Hz low-pass filter.

4.3.2 Results of comparing the sEMG and the MMG signals

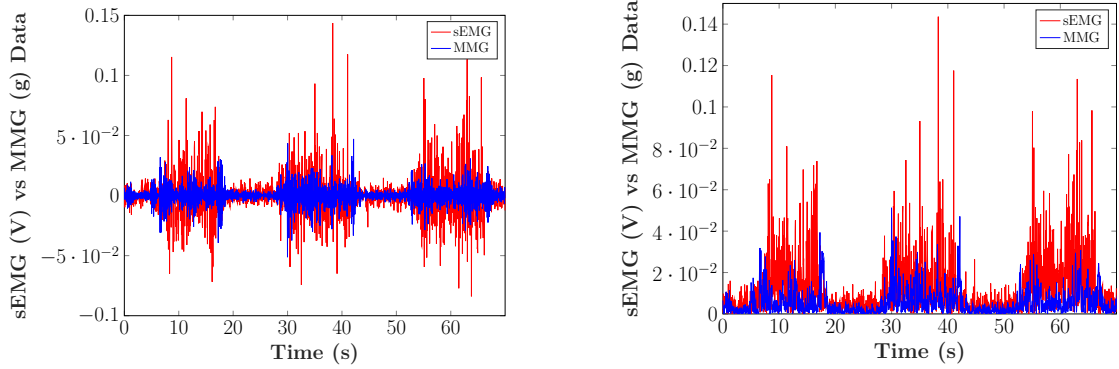
By comparing the data from the sEMG and MMG, the mechanomyography technique can be used to identify the mechanical vibrations of the muscle and classify them as muscle contractions. It is evident from both the realignment and envelopes analyses that the two signal types detect identical activations.

An *elbow flexion* acquisition compares the MMG and sEMG signals, as shown in Figure 4.7. The subject has to perform three contractions in this acquisition: first, he stretched his arm fully in the rest position and then raised his forearm until the angle produced by his arm and forearm equaled 90°. During this exercise the subject use a weight equal to the 70% of his MVC.

It is feasible to compare the two signals following the realignment operation, realigned data are shown in Figure 4.7a. The rectified signals are depicted in Figure 4.7b, while the signal envelopes are compared in Figure 4.7c.

Because sEMG envelope data are used in the literature to detect muscle activations, it was decided to validate MMG signals to identify muscular contraction by comparing sEMG and MMG envelopes.

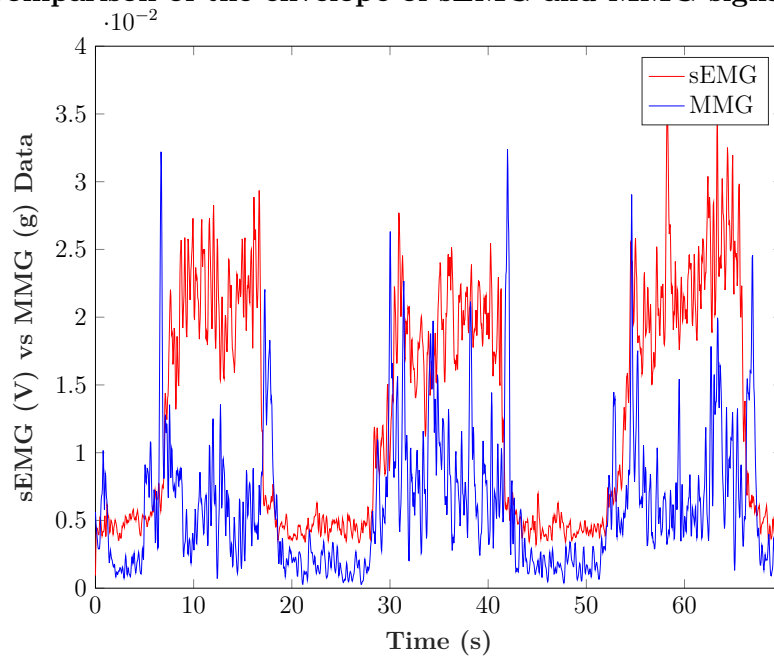
Comparison of Surface ElectroMyoGraphy (sEMG) and MechanoMyoGraphy (MMG) signals



(a) sEMG and MMG Data Realigned

(b) sEMG and MMG Data Rectified

Comparison of the envelope of sEMG and MMG signals



(c) Envelope of sEMG and MMG Data

Figure 4.7: Comparison of Surface ElectroMyoGraphy (sEMG) and MechanoMyoGraphy (MMG) signals acquired from *biceps brachii*. These signals are acquired during an *elbow flexion* using a weight equals to the 70% of the MVC.

4.4 MMG cross-effect

Another aspect of the analysed MMG signal concerns the cross-effect when evaluating the interference caused by the activity of multiple muscles during complex exercises. Specifically, the cross-effect between the *biceps brachii*, *upper trapezius*, and *deltoid medius* was investigated during exercises that provide a synergic movement. This comparison was made with respect to the actual activations observed in the sEMG signal.

Different exercises were performed to determine whether cross-effect exists in the MMG signal and if it can be mitigated through signal processing however, this discussion will be focused on the following:

- **Exercise 1:** The subject stands with the arm resting on the hip and the weight positioned on a support. After 10 s in this position, the subject lifts the weight until the elbow reaches a 90° angle relative to the floor, holding this position for 10 s. An example is reported in Figure 4.8.
- **Exercise 2:** Starting from the resting position with the arm hanging vertically, the subject abducts the shoulder with the arm straight until it reaches a 90° angle (ascent phase). The position is held for 10 s, followed by returning to the resting position (descent phase) for another 10 s. An example is reported in Figure 4.9.

All exercises are repeated 5 times, alternating 10 s of rest and 10 s of contraction.

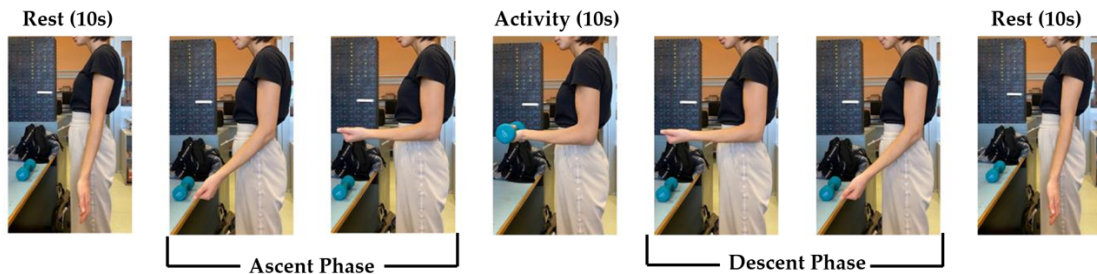


Figure 4.8: Exercise 1: elbow flexion.

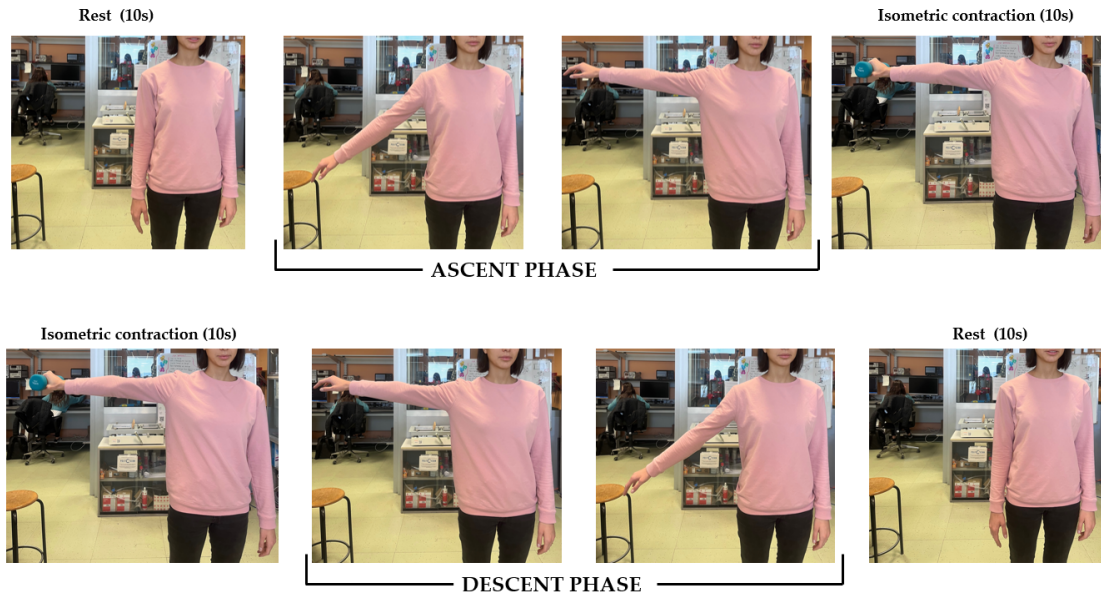


Figure 4.9: Exercise 1: shoulder abduction.

4.4.1 Cross-effect between *biceps brachii*, and *deltoid medius*

Firstly, there will be an analysis of the cross-effect between *biceps brachii* and *deltoid medius*. It is important to note that the gold standard technique (sEMG) is also affected by cross-effect induced by the proximity of the electrodes or volume conduction through the skin.

However, the sEMG and MMG spectrum are analysed during exercises n. 1 (in which the main activations should be present over the *biceps brachii*) and n.2 (movement is mainly performed by *deltoid medius*).

In Figure 4.10, there is a comparison of the Power Spectral Density (PSD) evaluated over the two muscles during exercise 1. The upper plot represents the PSD evaluated over signals detected from the MMG sensors, while the lower plot shows the sEMG signals. As can be seen, in the sEMG signal, both muscles exhibit the highest PSD intensity in the same frequency band from 30 Hz to 200 Hz; however, the PSD amplitude of the *biceps brachii* is much higher than that of the *deltoid medius*, as it is anticipated. Although it is impossible to determine whether the activations found in the *deltoid medius* are due to cross-effect or co-activations, these signals are considered in this project as the reference.

Conversely, by examining the MMG signals, a different behavior can be observed. Both muscles present similar peaks at approximately 12 Hz and 15 Hz; furthermore,

the PSD amplitude is comparable between the two signals. Thus, a cross-effect in the MMG signals can be noticed between the *biceps brachii* and *deltoid medius*. Additionally, since both MMG spectra present peaks in the MMG signal bandwidth (5 Hz to 25 Hz), this cross-effect cannot be removed by filtering.

On the other hand, during exercise 2, the cross-effect is even more accentuated. Indeed, in Figure 4.11, the same comparison is present.

As it can be seen, the *biceps brachii* activity in the sEMG is really low, while the *deltoid medius* power content is much higher. In contrast, from the MMG signals of the two muscles, it is possible to notice that the opposite behavior is found. This can be expressed as cross-effect induced by the oscillation found on the overall arm when the activity position is reached. Indeed, the shoulder is abducted till 90° with respect to the vertical line. Since the activity position is kept for 10 s, a fatigue effect due to the arm's weight (and the % of the MVC lifted) induces physiological oscillations of the segment. Even though the *biceps brachii* is not working, those fluctuations of the arm are detectable through the MMG signal and are present in the MMG bandwidth.

PSD comparison between MMG and sEMG: ex.1 70%MVC

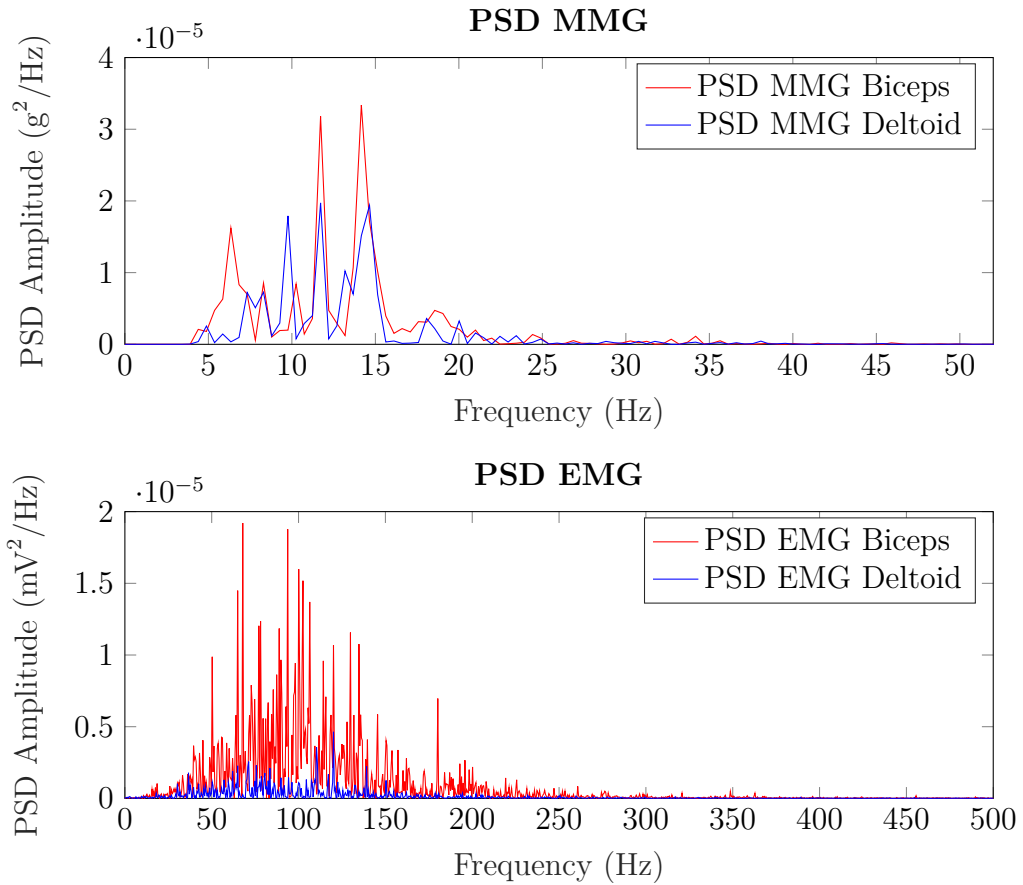


Figure 4.10: Power Spectral Density (PSD) comparison of Surface ElectroMyoGraphy (sEMG) and MechanoMyoGraphy (MMG) signals acquired from *biceps brachii* and *deltoid medius*. The exercise performed is n.1: lifting the 70% MVC from a vertical position of the arm to 90° with respect to the vertical line.

PSD comparison between MMG and sEMG: ex.2 70%MVC

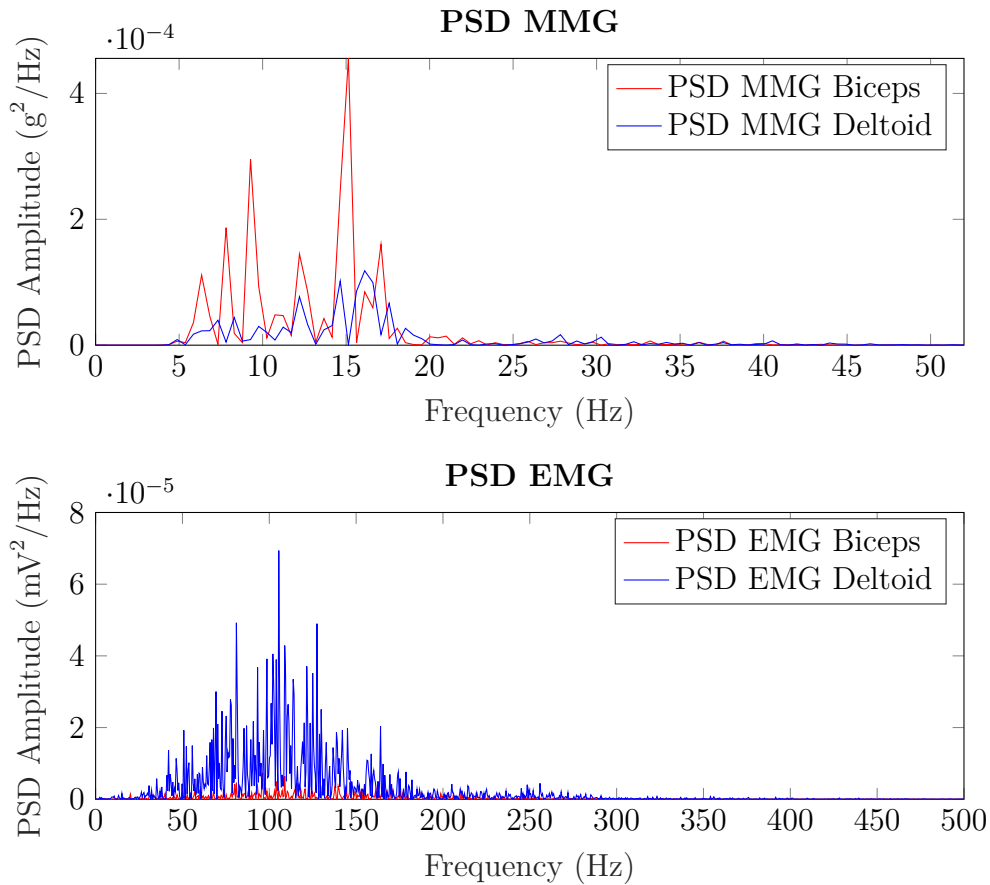


Figure 4.11: Power Spectral Density (PSD) comparison of Surface ElectroMyoGraphy (sEMG) and MechanoMyoGraphy (MMG) signals acquired from *biceps brachii* and *deltoid medius*. The exercise is n.2: the subject abducts the shoulder (while lifting the 70% MVC) with the arm straight until it reaches a 90° in respect to the vertical line.

4.4.2 Cross-effect between *biceps brachii*, and *upper trapezius*

Moreover, to understand better the effect of the cross-effect induced by the arm swinging during the contraction phase, the same exercises are performed with the signal detected from *biceps brachii* and *upper trapezius*.

In addition, the objective in this phase is to test if this cross-effect induced by the overall arm oscillation is present in a lower frequency band (from 0 Hz to 5 Hz), so the signals are filtered with a 0.1 Hz high-pass filter.

It is expected a higher work (so PSD amplitude) of the *biceps brachii* during exercise n.1, while during exercise n.2 the *upper trapezius* should present a higher amplitude.

In Figure 4.12, there is the comparison between the PSD evaluated over the *biceps brachii*, and *upper trapezius* with the MMG and sEMG signals during exercise n.1. It can be seen from the sEMG that both muscles are working, indeed the MMG signal confirms so. A slightly enhanced activity can be found in the *biceps brachii*.

However, in exercise n.1, this cross-effect is absent since the arm's position does not oscillate. When evaluating the same results over exercise n.2 (Figure 4.13), it is possible to see that even though the *upper trapezius* muscle is working more (from the sEMG PSD), in the MMG signal a higher content is present in the *biceps brachii* power. This confirms the results obtained in the comparison of the *biceps brachii* and *deltoid medius*.

Moreover, it is impossible to have some consideration about the 0 Hz to 5 Hz PSD band because all signals present a great impact on the PSD amplitude during this frequency range.

To conclude, this analysis was conducted on two subjects who exhibited the same cross-effect behavior induced by arm oscillation when placed in an abducted position relative to the body. This cross-effect cannot be eliminated by any filtering techniques because the artifact bandwidth coincides with that of the MMG signal.

However, the hypothesis proposed is that this effect does not significantly impact the results when using the MMG signal during FES for a closed-loop system. This is because, during the closed-loop analysis purposed in this thesis, to understand the effectiveness of a certain intensity of injected energy, two measurements are made: the MMG from the stimulated muscle (proximal segment) and the angle data from the distal segment. The combination of the two outputs made a conclusion of

the effect on the patient. This means that we are conscious of the MMG and angle results that should be obtained, and only if both measurements provide the desired result the stimulation results be efficient. Moreover, when we are stimulating only one muscle, we can consider that the activations detected belong only to that specific muscle. So, this cross-effect has been neglected through the following phases of the study, otherwise if the MMG increase is due to synergic muscles, the angle data will provide an output that is discordant with the desired one.

PSD comparison between MMG and sEMG: ex.1 30%MVC

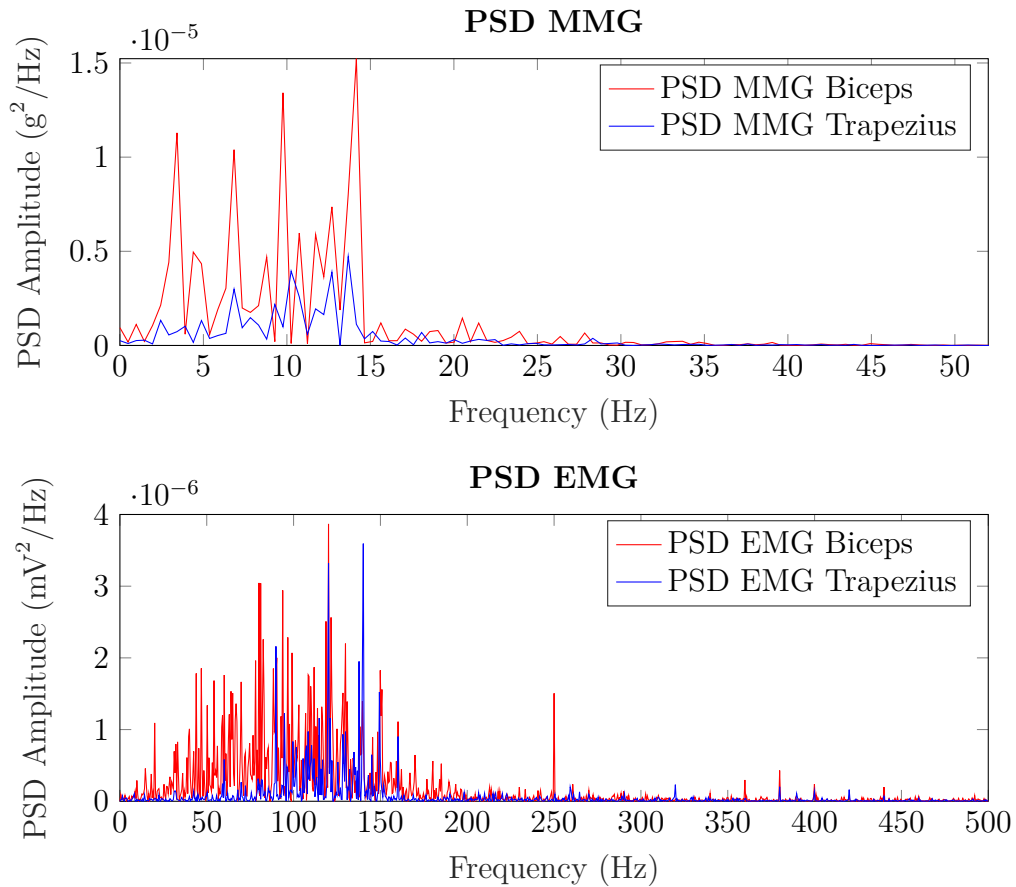


Figure 4.12: Power Spectral Density (PSD) comparison of Surface ElectroMyoGraphy (sEMG) and MechanoMyoGraphy(MMG) signals acquired from *biceps brachii* and *upper trapezius*. The exercise performed is n.1: lifting the 30% MVC from a vertical position of the arm to 90° with respect to the vertical line.

PSD comparison between MMG and sEMG: ex.2 30%MVC

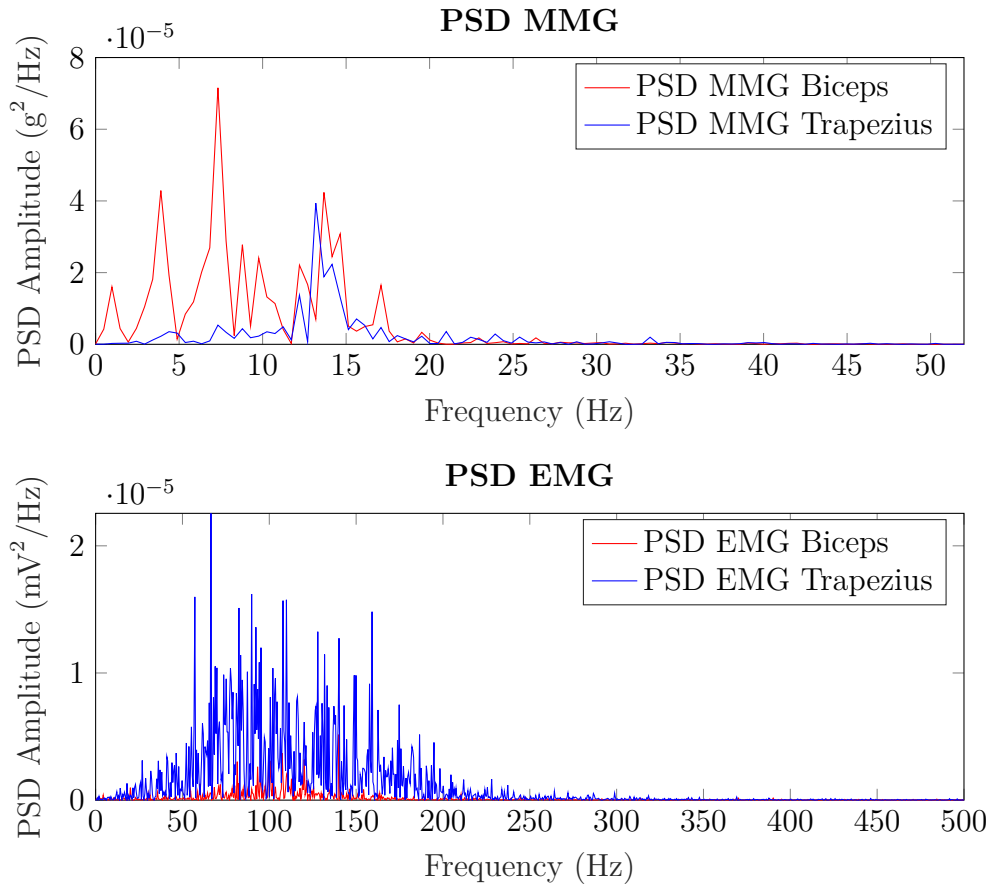


Figure 4.13: Power Spectral Density (PSD) comparison of Surface ElectroMyoGraphy (sEMG) and MechanoMyoGraphy (MMG) signals acquired from *biceps brachii* and *upper trapezius*. The exercise is n.2: the subject abducts the shoulder (while lifting the 30% MVC) with the arm straight until it reaches a 90° in respect to the vertical line.

4.5 MMG during stimulated contractions

The last step of the MMG signal analysis tends toward the feasibility of using this technique to investigate FES-induced contraction. As said in Chapter 2 during Section 2.2.1, the gold standard for the evaluation of muscle activity (sEMG) is highly affected by electrical interference that is difficult to remove. So, considering the disadvantages of the MMG signal described in Section 4.4, the aim is to test how this signal reacts during FES contractions.

So, the MMG signal has been tested over four muscle groups (*biceps brachii*, *triceps brachii*, *flexor ulnaris*, and *extensor ulnaris*) during voluntary and stimulated contractions.

Moreover, the MMG acquisition was performed on over nine subjects to compare the differences in terms of PSD between voluntary and stimulated contractions. Stimulation is given with a stimulation frequency of 40 Hz in triplet mode (so three pulses with 8 ms distance between each other will be injected every 25 ms), and the injected current is subject-specific and is the one that produces the full movement over the subject.

A detailed description of the muscles and the number of subjects considered is presented in Table 4.1.

Figure 4.14 shows the median frequency over the MMG acquisitions results. From the data obtained, it is possible to see that even when considering different genders, body sizes, currents, and muscles, the results are comparable regarding spectrum distribution. That suggests that the MMG measurement is a robust method that can be used to monitor muscle activity while performing either voluntary or FES contractions.

In addition, the MMG signal does not significantly modify its PSD while considering voluntary and stimulated contractions. So the MMG detects the stimulated contractions, without suffering a lot of the electric interference as happens in the surface ElectroMyoGraphy (sEMG) (Chapter 2, Section 2.2.1). So, the MMG signal can be used in a closed-loop system for the evaluation of the muscle activations.

Table 4.1: Table of muscle and number of subjects for the MechanoMyoGraphy (MMG) evaluation: those subjects and those muscles are used to evaluate boxplot in Figure 4.5. For each measurement, ten repetitions are considered.

Muscle	N. Subjects	N. Females	N. Males
Biceps Brachii	9	6	3
Triceps Brachii	8	5	3
Flexor Ulnaris	3	2	1
Extensor Ulnaris	3	2	1

MMG PSD fmed during voluntary and stimulated contractions

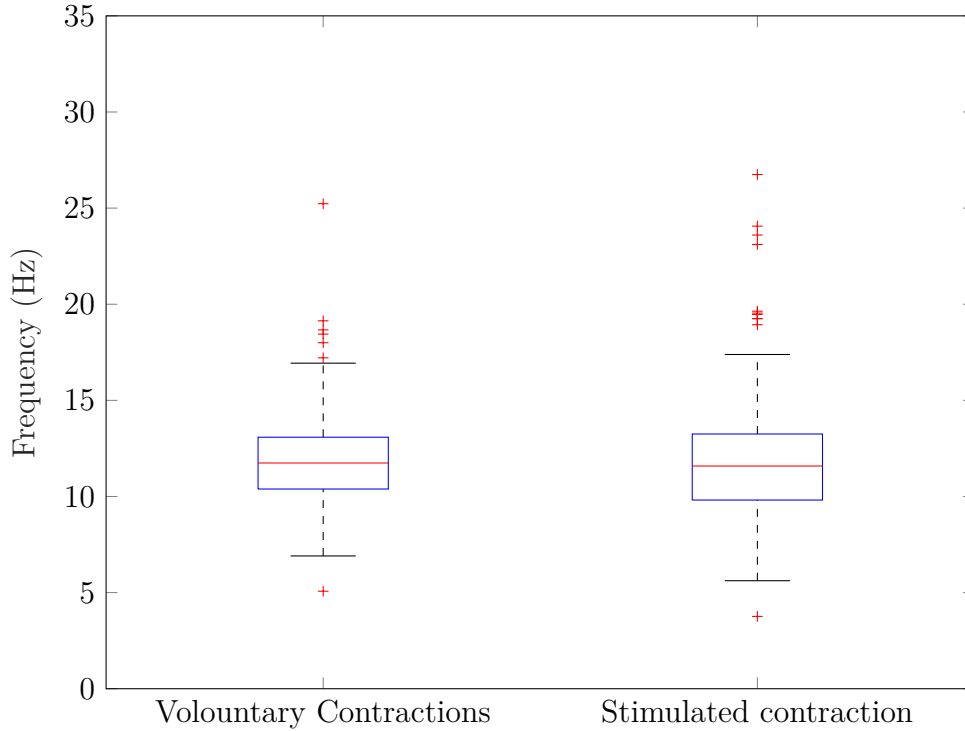


Figure 4.14: Median frequency (fmed) of the MechanoMyoGraphy (MMG) signal acquired from 4 muscle groups (*biceps brachii*, *triceps brachii*, *flexor ulnaris*, and *extensor ulnaris*). Results are evaluated over subjects expressed in Table 4.1. For each acquisition, ten repetitions are considered.

Chapter 5

Software enhancement

In this chapter, there will be an explanation of the Software (SW) enhancement discussed in Chapter 3 Section 3.5. This discussion will focus on the changes to the FES SW and the IMU SW. For both SWs, a comparison of the old and new Graphical User Interface (GUI) will be done.

The SW upgrades aim to put this thesis project into practice. The goal is to simultaneously obtain data from the IMU on the Apollux devices while the subject is undergoing functional electrical stimulation. Furthermore, closed-loop control and management will be implemented in the project's subsequent phase.

Specifically, the entire developed SW seeks to obtain the Euler's angle from the distal segment and the MMG from a single Apollux on the muscle to be stimulated. For example, the back of the forearm is the *distal segment* if the stimulated muscle is the *biceps brachii* during the *elbow flexion*. The acquisition system is the same as that which is outlined in Section 3.3 of Chapter 3 and shown in Figure 3.7.

Figure 5.1 illustrates the SW's block diagram that reports all the modifications explained in this chapter to obtain an open-loop system and show the experimental set-up realized for using the SW.

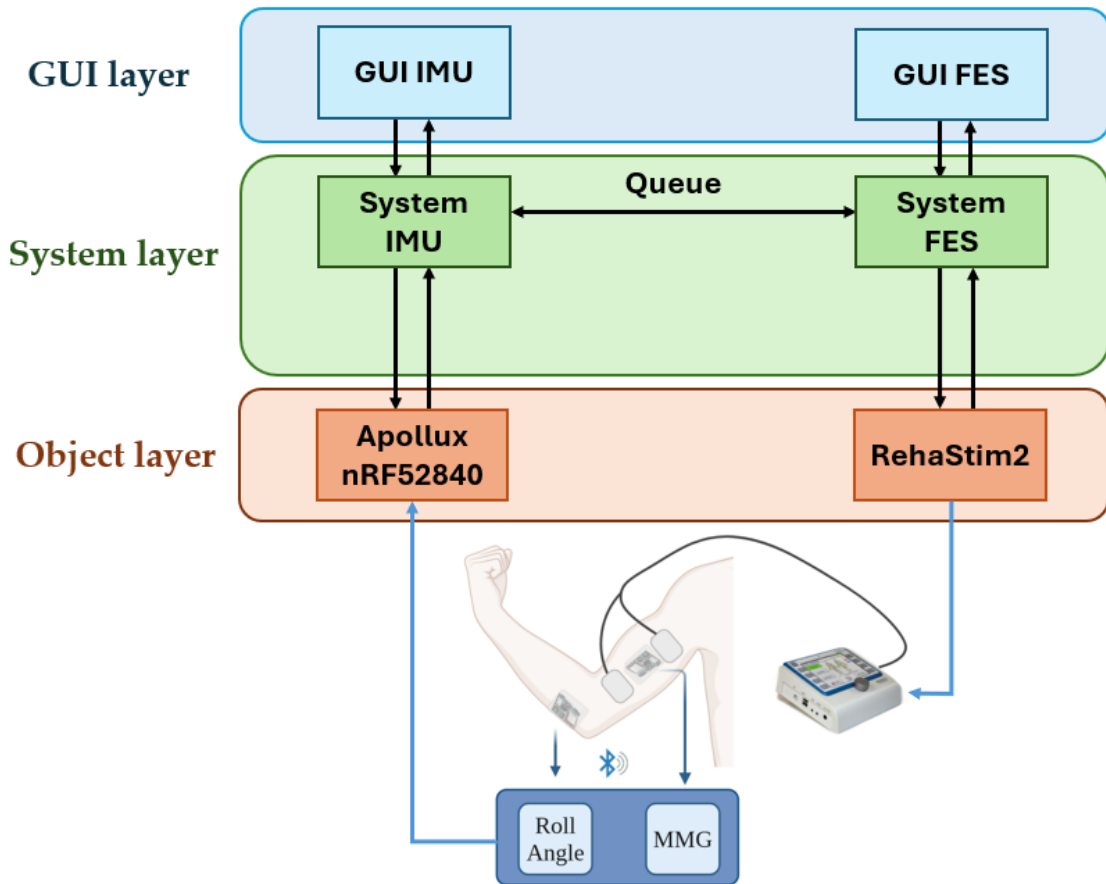


Figure 5.1: Block Diagram of developed software used to realize an open-loop system using Apollux devices and functional electrical stimulation. The figure illustrates the enhancement done on the SW, which will be explained in this chapter, and shows the experimental setup for these modifications. In the experimental set-up are illustrated the two Apollux devices located one on the *biceps brachii* and the other on the *distal segment* (the back of the forearm), from the first MMG data are acquired and from the second Roll angle data. Figure shows also the RehaStim2 stimulator and the relative electrodes positioned on the belly of the *biceps brachii*.

5.1 Software connection

Firstly, it is necessary to underline the aim of the realized closed-loop system. Indeed, the closed-loop should combine the data from the Apollux device and the stimulator in order to give an output of the results of the injected energy on the patient.

To do so, the synchronous activity of the Inertial Measurement Unit (IMU) sensors (contained in the Apollux devices, described in Section 3.1) and the RehaStim2 stimulator (Section 3.2) is necessary.

As mentioned in Chapter 3 Section 3.5, two SWs were already provided: the 'IMU SW' manages the connection between the PC and the Apollux devices, while the 'FES SW' handles the stimulation inputs sent from the PC to the device using the ScienceMode2 protocol. Nevertheless, there was no communication between the two SWs, and they could not exchange any information. In order to work in real-time, the first requirement to satisfy is to synchronize the two SWs.

5.1.1 Software communication by queue

The first step in SW development was to create a form of communication between the two SWs. The SWs are designed in Python[®] with the Object Oriented Programming (OOP) model. The dialogue between them has been achieved through multiprocessing with *multiprocessing* module that allows the creation of multiple processes and leverages multiprocessing to perform concurrent and parallel tasks [102].

In particular, the parent process is the IMU SW, which is run by the *Process* object and then calls its `start()` method (parent process). After the IMU (GUI) initialization, a checkbox is present with the label 'FES', and when it is active, the IMU SW runs `spawn start()` method by beginning a fresh Python interpreter for the FES SW (that will be a child process).

However, the *multiprocessing* does not allow the child process to inherit the attributes or the operational state of its parent process. Thus, a queue connection has been created for the information exchange between the SWs. This queue is created via `multiprocessing.Queue`, it is a data structure that manages a collection of elements in a specific order.

As shown in Figure 5.1, the queue is the SW connection between the two SWs and is used to exchange information and messages.

It has especially been used to exchange messages regarding the SW state. Indeed, the queue created a link between the layer System of the IMU SW and the layer System of FES SW (Figure 3.9). Every time an operational state changes in one SW (that would require another alteration in the other SW), a message is sent from one SW to the other. Nevertheless, queues are an asynchronous way of communication since one SW adds an element to the queue, but the other SW does not know when a new element has to be removed from the queue.

To create a sort of synchronous relationship between the SW, a thread is added on each SW to control the presence of new messages in the queue. In particular, it checks every 0.01 s if the queue is empty; if it is not, it checks if the receiver of the message is itself. Each message corresponds to a specific command that a SW should execute to match its operational state to that of the other SW.

The message is sent using the command:

```
self.appIntercommunicationQueue.put(([0], [1], ..., [-1]))
```

So the message is structured in this way: in the position [0], there is the sender; in the position [1], the text of the message; in the position [-1], the receiver. Between the text of the message and the receiver, adding some attributes to send with the message is possible. The message is read using the command:

```
self.appIntercommunicationQueue.get()
```

Followed by:

- sender = message[0]
- receiver = message[-1]
- text = message[1]

For example, when the 'Start' button on the IMU GUI is pressed, the layer `System IMU` sends to the layer `System FES` a message: *IMU start acquisition*. So, the FES stimulation also starts, and the two SWs work simultaneously. This message will be sent with this command:

```
self.appIntercommunicationQueue.put((self.myName, "IMU start acquisition", "System FES"))
```

Instead, an example of a message sent from the layer `System FES` to the layer `System IMU` is: *FES repetition number*. This message is sent each time a new repetition starts on the FES SW. This message will be sent with this command:

```
self.appIntercommunicationQueue.put((self.myName, "FES repetition number", self.dictRepetition, "System IMU"))
```

`self.dictRepetition` contains information about the number of current repetition, and the time in which the repetition starts.

5.1.2 Data synchronisation

A fundamental step in developing the closed-loop software was matching the IMU samples with the injected current at the exact time they were recorded. Since IMU and FES SWs are run by *multiprocessing*, they are executed in two different processes. In this way, the Central Processing Unit (CPU) processing times are different between them.

The IMU data is received from Apollux devices by BLE connection (thanks to an nRF52840 USB dongle) in a packet of 10 samples each. Each packet is unpacked by the IMU SW in a dictionary containing the sensor's information for each sample. This information comprises the packet number (ranging from 0 to 255), the sensed measure (could either be the acceleration data in the three dimensions or the three Euler's angles), and the acquisition time (timestamp of the sensed values). On the other hand, the FES SW controls the value of the current to inject every 100 ms.

Another important aspect that should be considered when linking this information is related to the fact that the FES SW gives real-time information on the current that is injected. Indeed, every time a packet is received, the acquired value refers to a past-time that can be shorter or longer due to various factors, such as BLE communication time, SW performances in data processing, or distance between the Apollux device and the Bluetooth dongle.

To solve this, a time comparison between the event occurrence of the FES and the time samples of the IMU data is performed in real-time. Specifically, the FES events that can occur are:

1. The start of a new FES repetition;
2. Every time there is a variation in the injected current value.

Moreover, to account for the presence of different processing times between the SWs, the time is evaluated with the `time.time()` Python function, that evaluates the number of seconds that have passed since a fixed point in time (January 1, 1970, 00:00:00 (UTC)). This value measures real-time as perceived by the operating system and hardware rather than just the CPU process time. When running multiple processes or threads concurrently on a computer, their execution times can overlap and be interleaved by the operating system. Consequently, it is necessary to measure the actual wall-clock time that has passed, regardless of how the operating system schedules the processes. So, evaluating the time that has passed between two points in two different processes is possible by calculating the

difference between the two-time values acquired with `time.time()` Python function.

In addition, another possible source of delay is related to the queue communication between the SWs. Indeed, as said in Section 5.1.1, each SW has its own thread that interrogates the presence of a new message every 10 ms. However, this time can be prolonged due to various factors, such as the process running a specific function/attribute or higher CPU latency.

So, a time synchronization protocol has been developed to address these issues comprehensively and has been enhanced to reduce the required processing time of the software. In particular, each SW records a time of an event occurrence with `time.time()` Python function, and exchanges a message by queue that contains both the event information and the evaluated time. Finally, when evaluating the current injected when a specific IMU data was acquired, the following processing path is shown in Figure 5.2. The start time of the acquisition is evaluated by the IMU SW and passed by queue to the FES SW, which saves this information and keeps running its process. Once an FES event happens, the occurrence time is evaluated as the difference between the start time of the acquisition and the present time. A message is sent to IMU SW containing the FES event information (i.e., an update in the current value) and the timing instance. So, the IMU SW will save this information in a structure that contains all the events that arise and their happening time.

At last, when the IMU SW is processing a data sample, it compares the time of the samples (contained in the information sent from the Apollux devices to the SW) with the list of the timing of FES events and evaluates the injected current as the one that was injected at the moment the sample was acquired. Indeed, this protocol functions thanks to the fact that every IMU sample refers to a past-time. Thus, once it is processed by the IMU SW, the current injection is already known by SW because the FES update is processed in the occurrence time.

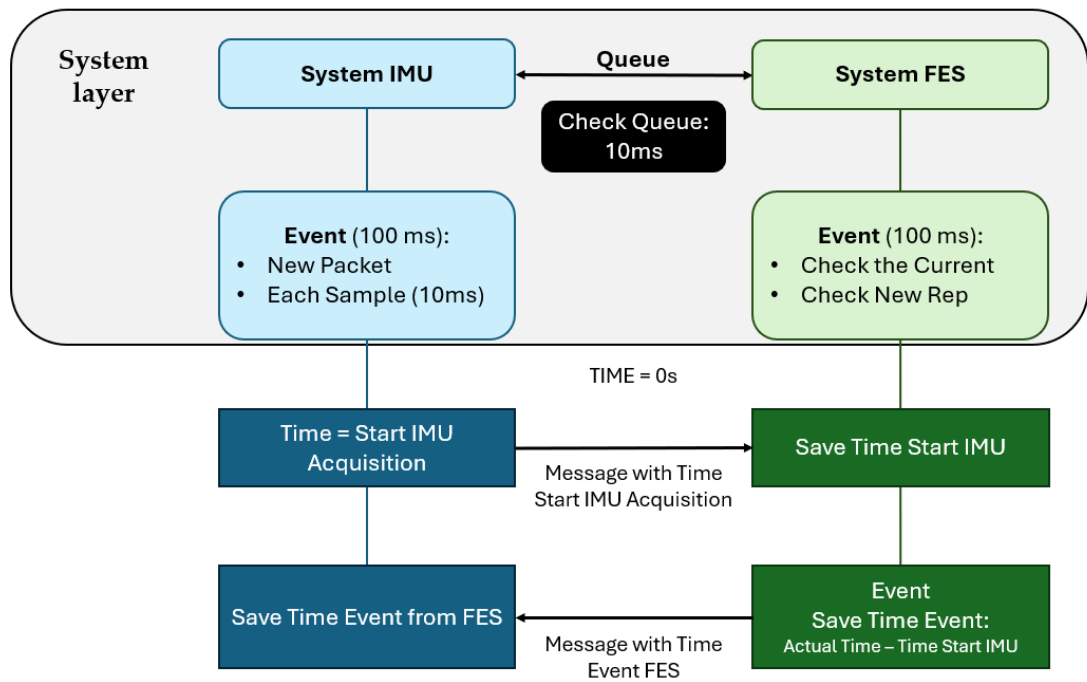


Figure 5.2: Synchronisation of FES and IMU processes time. The IMU SW receives every 100 ms a data packet from the Apollux devices. The FES SW checks every 100 ms if there is a new FES event. Both SWs check every 10 ms if there is a new message in the queue. The IMU software evaluates the start time of acquisition and sends it via queue to the FES software. When an FES event occurs, the time of occurrence is calculated as the difference between the start time of acquisition and the current time. A message containing the FES event details (such as an update in the current value) and the timing instant is then sent to the IMU software.

5.2 Main changes in the software

In this section, there will be a description regarding the main upgrades on two SWs at the system level and Graphical User Interface (GUI) level.

5.2.1 Inertial Measurement Unit (IMU) software main changes

In this subsection, an analysis of the improvements in IMU SW will be made. In Figure 5.3, there is an overview of the previous GUI for the IMU acquisition, while in Figure 5.4, the representation of the final GUI is provided.



Figure 5.3: Previous GUI IMU: the top layer contains the widgets that allow the user to interact with the Apollux devices. The bottom contains the graphic elements that will plot the acquired data.

The old IMU SW was developed to acquire IMU data from a maximum of four Apollux devices simultaneously, and three modes were selectable by checkboxes (present at the top of the left side of the GUI in Figure 5.3): acceleration data (or ACC), gyroscope data (or GYR), and Euler’s angles (or ATT).

One modification was performed regarding the mode acquired from each Apollux data. Indeed, for the closed-loop, at least two Apollux devices are needed; at least

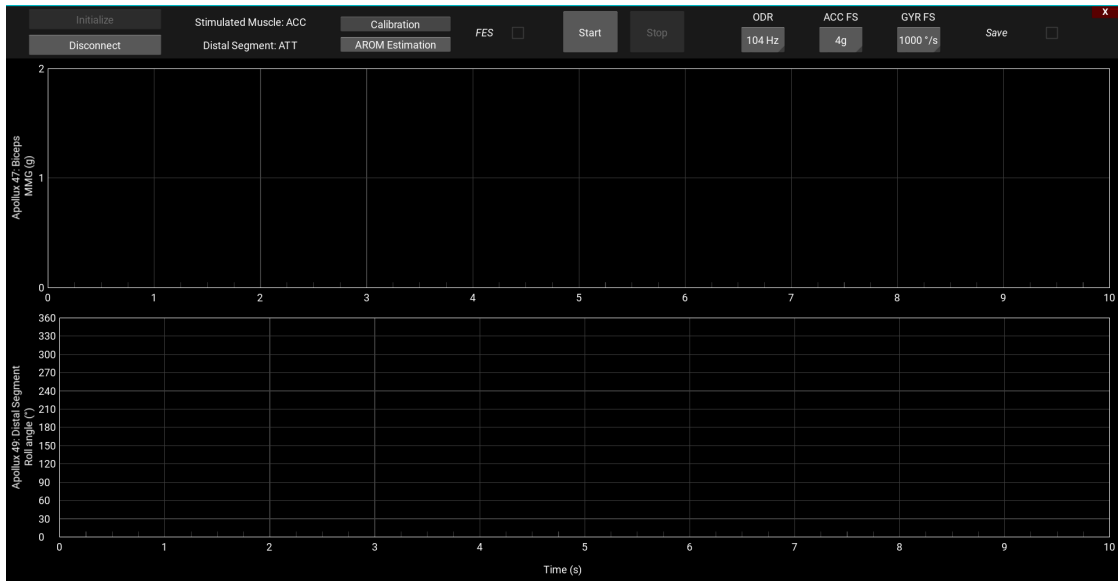


Figure 5.4: Actual GUI IMU: the top layer contains the widgets that allow the user to interact with the Apollux devices. The bottom contains the graphic elements that will plot the acquired data.

one should acquire MechanoMyoGram (MMG) data from the stimulated muscle, while another is needed to acquire the reached angle during the stimulation.

For this purpose, the labeling operation of the acquisition devices is imposed. Indeed, the user has to assign a name to each sensor used. The name corresponds either to the monitored muscle (insert with the first capital letter, i.e., *Biceps Brachii*) or should be *Distal Segment* if it senses the angular motion.

Labeling is performed when pressing the 'Initialize' button (present at the top of the left side of the GUI in Figure 5.4). The user will be asked to select the device to connect and write the name in the apposite text input, as shown in Figure 5.5.

Thanks to this labeling step, it is possible to impose both the sensor acquisition mode (acceleration data for the muscles or Euler's angles for the *Distal Segment*) and an association between the sensing device and the stimulation channel.

A button for the Active Range Of Motion (AROM) estimation is added: it acquires Euler's Angle data from *Distal Segment* and evaluates the AROM as the difference between a rest position and the maximum value reached during the full movement. As already mentioned, for the muscle and the movement performed in this thesis, the roll angle has been selected as the indicator of the movement; it is evaluated in a range from 0° to 360° .

In particular, it evaluates the baseline roll angle during 5s of rest and then the

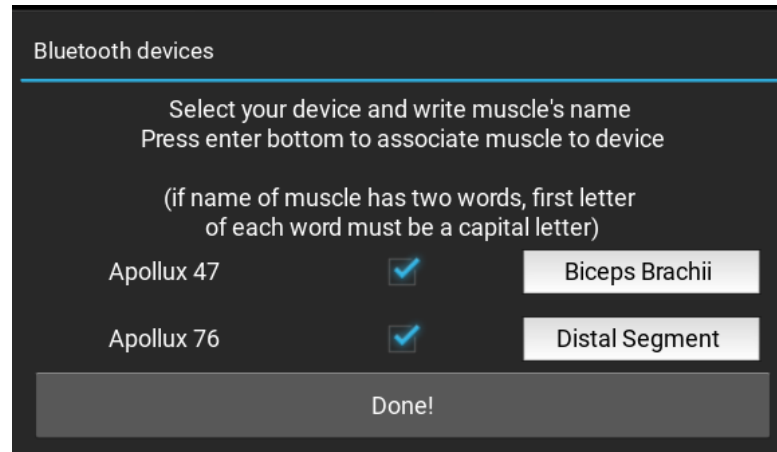
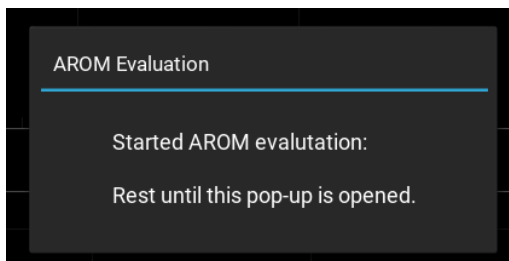
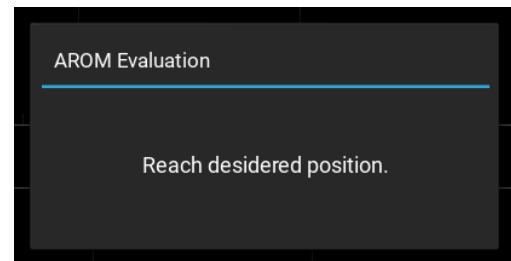


Figure 5.5: GUI IMU labels assigned to Apollux devices. When pressing the *Initialize* button on the GUI, a pop-up opens that permits selecting the Apollux device. Each of them has to be labeled with a muscle name or with *Distal Segment*.

maximum value that is reached while contracting (the complete movement should be performed in maximum 5 s). By pressing the '*AROM evaluation*' button, the user is informed of the acquisition step to perform thanks to some pop-up that appears during the acquisition (reported in Figure 5.6).



(a) Baseline evaluation pop-up.



(b) Perform full movement pop-up.

Figure 5.6: Active Range Of Motion (AROM) evaluation: software pop-up. (a) Baseline evaluation pop-up (5 s) (b) Perform full movement pop-up (5 s).

At the end, a pop-up will inform the user of the AROM evaluated; an example of it is shown in Figure 5.7.

After AROM estimation, the y-axis of the *Distal Segment* roll angle modifies its range (before it ranged between 0° to 360°) to a smaller range based on the estimated AROM value, in order to make the plot more understandable for the user.

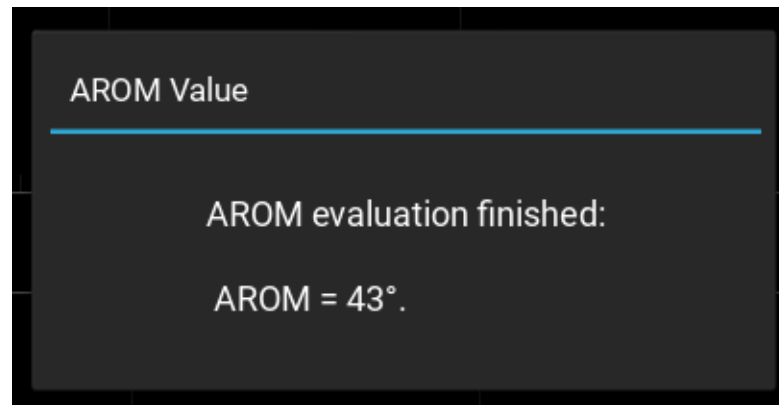


Figure 5.7: GUI IMU evaluated AROM value. This pop-up is open at the end of the AROM evaluation, it indicates the measured AROM value.

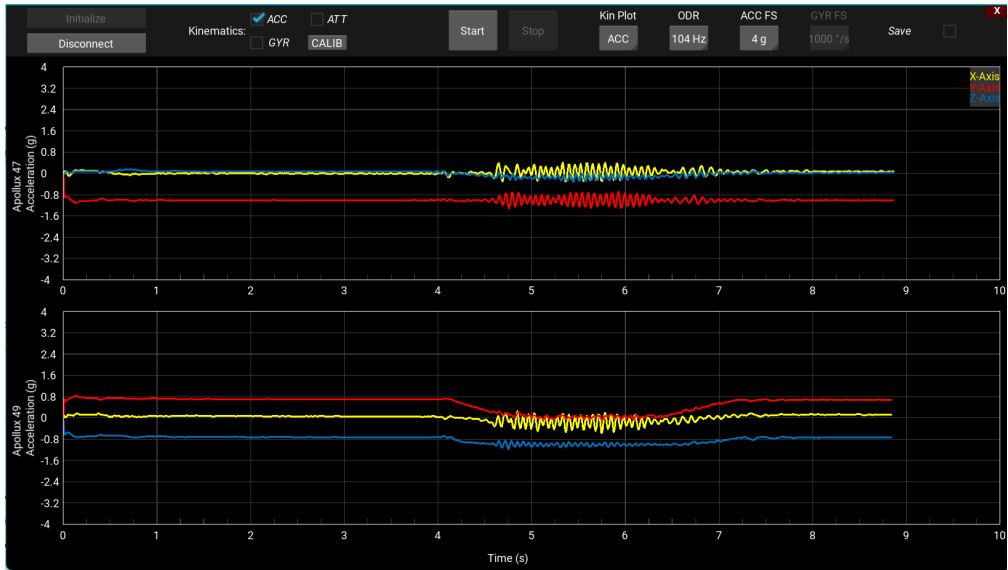
Another improvement regards the real-time plots of the IMU data. In particular, in the previous version, the GUI had a number of plots that corresponded to the number of Apollux devices connected, and the plots were ordered in a rising order with respect to the number of devices. In the updated version, the *Distal Segment* always occupies the bottom plot, and even though three Euler's Angles (Roll, Pitch, and Yaw) are detected, only the Roll angle is plotted. On the other hand, the Apollux devices placed on the muscles collect acceleration data, and the unfiltered MMG value (evaluated as defined in Equation 4.1) is plotted.

Figure 5.8 compares the previous plots in the original version of the IMU SW and the actual plots. In Figure 5.8a are represented old plots, while in Figure 5.8b the new.

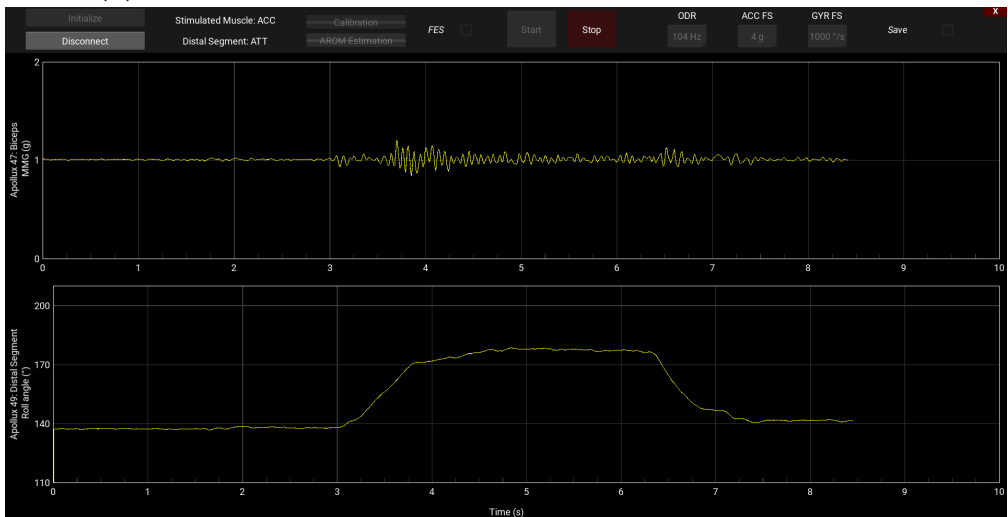
Moreover, a checkbox is added for the initialization of the FES SW through *multiprocesing*; when it is active, the FES SW is open, while it is closed when it is inactive.

On the other hand, there are some widgets whose functionality has not been modified. They are:

- *Disconnection* button: permits the disconnection of the Apollux devices;
- *Calibration* button: performs the gyroscope calibration;
- *Start* button: permits the start of the Apollux devices acquisition. The gyroscope calibration must be performed before the user presses this button. If the FES SW is running, it will also start the stimulation (after waiting a



(a) IMU GUI Example of Acquisition using the initial software.



(b) IMU GUI Example of Acquisition using the actual software.

Figure 5.8: IMU GUI Example of Acquisition: comparing the previous and the new plot. In Figure (a), the previous plots are illustrated; in this case, the acceleration data was selected to be plotted, and for both Apollux devices, the three axes (X, Y, Z) are represented in three different colors (yellow, red, blue). In Figure (b), the actual plots are shown; in this case, the MMG data is plotted for the Apollux located on the muscle of interest (top graph), and the roll angle for the Apollux is shown on the distal segment (bottom graph).

variable amount of time due to a transitory presence in the Euler's Angle). Otherwise, it will acquire data from voluntary contractions;

- *Stop* button: permits the stop of the Apollux devices acquisition. If the FES SW is running, it will stop the stimulation, too, or if the stimulation is ended, the acquisition will automatically stop;
- *Disconnection* button: permits the disconnection of the Apollux devices;
- *ODR* menu: permits the selection of the sampling frequency, the recommended one is 104 Hz to not decrease the SW performances;
- *ACC or GYR fs* menu: permits the user selection of respectively the accelerometer and gyroscope full scale;
- *Save* checkbox: allows the save of the acquired Apollux data. If FES and closed-loop SW are running, their data will also be saved.

5.2.2 Functional Electrical Stimulation (FES) software main changes

The initial modification made to the FES SW was to divide up the previous SW's methods in order to create a more functioning SW. This project began with just one SW that provided system and graphical commands. Thus, it was decided to divide them into two distinct parts: System FES, which oversees the system's operations, and GUI FES, which contains all graphical methods.

A comparison between the overview of the FES GUI as it was and as it is currently is provided. The previous GUI taken at the start of this thesis project is shown in Figure 5.9.

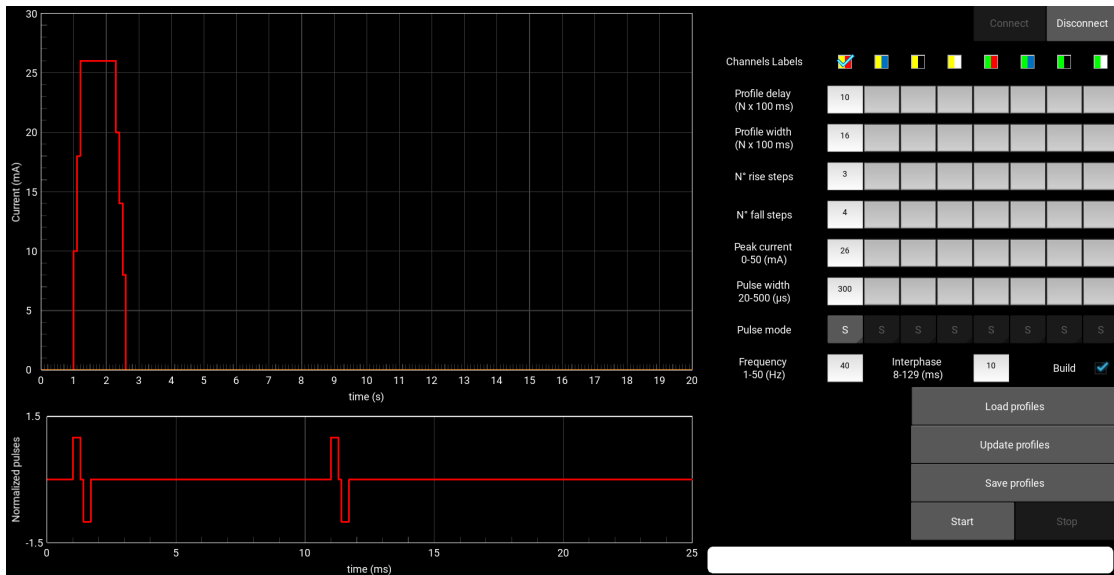


Figure 5.9: Previous GUI FES. The input parameters and all the buttons used to manage the stimulation are on the right. On the left are two graphs: the top graph shows the stimulation profile defined by the user, and the bottom graph illustrates the selected mode of pulses.

Alternatively, all of the enhancements and modifications made to the FES GUI are displayed in Figure 5.10. In Chapter 7, the GUI modifications required for the closed-loop operations will be described.

In the beginning, the FES SW was unable to provide sequential stimulation. This means that the first requirement for this SW is to enable it to surpass this limit by enforcing the number of consecutive repetitions that the user desires.

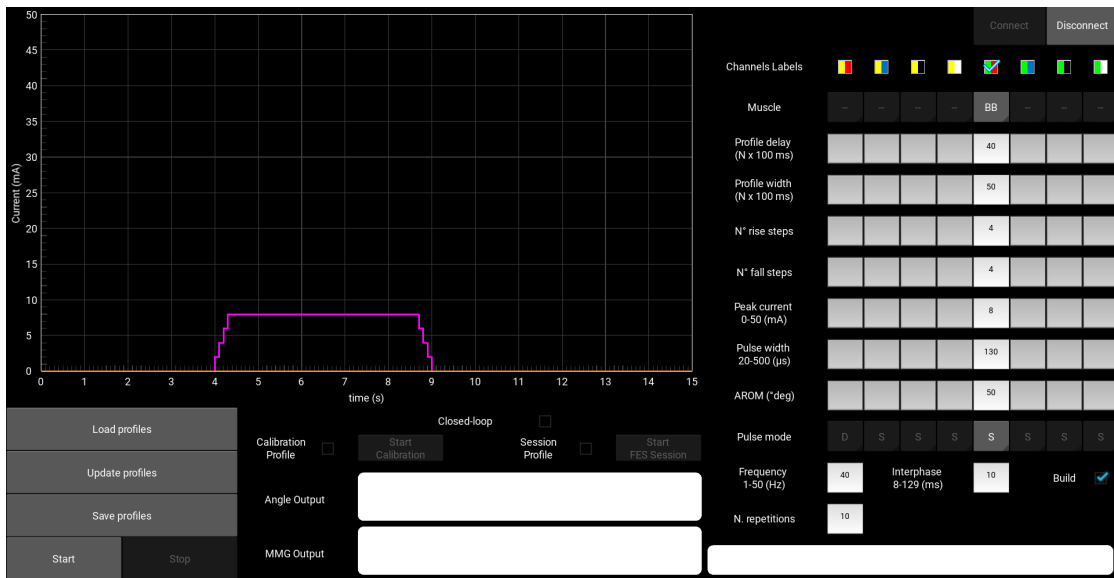


Figure 5.10: Actual GUI FES. The main changes present in this overview are the position of buttons used to manage the stimulation (in this version, they are located on the bottom at left), the addition of all the objects necessary for the closed-loop system (located on the bottom at center), and the addition of some new input parameters (on the right).

Following the connection of the two SWs, due to the FES SW's ability to pick the stimulation channel, the possibility for the user to choose which muscle is stimulated on each channel was added. For this choice, the user must select the initial letter of muscle from a drop-down menu, defined by the IMU SW.

Indeed, the labels of the muscles present in the selection were sent from IMU SW when the FES SW was launched, and the list of muscles is composed of the initial capital letter of each word that composes the name of the muscle. For instance, *Biceps Brachii* label became 'BB' in the drop-down menu. This linking between the channel selected and the muscle is essential. Thanks to that, the SW can create a direct connection between the Apollux device, the relative muscle that Apollux monitors, and the stimulation channel used for that muscle.

The last modification done regarding the input parameters of the FES GUI is adding the AROM value for each channel. This is an input that the closed-loop system requires. The explanation of every implementation needed for the closed-loop will be provided in Chapter 7. All the input changes are shown in Figure 5.11.

Channels Labels								
Muscle	--	--	--	--	BB	--	--	--
Profile delay (N x 100 ms)					40			
Profile width (N x 100 ms)					50			
N° rise steps					2			
N° fall steps					2			
Peak current 0-50 (mA)					2			
Pulse width 20-500 (µs)					130			
AROM (°deg)					50			
Pulse mode	D	S	S	S	S	S	S	S
Frequency 1-50 (Hz)	40		Interphase 8-129 (ms)		10		Build	<input checked="" type="checkbox"/>
N. repetitions	10							

Figure 5.11: Actual Input GUI FES: changes in input parameters. Under the channel selection, choosing the muscle to stimulate using a drop-down menu is possible. Other changes that emerged from these input parameters are the input text for the AROM of each muscle and the input text for the number of consecutive repetitions.

It is possible to resume all the input parameters of FES GUI:

- *Channel Labels*: selection of stimulation channel;
- *Muscle*: selection of stimulated muscle;

- *Profile delay*: indicates the time of start of injecting current, to obtain this time, it is necessary to multiply the factor inserted in the text input and 100 ms;
- *Profile width*: indicates the time of the entire stimulate, to obtain this time, it is necessary to multiply the factor inserted in the text input and 100 ms;
- *N^orise/fall steps*: these two inputs indicate the steps of ascent and descent necessary to reach the wanted current. So this stimulation doesn't have a rectangular waveform, but the pulse shape, created with this SW, could change based on these steps;
- *Peak current*: indicates the current to inject into the subject, it is measured in mA;
- *Pulse width*: indicates the duration of a single pulse (in μ s);
- *AROM*: indicates the AROM to reach in $^{\circ}$ (it is a requirement for the closed-loop operation);
- *Pulse Mode*: choosing between single, double, or triplet mode can be possible.
- *Frequency*: indicates the stimulation frequency, it is measured in Hz;
- *Interphase*: is the time between the two phases on a biphasic pulse. It is measured in ms;
- *N. repetitions*: indicates the number of consecutive repetitions with the same stimulation energy to perform;
- *Build* check-box: it is necessary to create the stimulation profile.

The buttons present in the FES GUI are illustrated in Figure 5.12, following a brief description:

- *Load profiles*: this button uploads a stimulation profile that was previously saved;
- *Update profiles*: this button updates the actual stimulation profile based on the input parameters inserted by the user; moreover, when this button is pressed, all the input parameters of the stimulation are sent to IMU SW;
- *Save profiles*: this button consent to save a stimulation profile for the next session of stimulation;
- *Start*: this button consents to use the FES SW apart from the IMU system acquisition; thus, pressing this button makes it possible not to acquire the IMU signal using the Apollux but to start only the stimulation part. If the user wants to acquire the IMU signal while the stimulation is going, it's necessary to press *start* at the button of the IMU GUI;
- *Stop*: this button stops the stimulation in both if the two SWs are working together or if only the FES is working.
- *Connect*: this button allows the user to connect the stimulator. There is also a simulated version of the RehaStim2 that can be connected.
- *Disconnect*: this button consents to disconnect the stimulator in security.

If the closed-loop checkbox is active, all the buttons just described are disabled, and the stimulation and acquisition are managed from closed-loop buttons. These

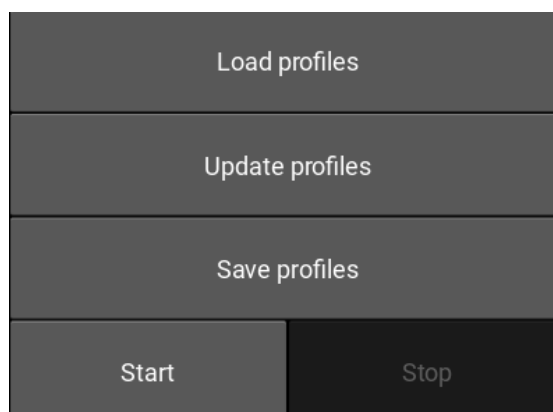


Figure 5.12: Actual GUI FES: buttons used to manage the stimulation.

functionalities will be described in the Chapter 7.

A physical emergency button is also connected to the RehaStim2 to stop the stimulation when pressed.

Under the input parameters, a white panel is used to print some useful messages to interact with the user. Some examples of these communications are: *number of repetition*, problems like *RehaStim2 is not connected*, *Electrode's error*. Only the profile stimulation graph was left in the actual FES GUI version; the current ranges from 0 mA to 50 mA, and for each repetition last 15 s.

The reason why a saving file wasn't created in the prior FES SW is likely that successive repeats weren't permitted. Following this implementation, information about the stimulation had to be saved after connecting to the FES and IMU SW. For each repetition, it is required to save the current and the corresponding time, the channel being stimulated, and the associated muscle. Additionally, all other input parameter data must be saved.

It was explained that the IMU SW and the FES SW are linked through the queue and that the IMU SW launches the FES SW using a multiprocessing. There are some messages that FES sends to IMU that are crucial for the synchronous working of the two SWs:

- Messages of errors:
 - *FES error: no profiles*. This indicates that the stimulation profile wasn't created, so the IMU acquisition should be stopped.
 - *FES RehaStim2 not connected*. This indicates that the stimulator is not connected, so the IMU acquisition should be stopped.
 - *FES ScienceMode2 not entered*, *FES RehaStim2 problem while connection*, *FES Stimulation Error*: all these error messages are sent from FES SW to warn the IMU SW that something is wrong, thus the IMU SW must stop the acquisition.
- Message of initialization:
 - *FES Muscle Accepted Input*. This message is sent from the FES SW when it is connected (when the *connect button* is pressed) and it has configured the drop-down menu composed by the abbreviation of muscles.
 - *New stimulation parameters*. This message is sent from the FES SW when it updates (when the *update button* is pressed) its stimulation profiles and sends all their information to the IMU SW.

- Messages that manage the synchronous working:
 - *FES is started*. This message is sent from the FES to warn the IMU that it will start after the analysis of the initial transitory done by the IMU SW ends.
 - *FES repetition number*. This message refreshes the number of repetitions from time to time.
 - *FES has completed rep n*. This message is used to inform the IMU SW that FES SW has executed all the repetitions imposed by the user. Thus, the IMU SW has to stop the signal acquisition.
 - *FES pressed stop button*. This message serves to notify the IMU SW that the *stop button* of the FES GUI is pressed. Thus, the IMU SW has to stop the signal acquisition.
 - *FES Injecting Current*. This message advises the IMU SW of each change of current.

To sum up, in the section of software development covered in this chapter, two distinct SWs are combined using *multiprocessing* to create a single primary SW from which the second SW's process can be initiated. The two SWs are connected and capable of simultaneous operation based on the modifications that were just described.

The tests conducted with the SW—which is merely an illustration—will be detailed in the following chapter in order to ascertain which parameters may be extracted from MMG signals in order to identify the voluntary contribution during functional electrical stimulation.

Chapter 6

Software Testing on MechanoMyoGraphy (MMG) signals

This chapter will describe the first experimental protocol executed to test MMG signals during the FES. This phase aims to identify a parameter that permits distinguishing between a voluntary and a stimulated contraction using MMG signals.

6.1 Test Protocol Description

An initial experimental protocol was carried out to identify at least one measure capable of differentiating between different types of contraction. To realize the closed-loop system, it's necessary to have a parameter that detects some information from the acquisition signal and manages that in order to provide the output to the stimulation system. This is the reason for these preliminary tests.

The muscle tested is the *biceps brachii*, and the movement required is the *elbow flexion*. The protocol includes 7 healthy subjects, five female and two male. The participants had to sign a liability waiver certifying that they were aware of all test phases, how the FES operated, and that they were taking the exam voluntarily. In addition, at the end of the procedure, subjects have to compile a survey to leave feedback about their experience.

The test protocol is divided into three main phases:

- The **first phase** includes the evaluation of the AROM and the MVC values. The AROM value sets the angle to be reached during the stimulation. Instead, the MVC value determines the weight to use during trials.
- The **second phase** includes the calibration of the stimulation that defines the stimulation parameters that will be used in the last phase of the protocol. The stimulation parameters that allow the subject to reach his/her AROM value define the upper energy parameters. While the lower energy parameters are defined as the stimulation parameters tested before the last.
- The **third phase** includes the key test. Indeed, 7 tests are done in this part:
 1. Voluntary case with 0 % of the MVC;
 2. Voluntary case with 30 % of the MVC;
 3. Voluntary case with 70 % of the MVC;
 4. Only stimulated case at lower energy with 0 % of the MVC;
 5. Stimulated plus voluntary contribution case at lower energy with 30 % of the MVC;
 6. Stimulated plus voluntary contribution case at lower energy with 70 % of the MVC;
 7. Only stimulated case at upper energy with 0 % of the MVC;

6.1.1 Details regarding subjects and acquisitions

Two tables will be presented with more details about the subjects and the acquisitions.

All of the subject's information is summarised in Table 6.1; this information includes gender, age, sides, MVC, and AROM. The subjects' ages range from 24 to 28 years old, with women constituting the 70 % of the participants. Each subject decided whether to use the right or left side. The MVC and the AROM are also reported in this table. Indeed, the subjects have been tested to evaluate their own MVC measured in kg, and the AROM reached to complete the required movement is measured in °. The explanation of how these two parameters are estimated will be provided during this Chapter in Section 6.1.2.

Instead, in Table 6.2 are reported the stimulation parameters that will be used during the test. These are defined for each subject based on a manual FES calibration executed before the test. In this Chapter, Section 6.1.4 discusses more

information about this phase.

Table 6.1: Subjects data during the experimental protocol. The studied muscle is the *biceps brachii* during the *elbow flexion*. For each subject are indicated gender, age, side, MVC value in kg, and AROM value in °.

Subject n.	Gender	Age	Side	MVC (kg)	AROM (°)
1	F	24	Left	6	63
2	F	27	Right	9	74
3	F	24	Right	6	69
4	M	23	Right	18	70
5	M	24	Left	10	73
6	F	28	Right	5	80
7	F	24	Right	7	73

Table 6.2: Each subject’s stimulation parameters during the experimental protocol. The studied muscle is the *biceps brachii* during the *elbow flexion*. For each subject are shown Current (C) and Pulse Width (PW) at the Low Energy level and the High Energy level.

Subject n.	Low Energy		High Energy	
	C (mA)	PW (µs)	C (mA)	PW (µs)
1	16	160	18	160
2	18	160	18	170
3	12	140	14	140
4	26	200	30	200
5	20	180	22	180
6	16	150	16	160
7	26	200	27	200

6.1.2 Evaluation of MVC and AROM values

Maximal Voluntary Contraction (MVC) parameter

Scientific research frequently uses the Maximal Voluntary Contraction (MVC) parameter to standardize measurements for comparing muscle strength across groups and assessing the effectiveness of novel therapies or training approaches.

For this reason, it was decided to execute the trial using the 0 %, 30 %, and 70 % of the MVC to try to understand how the stimulation can respond at different levels

of contractions.

The MVC of the *biceps brachii* is obtained by asking the subject to produce her/his own maximal contraction using the dynamometer [103]. In order to execute the MVC estimation, the subject stands in front of a support with one side of the dynamometer attached, as indicated in the Figure 6.1 for this phase's setup. The volunteer holds the forearm at a 90° angle with respect to the arm and grips the other side of the dynamometer in her/his hand. The participant has to draw up the dynamometer by doing her/his maximal contraction from this posture.



Figure 6.1: Estimation of Maximal Voluntary Contraction (MVC): this is the experimental set-up followed during the measure of the MVC of each subject.

Active Range Of Motion (AROM) parameter

In order to increase awareness of the subject's movement, it was decided that the evaluation of the Active Range Of Motion (AROM) should be included in this project.

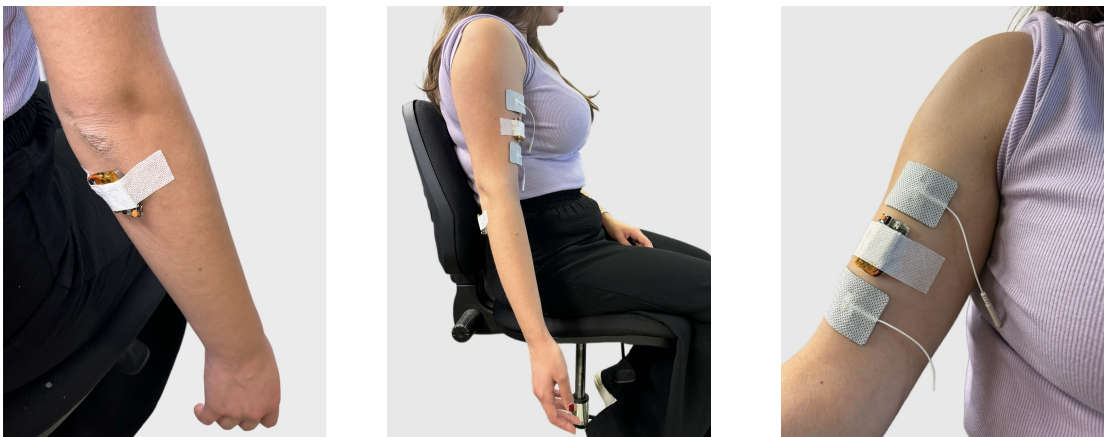
Each subject's AROM is measured during the first part of the test, and the various angles the individual achieves throughout the test are then compared to this. The Apollux device on the distal segment and the IMU SW are utilised to acquire the AROM. During the first five seconds of the "*AROM Estimation*", the

patient must remain in the rest position. After that, a pop-up message displays on the IMU GUI, directing the subject to move to the designated position. The difference between the angle of rest and the greatest angle obtained is the AROM.

6.1.3 Experimental set-up

During the trial, the subject executes all the tests sitting on an office chair. The patient's back should be well supported against the backrest. The arm is fully relaxed and extended along the body. The acquisition system comprises two Apollux devices, one positioned on the belly of *biceps brachii*, and the other on the back of the *forearm*. The electrodes of the stimulator RehaStim2 are positioned over the muscle to stimulate (Figures 3.7). The Apollux devices are fixed to the subject using a biomedical tape.

In Figure 6.2, it is shown the rest position of the subject during all tests (b) and the electrode placement for the *distal segment* (a) and *biceps brachii* (c).



(a) Apollux device positioned on the *distal segment*.

(b) Starting and rest position of *biceps brachii* contractions.

(c) Apollux and stimulation electrodes positioned on the *biceps brachii*.

Figure 6.2: Electrode placement and resting position of arm: in figure (a) there is the placement of the Apollux device of the *distal segment* (collecting Euler's angles); (b) resting position (during all tests, the subject must always return to this position, which is the reference position); (c) Apollux device on the *biceps brachii* (acquiring MMG data) and stimulation electrodes.

6.1.4 Research of optimal stimulation parameters

A manual FES calibration is done to obtain the optimal stimulation parameters. The subject is positioned as described in this Chapter during Section 6.1.3.

The manual FES calibration consists of researching the optimal stimulation parameters for the subject. These energy parameters allow the subject to reach the desired position only through functional electrical stimulation. In this phase, the subject must be completely relaxed and try not to add a voluntary contribution.

During this phase, the first set of energy parameters from which stimulation starts is: the current set to 0 mA, the pulse width set to 130 μ s, and 40 Hz as stimulation frequency. Each set of parameters is maintained for at least two repetitions, after which the efficacy of the stimulation is evaluated. If the stimulation is not effective, the current is increased by 2 mA every two repetitions up to 14 mA, then it is increased one time the current of 2 mA, and one time the pulse width of 10 μ s. The manual FES calibration is stopped when these parameters allow the movement to reach the AROM evaluated previously.

6.1.5 Comprehensive Testing: Integration of Voluntary and Stimulated Responses

This trial phase's seven tests all have the same main structure. Ten repetitions constitute each test, each lasting 15 s. Each repetition specifically consists of 4 s of rest, 5 s of voluntary or induced contraction, and 6 s of rest at the end. Between one test and the following one, there are 5 min of rest.

The set-up is the same as described for the manual FES calibration, and for the AROM Estimation in this Chapter during Section 6.1.3.

In particular, there are three typologies of cases:

- In the three voluntary cases (0 %, 30 %, and 70 % of the MVC), there is no electrical stimulation. The subject has to execute the ten repetitions only by her/himself.
- In the two only stimulated cases (both 0 % of the MVC), the subject did nothing and tried to relax and leave the stimulation to make the contraction without adding a voluntary contribution.
- In the two stimulated plus voluntary contribution cases (30 %, and 70 % of the MVC), the subject has to cooperate with the electrical stimulation to complete the movement.

The aim of this trial is to try to detect voluntary contributions during electrical stimulation. The three voluntary cases were performed to discover how electrical stimulation changes parameters such as the standard deviation, the root mean square, the median frequency, and the mean frequency.

It was decided to realize the cases with a percentage of the MVC to see how changes the parameters with a major activation.

Finally, after all cases were realized, a post-processing analysis of the data was done. In particular, the voluntary case with 0% of the MVC was compared to the two only stimulated cases. Instead, the voluntary case with 30% and 70% of the MVC was compared to the stimulated plus voluntary contribution case respectively with 30% and 70% of the MVC.

6.1.6 Statistical Analysis

When evaluating differences between various cases, an important aspect is to determine if the observed variations in the data are significant or merely due to random chance.

This protocol was designed to validate the feasibility of evaluating voluntary contractions using the MMG signal. Seven cases needed to be analyzed to identify a pattern that makes detecting voluntary contractions possible. Each case is represented by a data distribution, so an initial analysis of the means was required.

A statistical technique called ANOVA, or Analysis of Variance, compares the means of several groups to see if the means of at least one of the groups differs noticeably from the others [104]. However, this method has some strong assumptions that can be resumed in:

- Independence of observations;
- Normally distributed populations;
- Homogeneity of variances (equal variances among groups).

In cases where the assumptions of ANOVA are not satisfied, such as when the data are not normally distributed or the variances are not equal, the Kruskal-Wallis test is a non-parametric substitute for ANOVA [105].

To find out if the samples come from the same population (or, alternatively, from distinct populations with the same distribution), it compares the medians of the data groups in x .

The test statistics for the Kruskal-Wallis test are determined by ranking the data instead of using their numerical values. It uses the numeric index of this order

to assign ranks by sorting the data across all groups from least to largest. The average rank of all tied observations determines the rating for tied observations. The p-value in this test denotes the significance of the chi-square statistic, which takes the place of the F-statistic used in traditional one-way ANOVA. For this test, the null hypothesis (H_0) is that the distributions of all the groups are equal.

After evaluating the differences between at least one group's mean, it is necessary to identify which groups are significantly different from each other. This can be achieved through pairwise comparisons. Pairwise comparison is a statistical technique used to compare all possible pairs of groups to determine which specific pairs show significant differences.

6.2 Results of Test

6.2.1 Results over parameters analysed

The parameters extracted from the MMG signals are reported in Chapter 1 Section 1.6. The results are obtained by analysing the MMG data when the maximum current is injected. Moreover, the MMG technique is highly affected by the phases of ascending and descending the arm, so the MMG is evaluated only when the angle reaches a plateau stadium.

The acquisition types have been abbreviated to make the figures more comprehensible. Specifically, they are referred to as Voluntary Contractions (VC), Stimulation with Lower Energy (SLE), and Stimulation with Higher Energy (SHE).

Firstly, an analysis in the time and frequency domain has been performed; in particular, every subject performed 7 acquisitions, each comprehending 10 repetitions. So, ten values are extracted for each subject, test, and parameter considered. In Figures 6.3, 6.4, there is the analysis of respectively the Root Mean Square (RMS) and standard deviation (STD) evaluated over the 7 subjects and the 7 types of acquisition. On the other hand, the same comparison is present in Figures 6.6, 6.7, 6.5, which regards the frequency domain parameters of mean frequency (fmean), median frequency (fmed) and the sum of PSD (Psum).

This analysis shows an appreciable increase in the RMS, STD, and Psum value when considering the increase in the %MVC. It can be noticed in Figure 6.3 that if we consider the cases 1-2-3 (voluntary contractions with the increase of the % of the MVC) or the cases 4-5-6 (stimulated contractions lower energy with the increase of the % of the MVC), in both cases there is an increase in the RMS value when the % of the MVC is increasing. The same increase can be noticed in Figure 6.4 (regarding the STD parameter) and in Figure 6.5 (regarding the Psum parameter). Conversely, all three figures show that when considering 0% of the MVC, there are no appreciable differences between the cases of voluntary contractions (VC) and the two levels of stimulation (SLE and SHE).

Furthermore, it can be observed that as the % of the MVC increases, there is a corresponding increase in the variability of the parameter, as evidenced by the widening of the interquartile range (the difference between the third quartile and the first quartile, which represents the range within which the middle 50% of the data falls). Specifically, for case 4 (stimulation with lower energy), the interquartile range is 0.0023g, whereas in case 5 (stimulation with lower energy and voluntary contractions at 30% of the MVC), it increases to 0.0058g, and in

case 6 (stimulation with lower energy and voluntary contractions at 70 % of the MVC), it further increases to 0.030g. A similar trend is observed in the voluntary cases when comparing increases in % of the MVC, as well as in the STD and Psum parameters.

Moreover, a similar trend of augment, due to the % of the MVC growth, can be noticed from the median value of each of the seven distributions. An example of it is present in the RMS values: comparing the cases 4-5-6 (stimulation with lower energy with 0 % of the MVC, 30 % of the MVC and 70 % of the MVC), the median values are respectively equal to 0.0067g, 0.0149g and 0.0272g. So, an increase of 122 % is present when ranging from 0 % of the MVC to 30 % of the MVC, and an increase of 122 % when the % of the MVC rises from 0 to 70.

On the other hand, the analysis regarding the mean and median frequency (respectively Figures 6.6 and 6.7) do not report any appreciable trends. No appreciable variation is present due to the increase of the %MVC or the presence of stimulation.

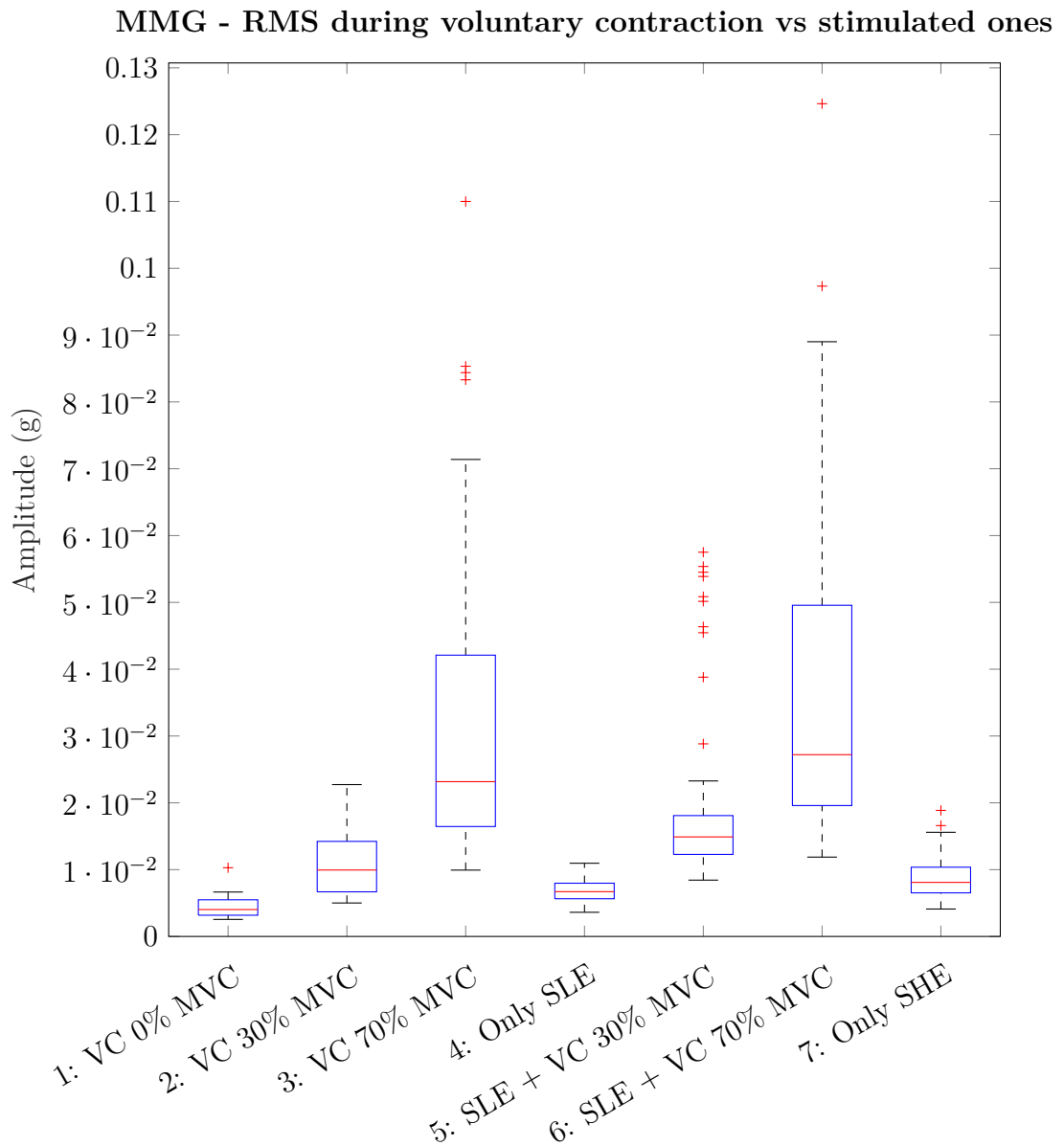


Figure 6.3: Root Mean Square (RMS) comparison between various levels of contraction (% of the MVC). Values were evaluated over 7 healthy subjects, ten repetitions of *biceps brachii* voluntary contractions (VC), stimulated with lower energy (SLE), or stimulated with higher energy (SHE).

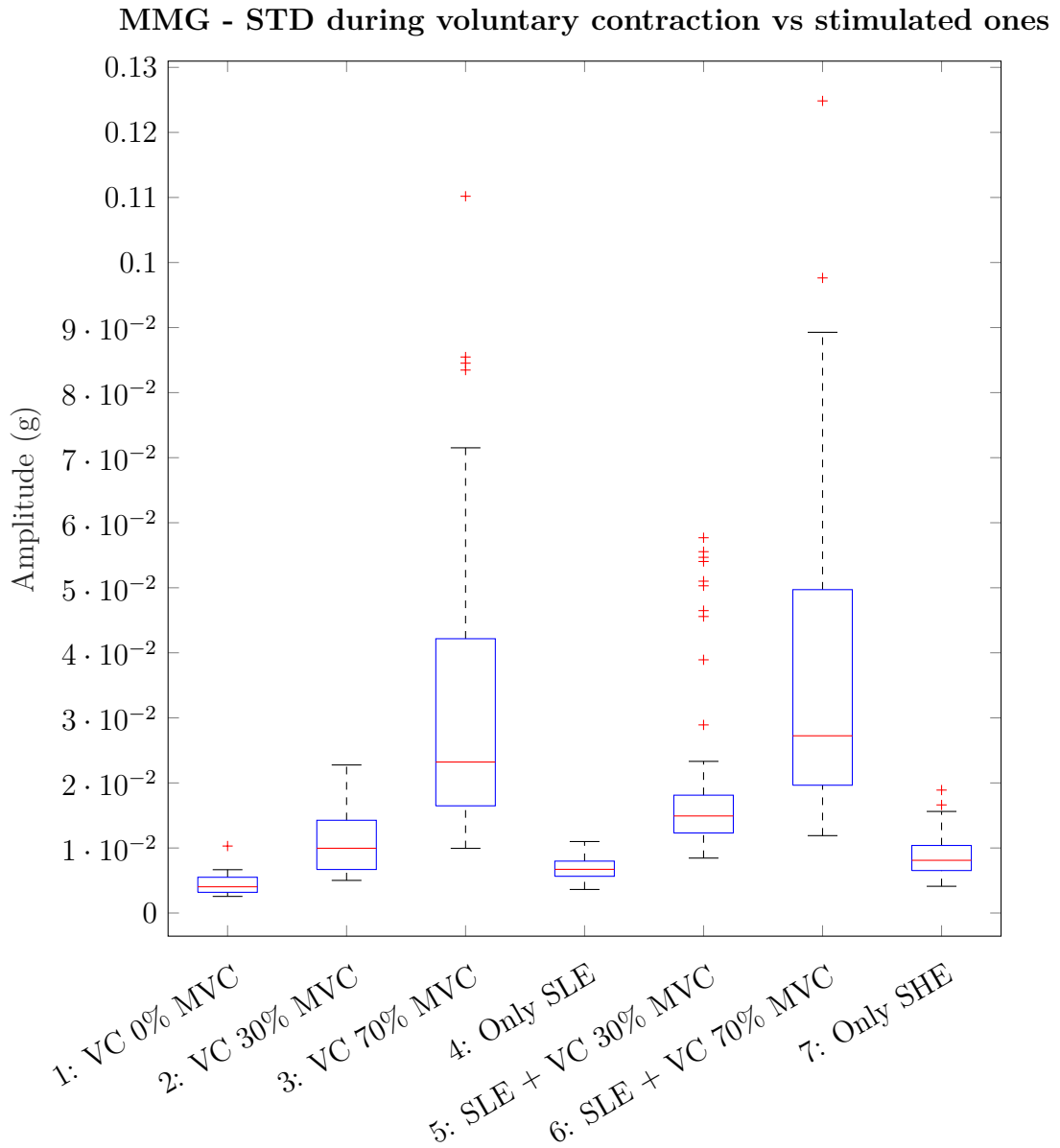


Figure 6.4: Standard Deviation (STD) comparison between various levels of contraction (% of the MVC). Values were evaluated over 7 healthy subjects, ten repetitions of *biceps brachii* voluntary contractions (VC), stimulated with lower energy (SLE), or stimulated with higher energy (SHE).

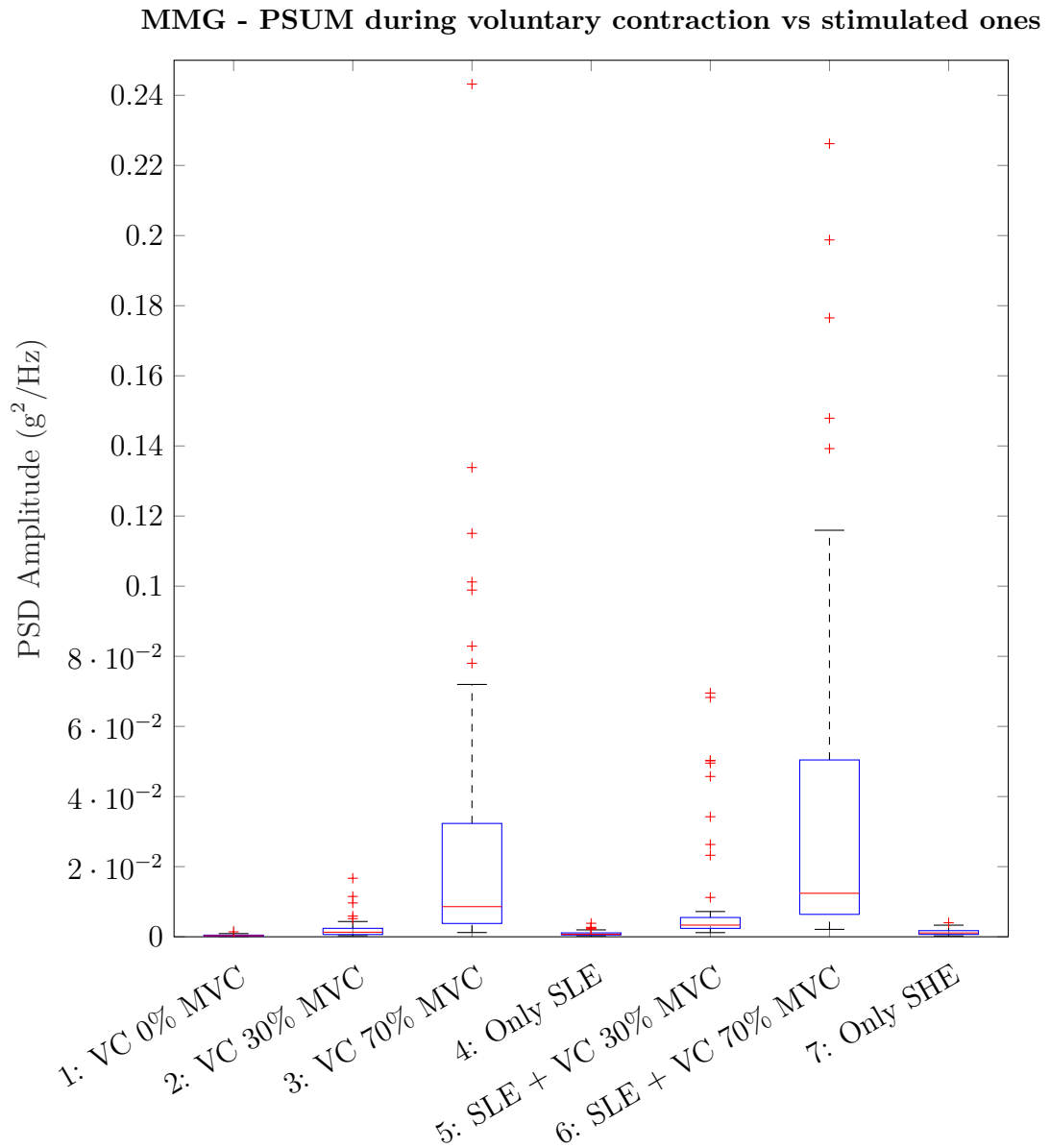


Figure 6.5: Sum of Power Spectral Density (Psum) comparison between various levels of contraction (% of the MVC). Values were evaluated over 7 healthy subjects, ten repetitions of *biceps brachii* voluntary contractions (VC), stimulated with lower energy intensity (SLE), or stimulated with higher energy (SHE).

MMG - FMEAN during voluntary contraction vs stimulated ones

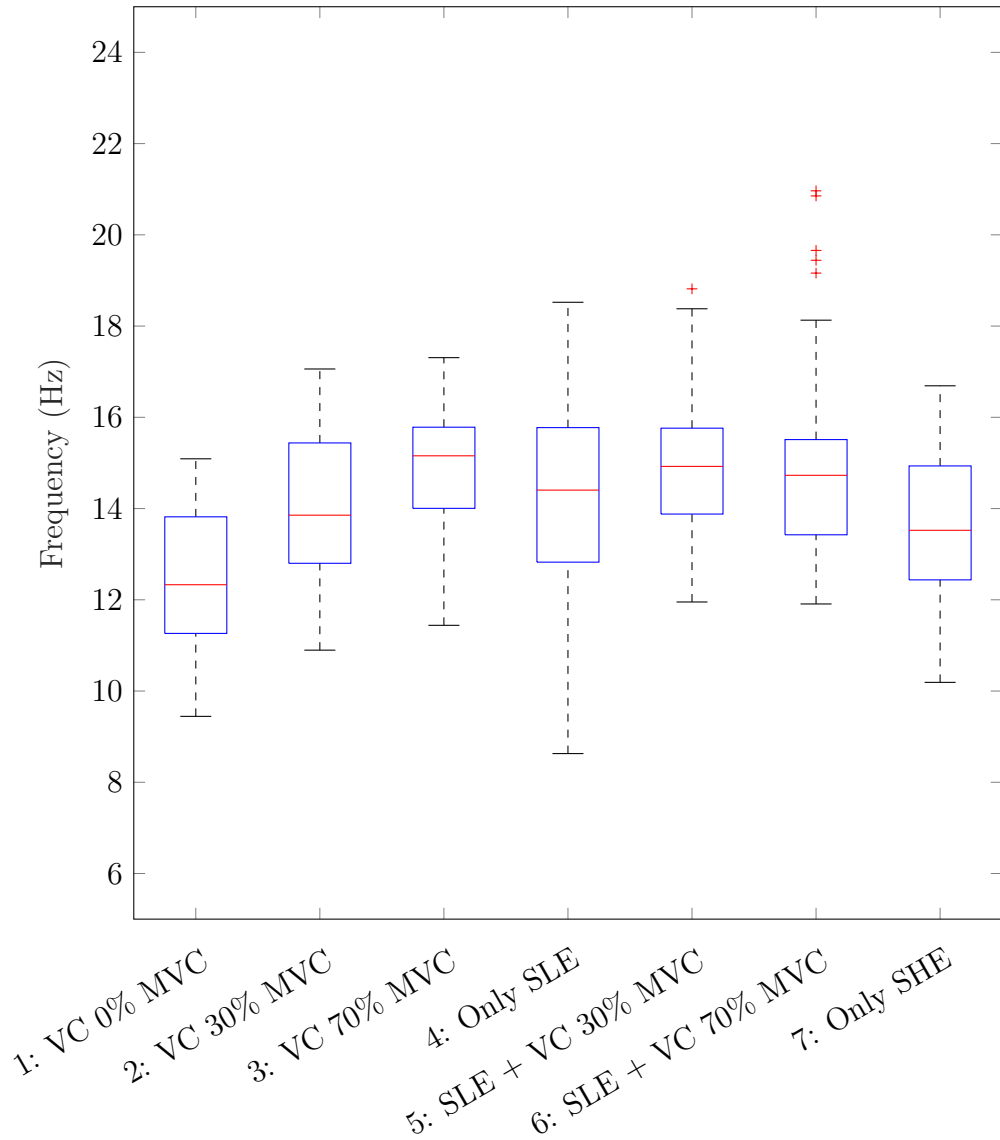


Figure 6.6: Mean frequency of Power Spectral Density (fmean) comparison between various levels of contraction (% of the MVC). Values were evaluated over 7 healthy subjects, ten repetitions of *biceps brachii* voluntary contractions (VC), stimulated with lower energy (SLE), or stimulated with higher energy (SHE).

MMG - FMED during voluntary contraction vs stimulated ones

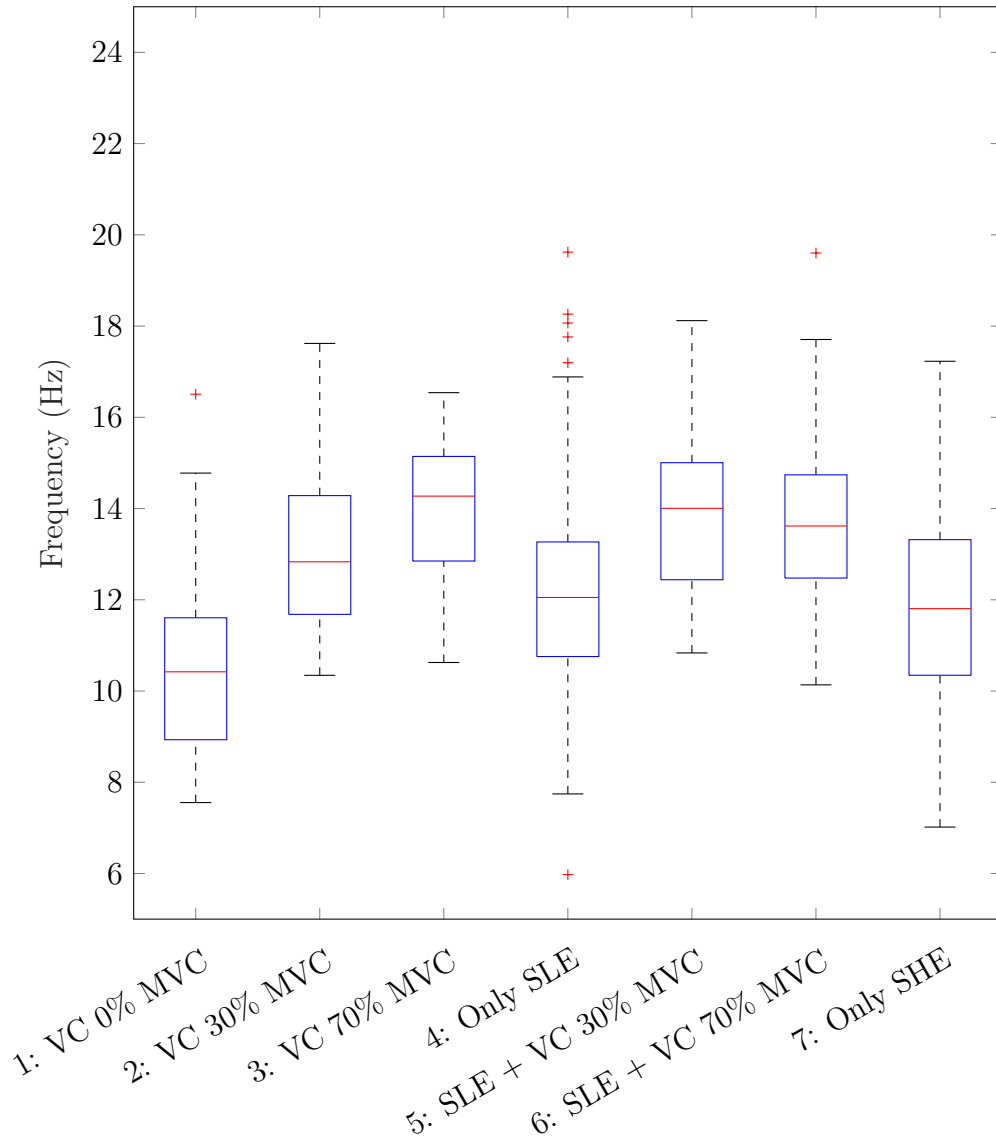


Figure 6.7: Median frequency of Power Spectral Density (fmed) comparison between various levels of contraction (% of the MVC). Values were evaluated over 7 healthy subjects, ten repetitions of *biceps brachii* voluntary contractions (VC), stimulated with lower energy (SLE), or stimulated with higher energy (SHE).

6.2.2 Statistical analysis result

However, a statistical analysis was needed in order to understand if the differences noticed in the RMS, STD, and Psum were significant.

To begin with, an investigation into the normality of the distribution was conducted using tests such as Shapiro-Wilk, Anderson-Darling, D'Agostino-Pearson omnibus, and Kolmogorov-Smirnov. However, all these tests confirmed that not all distributions were normal.

So, the Kruskal-Wallis test was used to study the statistical differences between the 7 cases in the STD, RMS, and Psum values. In particular, the results of this test are:

- for the RMS value, the *Chi-square* parameter is equal to 375.14 with a *p-value* of 6.143e-78;
- for the STD value, the *Chi-square* parameter is equal to 375.97 with a *p-value* of 6.375e-78;
- for the Psum value, the *Chi-square* parameter is equal to 364.86 with a *p-value* of 9.928e-76;

These values indicate statistically significant differences among at least some of the groups (7 cases) for each of the variables (STD, RMS, Psum) analyzed. In other words, the data distributions differ significantly across the groups for these variables, and the observed differences are unlikely to be due to chance but rather indicate genuine differences in the measured values among the cases studied.

Moreover, a pairwise comparison between each distribution is needed in order to understand which one differs from the others. So, the results of multiple comparison tests defined that there is a statistical difference between the cases in the RMS value:

- Voluntary contractions with 0 % of the MVC, 30 % of the MVC and 70 % of the MVC;
- Stimulated contractions at the same stimulation energy (lower one) with 0 % of the MVC, 30 % of the MVC and 70 % of the MVC;
- Voluntary contractions and stimulated one both at 0 % of the MVC;
- Stimulated contractions and voluntary contractions both at 30 % of the MVC.

No statistical differences were present between the stimulated contractions at 0 % of the MVC with different energy intensity; and between stimulated and voluntary contractions both at 70 % of the MVC.

Therefore, based on this analysis, assessing voluntary contributions in the MMG signal during stimulated contractions is feasible. This evaluation is particularly relevant for the goals of FES stimulation aimed at inducing neuromuscular rehabilitation. In a closed-loop system, an indicator of any voluntary activity should be present, which can be achieved through MMG measurements.

Specifically, the Root Mean Square (RMS) value of the MMG signal serves as the parameter for discriminating voluntary contributions. This choice is motivated by its computational efficiency compared to the sum of PSD while retaining all relevant information.

So, the voluntary contribution detection is performed by the comparison of contraction at the same level of stimulation energy, when an effort is needed (so a voluntary contribution must be performed to achieve the correct output), the RMS increases with the presence of a voluntary contribution.

Chapter 7

Closed-loop software

This Chapter will provide a description of the developed Closed-Loop (CL) Software (SW). Previous introduction and explanations of the system are present in Chapters 3 and 5.

A depiction of the real-time implementation, the communication between the closed-loop and the IMU and FES SW, and a first idea of how to use it in a rehabilitation session will be provided.

7.1 Closed-loop communication with IMU and FES SW

After conducting an offline evaluation of MechanoMyoGram (MMG) and angle data as discussed in Chapter 6, a real-time application has been developed. Specifically, an additional software component (CL SW) that processes data from Apollux sensors during the stimulation has been integrated into the software described in Chapter 5.

As described in Chapter 3 and in particular in Figure 3.9, the closed-loop analysis is performed thanks to the addition of a Closed-loop object and also a class system (CL System) that handles the communication with IMU and FES respective systems.

To summarize the functionality of the closed-loop SW, it receives input data from Apollux devices (MMG and roll angle) integrated over time with the corresponding injected current from the RehaStim2 (as explained in Section 5.1.2). It evaluates the state of each input by comparing a baseline level (rest) with the period when injected energy is present.

Both comparisons create an output that can be negative (indicating that muscle is not working or movement is not achieved), intermediate (indicating that there is partial muscle activity or movement), or positive (indicating that muscle is completely working or movement is achieved). These two outputs are then combined in order to give a result of the stimulation over the muscle activation and the movement performed. Afterward, this combined output will handle the update of the injected energy, which can be either increased, decreased, or kept constant.

7.1.1 System Closed-loop

The system layer of the CL SW must exchange the information with the other two system layers and with the CL object. In particular, what it does can be resumed in the:

- **Data reception:** receiving IMU data (already integrated with the injected current) from the IMU software;
- **Stimulation output delivery:** providing the stimulation results (evaluated by the CL object) to the FES software;
- **Operational message handling:** managing functional messages essential for the software's operation, such as initializing specific data structures or creating output files;
- **Communication with CL object:** commanding and cooperating with its respective object.

The connection between the systems is achieved through queues. Indeed, the System CL utilizes the same queue discussed in Chapter 5 Section 5.1.1 for the last three points of the previous bullet list.

Conversely, another queue has been created for the data exchange that links the IMU SW and the CL SW to upgrade overall SW performances. In particular, four types of data are exchanged by this queue:

- **MMG data during baseline:** contains a packet of MMG data during the baseline evaluation. For each sample in this packet, the MMG value (evaluated as MMG tot) and the muscle from which they are acquired are sent;
- **Angle data during baseline:** contains a packet of angle data during the baseline evaluation. For each sample in this packet, the roll angle value is sent;

- **MMG data after baseline:** contains a packet of MMG data during the stimulation. For each sample in this packet, the MMG value (evaluated as MMG tot), the injected current in that muscle, the timestamp of the sample, the repetition number, and the muscle from which they are acquired are sent;
- **Angle data after baseline:** contains a packet of angle data during the stimulation. For each sample in this packet, the roll angle value, the injected current, the timestamp of the sample, and the repetition number are sent;

Four types of messages are needed since the MMG data and the Angle data are evaluated in two different conditions: during a resting baseline that lasts 10s vs during FES stimulation (after baseline). Moreover, the data are processed asynchronously from the IMU SW since they are acquired from two different devices, sending them asynchronously to the CL system. Each queue is checked every 0.01s from a thread that controls the presence of a new queue message and conducts the requested operations.

In addition, one of these threads repeatedly checks the status of the outputs of the CL object that will be discussed in the following Section (7.1.2).

7.1.2 Closed-loop object

The closed-loop object is in charge of processing the data for bio-feedback. In particular, it analyses the data acquired from the IMU during the stimulation and produces two outputs (one for the muscle activations found from MMG data and the other for the reached angle) that depend on the stimulation result.

Then, the two outputs will be integrated into a single output that joins the information acquired from the muscle activations and the angle achieved. This merged output will be passed to the FES SW, upgrading its stimulation intensity based on the fused information.

This object contains different methods that perform the operation needed:

- *saveFile_init*: if the user requested to save the data acquired (by pressing the checkbox present in the IMU GUI, as seen in Chapter 5 Section 5.2.1), also a CL output file will be created. This file contains the values and the output of the CL analysis. In particular, this method initializes the output file that will be written by the other methods while the stimulation is performed.
- *initialize_dictionaries*: handles the data structures and the flags used for the CL operations. Indeed, it is called every time there is an update in the sent energy.

- *updatingFESafterClosedloop_Calibration*: combines the outputs given from the MMG data and the roll angle during the FES calibration phase. This phase will be discussed in this Chapter in Section 7.3. After a defined number of repetitions at the same injected energy are executed, the CL gives a combined output for that specific injected energy. This output can command the FES to either increase the stimulation energy (if the results are negative) or stop the calibration phase because the stimulation energy that allows to perform the complete movement (and so the MMG activation) is found.
- *updatingFESafterClosedloop_FES_Session*: combines the outputs given from the MMG data and the roll angle during the FES session phase. This phase will be discussed in this Chapter in Section 7.4 As the *updatingFESafterClosedloop_Calibration*, this method monitors at least two repetitions; if these two are equal, the stimulation parameters are updated, else there are other repetitions to obtain the output to change the parameters. After the monitoring, this method will give one output between these five cases: stop the session because there is something wrong with the starting parameters, increase the pulse width, increase the current, decrease the pulse width and the current, and good repetition. The FES session will stop when the subject executes the user's predefined number of good repetitions.
- *Angle_baseline*: saves roll angle data coming from *Distal Segment Apollux* during the 10 s baseline;
- *MMG_baseline*: saves MMG data coming from the Apollux placed on the muscle during the 10 s baseline;
- *evaluate_baselines*: after the 10 s baseline is ended, it evaluates the angle and MMG baseline. Angle is evaluated as the mean value of the samples acquired, while MMG signals are filtered with a high-pass filter with an 8th order Butterworth with a cut-off frequency of 5 Hz, then the Root Mean Square (RMS) value is evaluated;
- *euler_angle*: during the stimulation phase, it evaluates the angle baseline (when the injected current is equal to 0 mA), and the angle achieved during the activity phase (when the injected current is equal to the maximum sent current during that repetition). These values are evaluated as the mean value of the acquired samples. Then, it compares the reached angle (as the difference between the angle during the activity and rest phases) with some thresholds and determines the output of the angle. Moreover, it studies the derivative of the angle data to find the time at which the angle plateau is reached; this value will be used in the MMG evaluation.

- *MMG_amplitude*: it evaluates the MMG data during the activity phase by checking two conditions: whether the maximum injected current is present and the angle plateau is reached. This is achieved thanks to the time of the angle plateau evaluated in the method *evaluate_baselines*. The MMG value during activity is evaluated as the Root Mean Square (RMS) value of the filtered samples (MMG signals are filtered in this method with a high-pass filter with an 8th order Butterworth with a cut-off frequency of 5 Hz). Later, it compares the RMS of the MMG during the activity with thresholds imposed in the rest phase during the 10 s baseline to evaluate the MMG output.

It should be noted that for evaluating the stimulation output, both MMG and roll angle require threshold imposition. These thresholds are assessed in two different ways. The developed software uses the closed-loop (CL) system for two purposes: evaluating the correct stimulation energy needed for a subject to perform a full movement and a stimulation session aimed at the patient's rehabilitation. The implementation of the closed-loop system will be described later in Sections 7.3 and 7.4, where the threshold values will also be discussed.

However, it is important to highlight the asynchronicity in evaluating the outputs of the MMG and angle data, as the data is collected from two different Apollux devices. Data from the IMU software is received and processed in two separate threads, resulting in asynchronous transmission to the CL system. Consequently, two separate methods (one for the angle and one for the MMG) independently evaluate the stimulation output.

Finally, the combined output is assessed using another method, recalled by the CL System, once both outputs have been evaluated.

7.2 Introduction of the closed-loop operations and explanation of the area of FES GUI dedicated to the closed-loop.

Using the CL SW developed, there are two phases to follow. The first is the FES calibration, which searches for the stimulation parameters that allow the subject to complete the movement. After these parameters are defined, it is possible to execute the second phase, the FES session, which consists of the rehabilitative part of the protocol and uses stimulation parameters established in the FES calibration.

Figure 7.1 represents the FES GUI area allocated to the closed-loop operations.

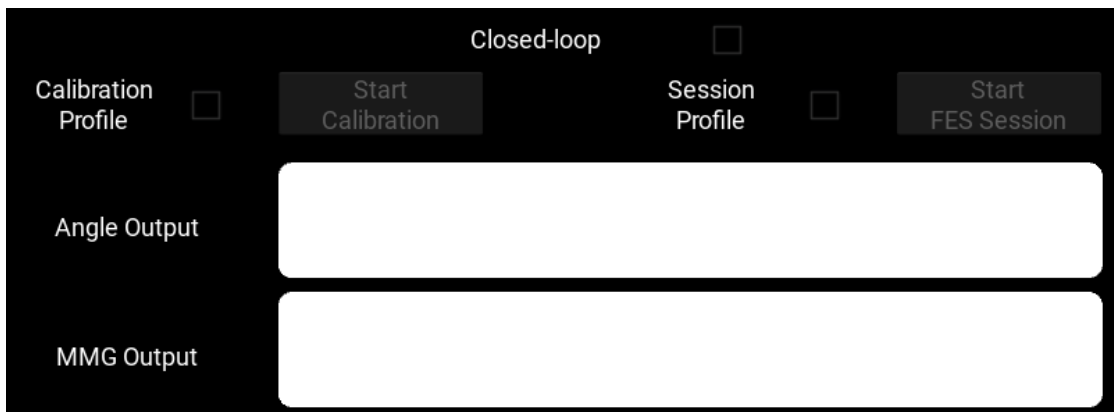


Figure 7.1: FES GUI area dedicated to the closed-loop: there is a checkbox to select which phase to do, and next to the checkbox, there is the relative button to start the chosen phase. The two text input spaces are for the output from the roll angle (that in the top) and the MMG (that in the bottom).

As illustrated in Figure 7.1, there are two checkboxes: one for the "*Calibration Profile*" and the other for the "*Session Profile*". When one of these checkboxes is active, the relative stimulation profile will be shown on the FES GUI. Next to each checkbox, there is a button: *Start Calibration*, and *Start FES session*. Thus, when one checkbox is selected, the relative button will be enabled, and by pressing it, the picked phase will start.

The stimulation profile of FES calibration is predefined based on the stimulation parameters imposed for this phase. Thus, the first stimulation profile of the calibration phase is always the same. There are the firsts 4.5s of rest, then 5s of stimulation.

Instead, the stimulation profile of the FES session is the last profile used during the previous FES calibration. Indeed, before performing the FES session, it's necessary to execute the FES calibration to obtain the optimal parameters to stimulate the subject. During the FES session, there are 4 s of initial rest, 5 s of stimulation and then 6 s of rest.

In Figure 7.2, the starting stimulation profile of the FES calibration phase for the *biceps brachii* during the *elbow flexion* is illustrated.

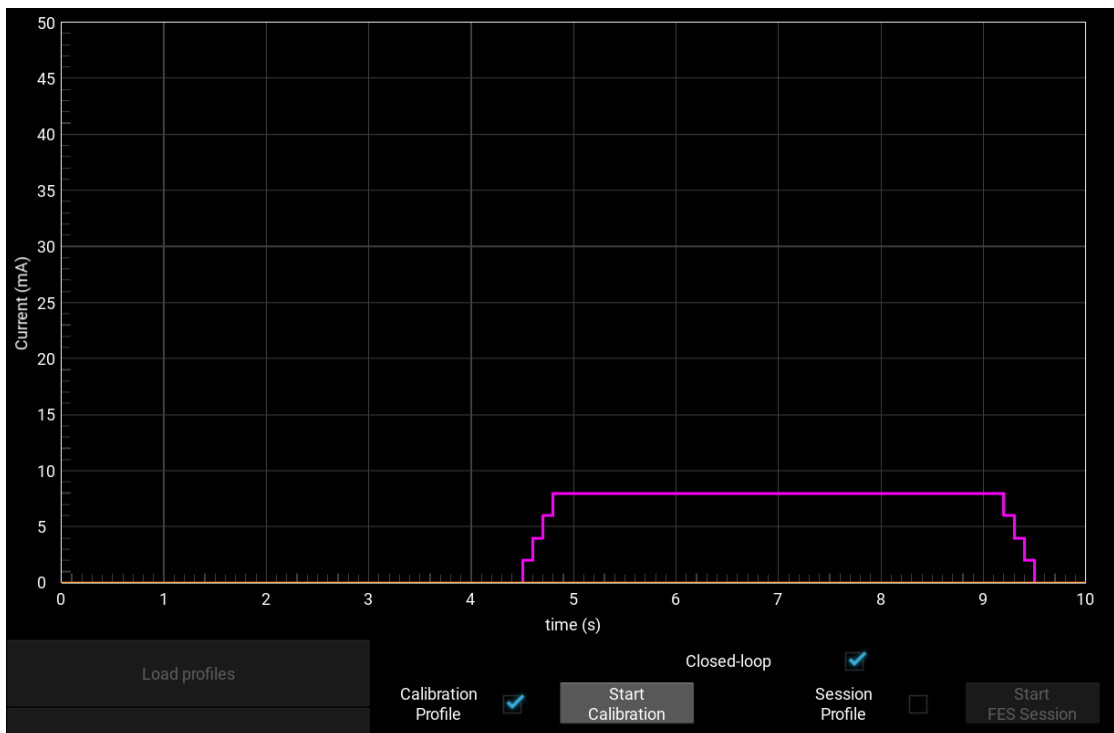


Figure 7.2: FES calibration starting stimulation profile: this is the starting stimulation profile for the *biceps brachii*. For each repetition, there are 4.5 s of rest, then 5 s of stimulation. In the case of calibration for the *biceps brachii*, the initial current is set to 8 mA, the pulse width to 130 μ s, and the rise and fall steps to reach the plateau are 4.

There are two blank spaces under the checkboxes and the buttons; this area is destined to print the outputs from the closed loop. As indicated from the label next to the spaces, the top space will produce the output relative to the roll angle signal, while the bottom is for the output of the MMG signal.

7.3 The FES calibration driven by closed-loop system

7.3.1 FES calibration aim and functioning

The FES calibration aims to determine which stimulation parameters, solely through electrical stimulation and without the subject's active participation, enable the subject to realize the full movement.

In fact, the subject is expected to engage in this phase only by allowing the electrical stimulation to accomplish the required action without providing any intentional contribution.

During the FES calibration, the energy stimulation is progressively increased based on the subject's response. The stimulation parameters increase during this phase until the participant reaches the predetermined AROM. As a result, the FES calibration ends when the planned movement is completed.

A Look Up Table (LUT) is implemented based on the actual energy required, indicating the necessary increases in pulse width and current to achieve this energy gain. The energy increase begins at 100 % and progresses to around 3 %.

A customized LUT is realized for each stimulated muscle since the RehaStim2 handbook specifies the proper pulse width based on the muscle to stimulate. Table 7.1 displays the LUT designed for the *biceps brachii*, and Table 7.2 that for the quadriceps. In the case of the *biceps brachii*, the FES calibration starts from the fourth step (Current at 8 mA, Pulse Width at 130 μ s); instead, in the case of the *quadriceps femoris*, the FES calibration starts from the sixth step (Current at 12 mA, Pulse Width at 250 μ s).

It is evident from both LUTs that in order to achieve a significant increase in total energy, the current was raised solely during the first calibration steps. Then, when it is almost at the current level that most people are stimulated, the current is increased once to 2 mA, and the pulse width is increased once to 10 μ s.

Table 7.1: Look Up Table (LUT) of stimulation parameters. Energy increases, current, and pulse width are adapted to stimulate the arm flexors, particularly the *biceps brachi* during the *elbow flexion*.

Real Energy (A s)	Energy Increase (%)	Current (mA)	Pulse Width (μ s)
2.6e-07	0.00	2	130
5.2e-07	100.00	4	130
7.8e-07	50.00	6	130
1.0e-06	33.33	8	130
1.3e-06	25.00	10	130
1.6e-06	20.00	12	130
1.7e-06	7.69	12	140
2.0e-06	16.67	14	140
2.1e-06	7.14	14	150
2.4e-06	14.29	16	150
2.6e-06	6.67	16	160
2.9e-06	12.50	18	160
3.1e-06	6.25	18	170
3.4e-06	11.11	20	170
3.6e-06	5.88	20	180
4.0e-06	10.00	22	180
4.2e-06	5.56	22	190
4.6e-06	9.09	24	190
4.8e-06	5.26	24	200
5.0e-06	4.17	25	200
5.2e-06	4.00	26	200
5.4e-06	3.85	27	200
5.6e-06	3.70	28	200
5.8e-06	3.57	29	200
6.0e-06	3.45	30	200

Table 7.2: Look Up Table (LUT) of stimulation parameters. Energy increases, current, and pulse width are adapted to stimulate the leg extensors, particularly the *quadriceps femoris* during the *knee extension*.

Real Energy (A s)	Energy Increase (%)	Current (mA)	Pulse Width (μ s)
5.0e-07	0.00	2	250
1.0e-06	100.00	4	250
1.5e-06	50.00	6	250
2.0e-06	33.33	8	250
2.5e-06	25.00	10	250
3.0e-06	20.00	12	250
3.5e-06	16.67	14	250
4.0e-06	14.29	16	250
4.5e-06	12.50	18	250
4.9e-06	8.00	18	270
5.4e-06	11.11	20	270
5.8e-06	7.41	20	290
6.4e-06	10.00	22	290
6.8e-06	6.90	22	310
7.4e-06	9.09	24	310
7.9e-06	6.45	24	330
8.6e-06	8.33	26	330
9.1e-06	6.06	26	350
9.8e-06	7.69	28	350
1.0e-05	5.71	28	370
1.1e-05	7.14	30	370
1.2e-05	5.41	30	390
1.2e-05	6.67	32	390
1.3e-05	5.13	32	410
1.4e-05	6.25	34	410
1.5e-05	4.88	34	430
1.5e-05	5.88	36	430
1.6e-05	4.65	36	450
1.7e-05	5.06	37	460
1.8e-05	4.94	38	470
1.9e-05	4.82	39	480
2.0e-05	4.70	40	490
2.1e-05	4.59	41	500
2.1e-05	2.44	42	500
2.2e-05	2.38	43	500
2.2e-05	2.33	44	500
2.3e-05	2.27	45	500
2.3e-05	2.22	46	500
2.4e-05	2.17	47	500
2.4e-05	2.13	48	500
2.5e-05	2.08	49	500
2.5e-05	2.04	50	500

7.3.2 FES calibration outputs

The first part of this subsection illustrates the distinct output from the MMG signal and the Roll angle signal, and then the last part of this subsection reports their combined output.

Single repetition outputs

The thresholds imposed over the MMG signal and the angle data will be discussed. In particular, in both measurements, three possible states are evaluated:

- No muscle activity (from MMG data) or no movement (from roll angle data);
- Partial muscle activity (from MMG data) or partial movement (from roll angle data);
- Complete muscle activity (from MMG data) or complete movement (from roll angle data).

Starting with the analysis of the muscle activation by the data collected with the MMG signal, the resting value of the MMG has been evaluated as the Root Mean Square (RMS) during the first 10 s of baseline. Indeed, when the FES calibration starts, there are these firsts 10 s in which only the IMU acquisition is running to collect the MMG data from the rest position. Instead, the activity zone of each repetition is considered as the moment in which the current reaches its maximum value for that repetition, and the angle achieves a plateau state. Also, during the activity, the MMG value was calculated as the RMS of the samples that respect the two conditions.

The thresholds imposed have been found from experimental data, and they are:

- **Muscle is not active:** MMG during activity doesn't reach 110 % of the MMG during rest;
- **Muscle is partially active:** MMG during activity is comprise between 110 % and 130 % of the MMG during rest;
- **Muscle is completely active:** MMG during activity overcomes 130 % of the MMG during rest.

On the other hand, regarding the roll angle data, the baseline value of the angle is calculated for each repetition. Despite the roll angle data being acquired in the firsts 10 s of baseline, it was preferred not to consider that rest position as the angle baseline but to update the angle baseline each repetition because it's possible that after the stimulation the subject's arm doesn't return exactly in the initial position.

Thus, to calculate the baseline angle, the firsts 4.5 s are collected, and to obtain the angle value, the mean of these data is computed. To measure the angle of the plateau, the roll angle data at maximum current is averaged. The last operation, to get the real angle reached by the subject during the activity, is the difference between the angle of the plateau and the baseline angle.

Moreover, before the FES calibration phase, the subject must perform the *AROM estimation*. Indeed, the angle values reached during the activity are compared to some percentage of the AROM estimated. Also, for the roll angle, some thresholds are imposed to distinguish the three cases:

- **No movement:** angle during the activity doesn't reach the 20 % of the AROM;
- **Partial movement:** angle during the activity is comprised between 20 % and 70 % of the AROM;
- **Complete movement:** angle during the activity reach at least the 70 % of the AROM.

Output of a certain stimulation energy

After the distinct output from the MMG and the roll angle signal are obtained, these are joined in a combined output produced for every repeat. It should be noted that changing the stimulation parameter requires at least two repeats rather than just one. In fact, the final result is generated, and the stimulation parameters are changed if the aggregate output from the two subsequent repetitions is the same. Rather, if the cumulative output from the first two repetitions differs, a third repetition is performed and considered as the final result, which is provided twice over the three repetitions.

There are three possible final outputs and their functions can be resumed in this way:

- There is neither muscle activity nor movement: increase the energy stimulation of two steps into the LUT;
- There is partial or complete muscle activity and a partial movement: increase the energy stimulation of one step into the LUT;
- There is muscle activity and complete movement: stop the FES calibration phase because the optimal stimulation parameters are found.

Table 7.3: Combined output of a single repetition during the FES calibration: it is possible to see which operation follows the combined output for all possible output combinations. This table represents how the combined output is obtained for each single repetition.

Movement achieved corresponds to stopping the FES calibration because optimal stimulation parameters are found. All other cases involve an increase in stimulation energy.

MMG output (<i>activity</i>)	Angle output (<i>movement</i>)		
	Not detected	Partial	Complete
Not detected	+2 LUT step	+1 LUT step	+1 LUT step
Partial	+1 LUT step	+1 LUT step	+1 LUT step
Complete	+1 LUT step	+1 LUT step	Movement Achieved

All the outputs generated can be resumed in Table 7.3, which reports how the combined outputs are obtained for each repetition.

Figure 7.3 illustrates three MMG and angle output examples. Figures 7.3a and 7.3b represent the case in which neither muscle activity nor movement is detected; the combined output will be *+2 LUT step*. Figures 7.3c and 7.3d represent the case in which complete muscle activity and partial movement are detected; the combined output will be *+1 LUT step*. Finally, Figure 7.3e and 7.3f is the case in which complete muscle activity and movement are found; the FES calibration will stop.



(a) MMG and angle outputs indicate that there isn't muscle activity and no movement.



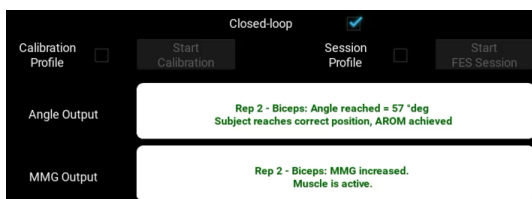
(b) Subject's arm position for the outputs in (a).



(c) MMG and angle outputs indicate muscle activity and partial movement.



(d) Subject's arm position for the outputs in (c).



(e) MMG and angle outputs indicate muscle activity and complete movement.



(f) Subject's arm position for the outputs in (e).

Figure 7.3: Example of distinct output of MMG and angle during the FES calibration phase. The combined output will be: figure (a) +2 LUT step, figure (c) +1 LUT step, and figure (e) stop FES calibration. The figures (b), (d), and (f) represent the subject's arm position during the stimulation to achieve that specific output.

7.4 The FES session driven by closed-loop system

7.4.1 FES session aim and functioning

FES session implements the closed-loop real approach during a rehabilitative session.

It aims to achieve a predefined number of 'good repetitions', which provide an angle that reaches the evaluated AROM. When a good repetition happens, the

stimulation energy should be kept constant because the subject performs the full movement.

The FES session has been developed in two different ways to evaluate two different rehabilitative scenarios:

- Voluntary contribution does not affect the number of good repetitions: all repetitions that achieve an angle within the AROM guidelines are considered good repetitions, regardless of voluntary contribution. In this FES session, while the software evaluates the presence of voluntary contributions, repetitions are still considered good even if no voluntary contribution is detected. The target is to achieve 10 good repetitions;
- Voluntary contribution affects the number of good repetitions: only repetitions with detected voluntary contribution are considered good. In this FES session, the goal is to perform 5 good repetitions. Even though repetitions without voluntary contributions are not considered good, they are still monitored and counted. If the achieved angle meets the AROM guidelines, and no voluntary contribution is detected, the injected current is reduced by 1 mA after 5 such repetitions. Once the current is lowered by 1 mA, full movement cannot be achieved by stimulation alone, requiring the subject to voluntarily contribute to reaching the imposed AROM.

On the other hand, the iterations that do not provide these conditions are considered 'bad repetitions'. When they occur, an increase or decrease in the injected energy is needed.

In particular, the FES session starts with the energy that allows the patient to perform the full movement without an intentional contribution. This energy is found in the calibration phase (which must be performed before it).

The subject is stimulated for 5 s, and before and after the stimulation, there is rest, respectively 4 s and 6 s. The angle baseline is evaluated during the 4 s rest prior to the stimulation (before every repetition), while the baseline for the MMG data is evaluated during a previous 10 s baseline at the beginning of FES session.

So, various repetitions are performed till the good repetitions achieved are equal to the required number. However, the effect of the stimulation over the subject and the presence of voluntary contractions dynamically vary during the various stimulation iterations, so a change in the stimulation parameters is needed in order to achieve the number of good repetitions imposed.

The following Section 7.4.2 will provide a detailed description of the calculations performed by the CL object for counting the reached angle and detecting voluntary

contribution. Additionally, it will cover the changes in injected energy based on the results obtained from muscle and movement analysis.

7.4.2 FES session outputs

Specific thresholds for the MMG and angle data have been set for the closed-loop evaluation of muscle activity and movement outputs. These thresholds assess the differences between values recorded during a baseline state (rest) and activity. Additionally, certain criteria are used to combine the results of the MMG and angle data. This section will explain the reasoning behind these decisions.

Voluntary contribution discrimination

During the FES session, the presence of a voluntary contribution has been evaluated. In particular, thanks to a first acquisition explained in Chapter 6, it has been discovered that there is a statistical difference between the MMG evaluated with the presence of a voluntary contribution and during purely stimulated contractions. To evaluate the effect of the voluntary contribution during FES contractions, the voluntary contribution has been standardized by the use of a weight corresponding to 30 % or 70 % of the MVC. Indeed, when considering the same amount of injected energy, the stimulation cannot lift the weight alone, so a voluntary contribution must be added.

In particular, the MMG Root Mean Square (RMS) value has been compared during the performance of both voluntary and stimulated contractions. It has been found in Section 6.2 that there is a statistical difference between the values of stimulated contraction with the same stimulation intensity when considering only stimulated contractions and the ones with a fixed % of the MVC. The same results are present when considering voluntary contractions during the increase of % of the MVC.

From these results, we conclude that a voluntary contribution can be seen when considering the difference between purely stimulated contractions (performed without any % of the MVC) and the presence of voluntary contribution (in the presence of a weight corresponding to a certain amount of % of the MVC).

However, a threshold should be imposed over the real-time acquired MMG data for this discrimination. Especially this threshold has been searched through the acquisition of over 10 subjects that will be explained in Chapters 8 and 9. In this experimental analysis, the MMG RMS value acquired during the calibration

phase in the last energy step (the one that makes the full movement performed) has been considered as the MMG value during purely stimulated contractions since, in the calibration phase, the subject is asked to do not perform any voluntary contribution.

It has resulted that a threshold of 120% with respect to the MMG RMS value during purely stimulated contraction allows detection of the voluntary contribution for 30% of the MVC case with an accuracy of 90%.

Single repetition outputs

The imposed thresholds for the MMG signal and the angle data will now be examined. Notably, in both measurements, various states are considered. Beginning with the analysis of muscle activation using the data collected from the MMG signal, the potential activation states are:

- No muscle activity;
- Muscle activity but no voluntary contribution;
- Muscle activity and voluntary contribution.

The resting and activity values of the MMG have been assessed using the Root Mean Square (RMS) of the collected samples. Specifically, the rest value is measured during a 10 s baseline period. The activity phase is defined by two conditions: the maximum injected current and the angle reaching a plateau state.

The experimental data led to the determination of the following thresholds:

- **Muscle is not active:** MMG during activity does not reach 120% of the MMG during rest;
- **Muscle is active but no voluntary contribution is present:** MMG during activity overcomes 120% of the MMG during rest, but does not overcome the 120% of the MMG during purely stimulated contractions;
- **Muscle is active and voluntary contribution is present :** MMG during activity overcomes 120% of the MMG during rest, and the 120% of the MMG during purely stimulated contractions.

On the other hand, regarding the roll angle data, the baseline value is determined by computing the average of the acquired data when the injected current is equal to 0 mA. The roll angle data at maximum current are averaged to find the plateau angle. The actual angle reached during the activity is the difference between the

plateau and baseline angles.

The selected thresholds are:

- **No movement:** Reached angle does not overcome 20 % of the AROM;
- **Partial movement:** Reached angle does overcome 20 % of the AROM but not the 70 % of the AROM;
- **Complete movement:** Reached angle is comprehended in the range between 70 % of the AROM and 120 % of the AROM;
- **Excessive movement:** Reached angle overcomes 120 % of the AROM.

Output of a certain stimulation energy

After evaluating both MMG and angle outputs, the closed-loop system generates a combined output that considers both muscle activation and the performed movement.

Regarding the FES session, there are 2 types of rehabilitative approaches considered:

- *Type A:* Voluntary contribution does not influence the number of good repetitions. Repetitions within the AROM guidelines are considered good, regardless of voluntary effort. The objective is to complete 10 good repetitions;
- *Type B:* Voluntary contribution impacts the number of good repetitions. Only repetitions with detected voluntary effort are counted as good, and 5 such repetitions are required. Additionally, if the achieved angle meets the AROM guidelines without detected voluntary contribution (good no voluntary repetition), the injected current is reduced by 1mA after 5 of these repetitions. This reduction aims to enhance the subject's effort in performing good repetitions.

There is a minor difference in the outputs generated by the combined results between these two types of FES sessions. Table 7.4 shows the final outputs for type A FES sessions, while Table 7.5 presents the outputs for type B. The distinction lies in the case of a complete movement (angle) with no voluntary activity (MMG): in type A, it is counted as a good repetition, whereas in type B, it is considered a good no voluntary repetition.

The effectiveness of a specific amount of injected energy is evaluated through three repetitions. If the first two repetitions yield the same output, the third repetition is not performed, as the result is already determined.

Table 7.4: Combined repetition output, FES session: MMG Output vs Angle Output. Some conditions are abbreviated, in particular, 'Good rep' is Good repetition, and 'Calib error' is calibration error. 10 good repetitions must be achieved during this protocol.

MMG output (<i>activity</i>)	Angle output (<i>movement</i>)			
	Not detected	Partial	Complete	Over
Not detected	Calib error	Calib error	Calib error	Calib error
No Voluntary	+1 mA	+1 mA	Good rep	-(10 μ s and 2 mA)
Voluntary	+20 μ s	+20 μ s	Good rep	-(10 μ s and 2 mA)

Table 7.5: Combined repetition output, FES session: MMG Output vs Angle Output. Some conditions are abbreviated; in particular, 'Good rep' is Good repetition, 'No vol rep' is good no voluntary repetition, and 'Calib error' is calibration error. 5 good repetitions must be achieved during this protocol. If 5 good no voluntary repetitions are achieved, the current is decreased by 1 mA.

MMG output (<i>activity</i>)	Angle output (<i>movement</i>)			
	Not detected	Partial	Complete	Over
Not detected	Calib error	Calib error	Calib error	Calib error
No Voluntary	+1 mA	+1 mA	No vol rep	-(10 μ s and 2 mA)
Voluntary	+20 μ s	+20 μ s	Good rep	-(10 μ s and 2 mA)

Figure 7.4 illustrates three MMG and angle output examples. Figures 7.4a and 7.4b represent the case in which partial movement and no voluntary activity are detected; the closed-loop combined output will be *increase the current of 1 mA*. Figures 7.4c and 7.4d the case with a complete movement but no voluntary activity detected, the output will be *+1 Good No voluntary repetition*. On the other hand, in Figures 7.4e and 7.4f the case with complete movement and voluntary activity, the combined output will be *+1 Good repetition*.

In Figure 7.5 there is an example of the real-time closed-loop SW during the FES session. In particular, the upper portion of the image contains the FES SW, while the second part the IMU SW. It is possible to see that the outputs of the closed-loop are given in real-time and they correctly correspond to the movement and type of contraction displayed.



(a) MMG output does not detect voluntary contribution, the angle does not provide full movement.



(b) Subject's arm position for the outputs in (a).



(c) MMG output does not detect voluntary contribution, the angle provides full movement.



(d) Subject's arm position for the outputs in (c).



(e) MMG output detects voluntary contribution, the angle provides full movement.



(f) Subject's arm position for the outputs in (e).

Figure 7.4: Example of distinct output of MMG and angle during the FES session phase. The combined output will be: figure (a) + 1 mA, figure (c) +1 Good No Voluntary Repetition, and figure (e) +1 Good Repetition. The figures (b), (d), and (f) represent the subject's arm position during the stimulation to achieve that specific output.

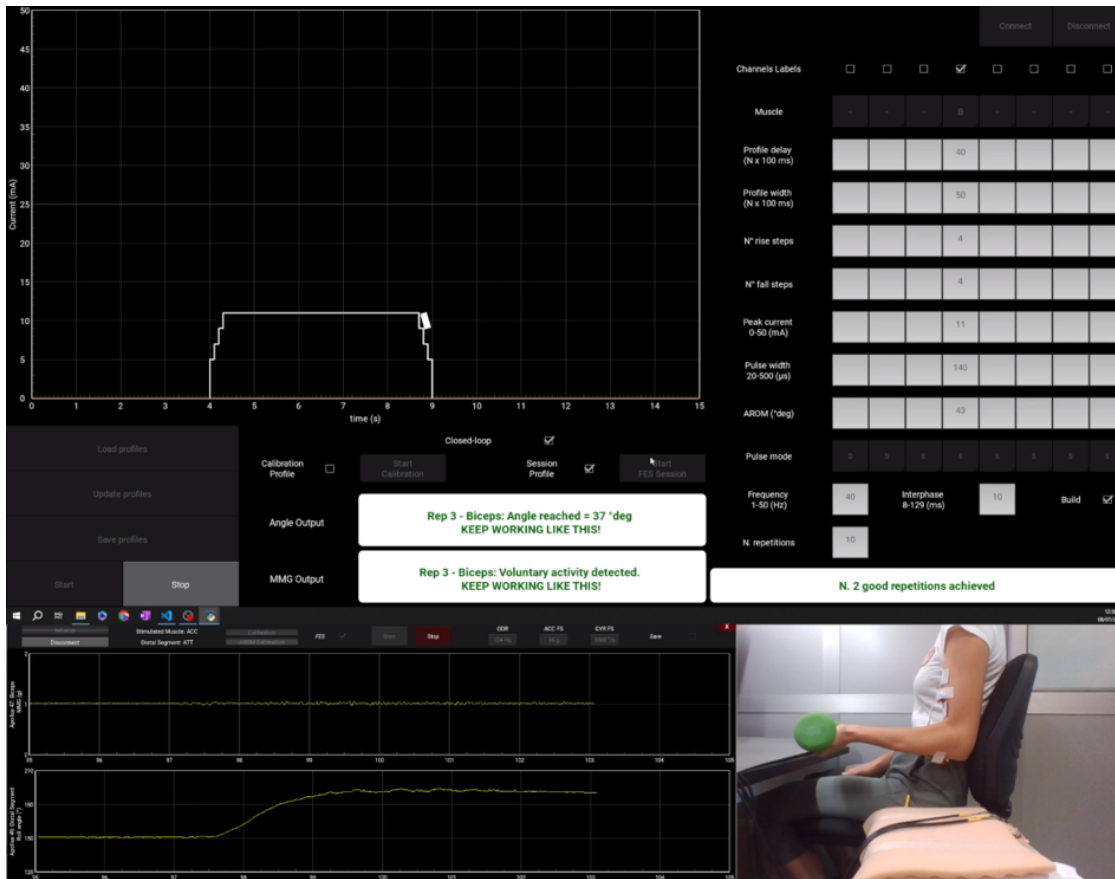


Figure 7.5: Real-time closed-loop software example. The upper part of this image contains the FES SW with the stimulation profile. The lower part is the IMU SW with two plots: the first one contains the MMG signal detected from the *biceps brachii*, while the second one is the roll angle from the *distal segment*. It is possible to see in real-time the movement performed (complete movement) and the activation level (voluntary contraction due to a weight corresponding to the 30%MVC). The outputs given by the closed-loop correspond to the contraction performed in the image. So, the software is correctly detecting the type of contraction and movement.

Chapter 8

Experimental Protocols description

This chapter will outline the two experimental procedures that were carried out to confirm that the closed-loop system created for the FES control was operating as intended.

The *first protocol* uses various MVC percentages to determine a threshold for detecting voluntary muscular activation during FES with the CL SW. Rather, the *second protocol* aims to improve the system's responsiveness in a simulated actual scenario by employing an elastic band to represent a sick patient.

8.1 First Protocol

During functional electrical stimulation, the first protocol's goal was to determine a threshold that would permit the identification of intentional contribution. The FES calibration and the FES session driven from a closed-loop system were tested in this protocol.

The aim of this trial was to examine how varying MVC percentages affect the ability to identify a purposeful contraction. Moreover, 0%, 10%, 20%, 20%, and 30% of the MVC of each subject were used in the execution of this protocol. This protocol includes two different muscles and movements: the *biceps brachii* during the *elbow flexion*, and the *quadriceps femoris* performing the *knee extension*.

The protocol, followed for both the muscles, is divided into three main sections:

1. **Estimation of the MVC and the AROM:** first of all, it is necessary to determine for each subject the value of the MVC that each subject can achieve with the muscle taken into consideration and the AROM reached by the subject to perform the desired movement.
2. **FES calibration:** this automated phase was explained in the Chapter 7, Section 7.3. This calibration serves to determine the optimal stimulation parameters for each subject to execute the wanted motion. Each repetition of calibration starts with 4.5s of rest followed by 5s of stimulation.
3. **FES session:** this phase was described in the Chapter 7, Section 7.4.2 considering as rehabilitative approach the *Type A*. In this protocol, the FES session was executed considering four cases:
 - Purely Stimulated;
 - 10 % of the MVC;
 - 20 % of the MVC;
 - 30 % of the MVC.

The FES session consists of performing 10 good repetitions for each of these four cases. Good repetition means a repetition in which there is a complete movement, and the presence of voluntary contribution could or could not be detected. During the FES session, the stimulation profile consists of 4s of initial rest, followed by 5s of stimulation and then 6s of rest.

In this test, 11 subjects participated in the study on the *biceps brachii*, and 10 subjects on the *quadriceps femoris*. They were all required to sign a permission waiver and were told of all phases prior to the test's beginning. They all participated in the experimental protocol for the intended purpose. In addition, after all protocol phases are finished, each participant is required to complete a survey to share their thoughts on the experiment.

Women constitute 70% of the volunteers. Each participant, who is between the ages of 23 and 28, can decide to engage both of their muscles on the right or left side.

8.1.1 Experimental set-up for *biceps brachii* performing an *elbow flexion*

As mentioned before, the first phase of this experimental protocol involves estimating the subject's maximal voluntary contraction (MVC). Thus, the subject must perform her/his maximal contraction using a dynamometer. The dynamometer utilised in this protocol is the same cited in Chapter 6, Section 6.1.2. Figure 8.1 illustrates how the MVC estimation is done. The subject standing in front of a support to which the dynamometer is fixed; from this position, he/she must execute the contraction.



Figure 8.1: Estimation of Maximal Voluntary Contraction (MVC) of *biceps brachii* performing the *elbow flexion*: this is the experimental set-up followed during the measure of the MVC of each subject.

After the estimation of MVC, the subject assumes the rest position that will be maintained for all the remaining phases. Indeed, during the trial, the subject executes all the tests sitting on an office chair. The patient's back should be well supported against the backrest. Next to her/his is a stool with support to which the subject leans her/his forearm. The angle formed from the position of *distal segment* with respect to the vertical axis is about 45° . The acquisition system

comprehends two Apollux devices, one on the belly of *biceps brachii* and the other on the back of the *forearm*, they communicate via BLE 4.0 with a dongle BLE connected to a PC. Both the two Apollux devices are fixed to the subject using a biomedical tape. The two stimulation electrodes are put on the belly of *biceps brachii*.

Before starting with the FES calibration and session phases, the AROM evaluation is also performed. The initial position of this phase is just described and illustrated in Figure 8.2b.

This phase lasts 10 s: the roll angle data from the firsts 5 s are collected and then mediated to obtain the angle baseline, and the maximum reached angle in the last 5 s is taken as max angle value. The AROM value is the difference between the max angle value and the angle baseline.

In Figure 8.2, there is an illustration of the experimental setup. Figure 8.2a shows how the Apollux device that collects angle data is positioned on the *distal segment*. Figure 8.2b exhibits the initial and resting position explained before. Figure 8.2c illustrates how the Apollux device that records MMG data and the stimulation electrodes are placed on the belly of *biceps brachii*.



(a) Apollux device positioned on the *distal segment*.



(b) Starting and rest position of *biceps brachii* contractions.



(c) Apollux and stimulation electrodes positioned on the *biceps brachii*.

Figure 8.2: Electrode placement and resting position of arm: in figure (a) there is the placement of the Apollux device of the *distal segment* (collecting Euler's angles); (b) resting position (during all tests, the subject must always return to this position, which is the reference position); (c) Apollux device on the *biceps brachii* (acquiring MMG data) and stimulation electrodes.

Table 8.1 resumed subjects' data as gender, age, side, MVC estimated, and AROM evaluated during the *biceps brachii* acquisition.

Table 8.1: Subjects data during the first experimental protocol. The studied muscle is the *biceps brachii* during the *elbow flexion*. For each subject are indicated gender, age, side, MVC value in kg, and AROM value in °.

Subject n.	Gender	Age	Side	MVC (kg)	AROM (°)
1	F	24	Left	6	50
2	F	27	Left	8	52
3	M	23	Left	8.5	54
4	M	25	Right	15	45
5	F	25	Right	6	39
6	F	24	Left	6.5	47
7	F	25	Left	15	55
8	M	24	Left	10	64
9	F	28	Left	10	49
10	F	27	Left	6.5	40
11	F	24	Right	7	53

In the case of the *biceps brachii* executing a *elbow flexion*, the FES calibration starts from the fourth step of Table 7.1. Thus, the first stimulation parameters are current 8 mA, pulse width 130 μ s, and there are four steps of rise and fall to reach the plateau of maximum current for each repetition.

As explained in Chapter 6 during Section 7.3, for each step of the LUT are executed at least two repetitions. A key point of this phase is that the subject must be completely relaxed during all calibration. If the first two repetitions done with those parameters provide the same angle and MMG output, based on the produced combined output, the energy stimulation will increase (of one or two steps in LUT), or the FES calibration will be stopped. Instead, if the combined outputs from the two repetitions are different, a third repetition will be executed to establish what to do.

The FES calibration will be stopped when the optimal parameters to achieve a complete *elbow flexion* stimulating the *biceps brachii* are found. The optimal energy level of each subject is reported in Table 8.2. The current measured in mA, and the pulse width in μ s reaches from each volunteer at the end of FES calibration are illustrated.

Once the ideal stimulation parameters are obtained, they are used to stimulate the subject during all four cases of the FES session. Between one trial and the following one, there are 5 min of rest.

Table 8.2: Each subject's stimulation parameters during the experimental protocol. The studied muscle is the *biceps brachii* during the *elbow flexion*. For each subject are shown Current (C) and Pulse Width (PW) at the Optimal Energy level.

Subject n.	C (mA)	PW (μ s)
1	18	160
2	18	160
3	14	150
4	28	200
5	14	150
6	20	180
7	18	170
8	16	160
9	18	160
10	24	190
11	26	200

8.1.2 Experimental set-up for *quadriceps femoris* performing an *knee extension*

As for the *biceps brachii*, also for the *quadriceps femoris*, the trial starts with the estimation of the subject's maximal voluntary contraction (MVC). Thus, the subject must perform her/his maximal contraction using the dynamometer cited in Chapter 6, Section 6.1.2. Figure 8.3 illustrates how the MVC estimation for the *quadriceps femoris* is executed. The subject, sitting on an office chair, must execute the contraction pulling up the dynamometer fixed to the chair's base.



Figure 8.3: Estimation of Maximal Voluntary Contraction (MVC) of *quadriceps femoris* performing an *knee extension*: this is the experimental set-up followed during the measure of the MVC of each subject.

After the estimation of MVC, the subject assumes the rest position that will be maintained for all the remaining phases. Indeed, during the trial, the subject executes all the tests sitting on an office chair. The patient's back should be well supported against the backrest. The subject is placed in front of a box, with the foot of the leg to stimulate resting on it. Particularly is the heel that is leaned to the box.

The angle formed from the position of the *distal segment* with respect to the vertical axis is about 45° . The acquisition system comprehends two Apollux devices, one on the belly of *quadriceps femoris* and the other on the *tibia*. They communicate via BLE 4.0 with a dongle BLE connected to a PC. Both Apollux devices are fixed to the subject using a biomedical tape. The two stimulation electrodes are put on the belly of *quadriceps femoris*.

Before starting with the FES calibration and session phases, the AROM evaluation is also performed. The initial position of this phase is just described and illustrated in Figure 8.4b.

This phase lasts 10s: the roll angle data from the firsts 5s are collected and then mediated to obtain the angle baseline, and the maximum reached angle in the last 5s is taken as max angle value. The AROM value is the difference between the max angle value and the angle baseline.

In Figure 8.4, there is an illustration of the experimental setup. Figure 8.4a shows how the Apollux device that collects angle data is positioned on the *distal segment*. Figure 8.4b exhibits the initial and resting position explained before. Figure 8.4c illustrates how the Apollux device that records MMG data and the stimulation electrodes are placed on the belly of *quadriceps femoris*.



(a) Apollux device positioned on the *distal segment*.

(b) Starting and rest position of *quadriceps femoris* contractions.

(c) Apollux and stimulation electrodes positioned on the *quadriceps femoris*.

Figure 8.4: Electrode placement and resting position of arm: in figure (a) there is the placement of the Apollux device of the *distal segment* (collecting Euler's angles); (b) resting position (during all tests, the subject must always return to this position, which is the reference position); (c) Apollux device on the *quadriceps femoris* (acquiring MMG data) and stimulation electrodes.

Table 8.3 resumed subjects' data as gender, age, side, MVC estimated, and AROM evaluated during the *quadriceps femoris* acquisition.

Table 8.3: Subjects data during the experimental protocol. The studied muscle is the *quadriceps femoris* during the *knee extension*. For each subject are indicated gender, age, side, MVC value in kg, and AROM value in $^{\circ}$.

Subject n.	Gender	Age	Side	MVC (kg)	AROM ($^{\circ}$)
1	F	24	Left	15	19
2	F	27	Left	10	23
3	M	23	Right	15	40
4	M	25	Right	20	42
5	F	25	Right	10	37
6	F	24	Left	15.5	33
7	F	25	Left	20	27
8	M	24	Left	25	22
9	F	28	Left	15	21
10	F	27	Left	20	18

From Table 8.3, it's possible to see how the AROM values change between the *quadriceps femoris* case and *biceps brachii* case. Indeed, unlike the *biceps brachii* case, where the arm reaches approximately 90° respect with the vertical line performing a complete *elbow flexion*, the subjects' values of AROM are approximately comprised between 40° and 60° ; in the case of the *quadriceps femoris* executing a complete *knee extension*, the tibia reaches approximately 60° respect the vertical line; as a result, the subjects' values of AROM will be lower, especially comprised between approximately 15° and 45° .

In the case of the *quadriceps femoris* executing a *knee extension*, the FES calibration starts from the sixth step of Table 7.2. Thus, the first stimulation parameters are current 12 mA, pulse width 250 μ s, and there are four steps of rise and fall to reach the plateau of maximum current for each repetition.

As explained in Chapter 6 during Section 7.3, for each step of the LUT are executed at least two repetitions. A key point of this phase is that the subject must be completely relaxed during all calibration. If the first two repetitions done with those parameters provide the same angle and MMG output, based on the produced combined output, the energy stimulation will increase (of one or two steps in LUT), or the FES calibration will be stopped. Instead, if the combined outputs from the two repetitions are different, a third repetition will be executed

to establish what to do.

The FES calibration will be stopped when the optimal parameters to achieve a complete *elbow flexion* stimulating the *biceps brachii* are found. The optimal energy level of each subject is reported in Table 8.4. The current measured in mA, and the pulse width in μs reaches from each volunteer at the end of FES calibration are illustrated.

Once the ideal stimulation parameters are obtained, they are used to stimulate the subject during all four cases of the FES session. Between one trial and the following one, there are 5 min of rest.

Table 8.4: Each subject's stimulation parameters during the experimental protocol. The studied muscle is the *quadriceps femoris* during the *knee extension*. For each subject are shown Current (C) and Pulse Width (PW) at the Optimal Energy level.

Subject n.	C (mA)	PW (μs)
1	26	330
2	26	350
3	16	140
4	34	430
5	24	310
6	36	430
7	26	350
8	34	430
9	21	330
10	34	430

8.2 Second Protocol

During functional electrical stimulation, the second protocol's goal was to verify the functioning of the closed-loop to detect the voluntary contribution in simulated real clinical case. Thus, a sick patient is imitated using an elastic band on healthy subjects. Indeed, the elastic band produced a force in opposition with that generated from the subject to perform the *elbow flexion*.

This protocol aimed to examine the subject's response during the FES session using the elastic band after two phases of calibration were performed to determine the stimulation's lower and upper energy limits. This protocol includes only the *biceps brachii* during the *elbow flexion*.

The elastic band used in this trial is a commercial gym product. This resistance band, offering 10 kg of resistance, is designed for muscle strengthening and rehabilitation. Its adjustable notches enable customization of length and resistance to suit individual requirements.

The protocol is divided into three main sections:

1. **Estimation of the AROM:** first of all, it is necessary to determine for each subject the value of the AROM reached by the subject to perform the desired movement wearing the elastic band.
2. **FES calibration:** this automated phase was explained in the Chapter 7, Section 7.3. Two calibrations are performed, the first without the elastic band to determine the lower stimulation energy limit and the second with the elastic band to define the upper stimulation energy limit. These energies represent the stimulation parameters that allow the subject to execute the complete movement (with or without the elastic band) only thanks to the electrical stimulation. Each repetition of calibration starts with 4.5 s of rest followed by 5 s of stimulation.
3. **FES session:** this phase was described in the Chapter 7, Section 7.4.2 considering as rehabilitative approach the *Type A*. The FES session is done only once with the elastic band in this protocol. This session starts from the stimulation parameters that determine the lower energy limit, and then the energy increases during the session up to reach the upper energy limit. At these stimulation parameters are executed 5 *no voluntary repetitions*, then the current is decreased by 1 mA and after 2 *bad repetitions*, the subject must add her/his voluntary contribution to perform 5 *good repetitions*.

In this second experimental protocol, repetitions are defined in this way:

- **Bad repetition:** during the repetition, there is no movement, and no muscle activity is detected.
- **No voluntary repetition:** during the repetition, the movement is completed, and a partial muscle activity is detected.
- **Good repetition:** during the repetition, the movement is completed, and a complete muscle activity is detected.

During the FES session, the stimulation profile consists of 4 s of initial rest, followed by 5 s of stimulation and then 6 s of rest.

In this test, 10 subjects participated in the study on the *biceps brachii*. They were all required to sign a permission waiver and were told of all phases prior to the test's beginning. They all participated in the experimental protocol for the intended purpose. In addition, after all protocol phases are finished, each participant is required to complete a survey to share their thoughts on the experiment.

Women constitute 60% of the volunteers. Each participant, who is between the ages of 23 and 28, can decide to engage both of their muscles on the right or left side.

8.2.1 Experimental set-up for *biceps brachii* performing an *elbow flexion* using an elastic band

During this protocol, the MVC of each subject is not measured because the elastic band utilized is not standardizable.

For the test duration, the subject executes the trials sitting on an office chair. The patient's back should be well supported against the backrest. Next to her/his is a stool with support to which the subject leans her/his forearm. The angle formed from the position of *distal segment* with respect to the vertical axis is about 45°. The acquisition system comprehends two Apollux devices, one on the belly of *biceps brachii* and the other on the back of the *forearm*. They communicate via BLE 4.0 with a dongle BLE connected to a PC. Both Apollux devices are fixed to the subject using a biomedical tape. The two stimulation electrodes are put on the belly of *biceps brachii*.

Only the first FES calibration is done without the elastic band, and then the second calibration and the FES session are performed utilizing the elastic band. This band has some holes to modulate the resistance.

One extremity of the elastic band is fixed, the last hole inside one foot of the office chair, and by the other extremity, the second hole is put on the wrist of the subject.

Also in this protocol, before starting with the FES calibration and session phases, the AROM evaluation is performed. The initial position of this phase is just described and illustrated in Figure 8.5b.

This phase is executed as explained in this Chapter during Section 8.1.1 with the difference that the AROM evaluation is done using the elastic band.

In Figure 8.5, there is an illustration of the experimental setup with the elastic band. Figure 8.5a shows how the Apollux device that collects angle data is positioned on the *distal segment*. Figure 8.5b exhibits the initial and resting position using the elastic band. Instead, the initial and resting position for the first FES calibration (performed without the elastic band) is that explained for the first protocol 8.1.1 and illustrated in Figure 8.2b. Figure 8.5c illustrates how the Apollux device that records MMG data and the stimulation electrodes are placed on the belly of *biceps brachii*.



(a) Apollux device positioned on the *distal segment*.

(b) Starting and rest position of *biceps brachii* contractions.

(c) Apollux and stimulation electrodes positioned on the *biceps brachii*.

Figure 8.5: Electrode placement and resting position of arm using the elastic band: in figure (a) there is the placement of the Apollux device of the *distal segment* (collecting Euler's angles); (b) resting position with elastic band (during all tests, the subject must always return to this position, which is the reference position); (c) Apollux device on the *biceps brachii* (acquiring MMG data) and stimulation electrodes.

Table 8.5 resumed subjects' data as gender, age, side, and AROM evaluated during the *biceps brachii* acquisition using the elastic band.

Table 8.5: Subjects data during the second experimental protocol. The studied muscle is the *biceps brachii* during the *elbow flexion* using the elastic band. For each subject are indicated gender, age, side, and AROM value in °.

Subject n.	Gender	Side	AROM (°)
1	F	Left	57
2	F	Right	57
3	F	Right	40
4	F	Left	53
5	F	Right	45
6	M	Right	50
7	M	Right	49
8	F	Right	44
9	M	Left	46
10	M	Right	43

In the case of the *biceps brachii* executing a *elbow flexion* using the elastic band, two calibrations are performed: the first without and the second with the elastic band. In both cases, the FES calibration starts from the fourth step of Table 7.1. Thus, the first stimulation parameters are current 8 mA, pulse width 130 μ s, and there are four steps of rise and fall to reach the plateau of maximum current for each repetition.

As explained in Chapter 6 during Section 7.3, for each step of the LUT are executed at least two repetitions. A key point of this phase is that the subject must be completely relaxed during all calibration. If the first two repetitions done with those parameters provide the same angle and MMG output, based on the produced combined output, the energy stimulation will increase (of one or two steps in LUT), or the FES calibration will be stopped. Instead, if the combined outputs from the two repetitions are different, a third repetition will be executed to establish what to do.

The FES calibration will be stopped when the optimal parameters to achieve a complete *elbow flexion* stimulating the *biceps brachii* are found. The optimal energy corresponds for the first calibration to the lower energy limit, and for the second calibration to the upper energy limit.

Each subject's energy parameters are reported in Table 8.6. The current measured

in mA, and the pulse width in μs reaches from each volunteer at the end of both calibrations are illustrated.

Table 8.6: Each subject's stimulation parameters during the second experimental protocol using the Elastic Band (EB). The studied muscle is the *biceps brachii* during the *elbow flexion* using an elastic band in opposition to the movement. For each subject are shown Current (C) and Pulse Width (PW) that define the Lower (from FES calibration without elastic band) and Upper (from FES calibration with elastic band) Energy limit.

Subject n.	Lower Energy Limit calibration no EB		Upper Energy Limit calibration with EB	
	C (mA)	PW (μs)	C (mA)	PW (μs)
1	18	170	22	180
2	18	160	22	180
3	18	160	20	180
4	22	190	24	190
5	14	150	18	160
6	12	130	14	140
7	27	200	31	200
8	20	170	22	180
9	20	170	22	180
10	18	170	22	180

After each calibration, there are 5 min of rest to allow to subject to repose. In both the calibration and during the first part of the session, the subject must be completely relaxed and ensure that the electrical stimulation moves the arm.

Once these parameters are obtained, they are used to stimulate the subject during the FES session. This phase starts from a lower energy limit; the subject performs three repetitions at the same stimulation parameters, and then the energy increases of one step of the LUT (7.1). When the upper energy limit is achieved, the subject executes 5 no voluntary repetitions, and then the current is decreased of 1 mA. At these new stimulation parameters, it is expected that the subject cannot reach the complete movement without a voluntary contribution, so there are first two repetitions in which the subject continues to be completely relaxed and doesn't reach the complete movement, and in the end, he/she must add a voluntary contribution to complete the exercise.

Chapter 9

Results and discussion of the results obtained from experimental protocols

In this chapter, there will be a description and a discussion of the obtained results over the two protocols described in Chapter 8.

9.1 First protocol

In this section, the results obtained during the First Protocol are presented. Specifically, this protocol aimed to evaluate the feasibility of the closed-loop software in assessing voluntary contributions.

This protocol focused on identifying a threshold for the *biceps brachii* and *quadriceps femoris* (*vastus medialis* and *rectus femoris*) that allows for the discrimination between purely stimulated contractions and those with a voluntary contribution (standardized using specific percentages of Maximum Voluntary Contraction (MVC)).

9.1.1 Results of *biceps brachii*

The results are evaluated as the accuracy (%) in detecting a voluntary contribution. Accuracy is evaluated as in Equation 9.1:

$$\text{Accuracy (\%)} = 100 \times \frac{\text{Number of Correctly Identified Repetitions}}{\text{Total Number of Repetitions}} \quad (9.1)$$

In Table 9.1, an overview of the accuracy detection results for the 11 subjects across various thresholds is presented.

For the threshold evaluation, the 'purely stimulated' RMS of the MMG signal value used is calculated during the last step of the calibration phase. During this phase, the subject is instructed not to contribute voluntarily, and the RMS of the MMG value recorded at the highest level of injected energy (which elicits the full movement) serves as the baseline for setting thresholds.

This baseline value is then used to set thresholds for subsequent FES session acquisitions, where the thresholds are defined as specific percentages of this value. The tested percentages for the thresholds are 110 %, 120 %, 130 %, 140 %, and 150 % of the threshold evaluated in the calibration phase.

Table 9.1: Accuracy (%) for different MVC levels vs purely stimulated contractions of *biceps brachii*. The imposed thresholds are given as percentages of the MMG - RMS value found during the purely stimulated contraction in the calibration phase. Data are evaluated over 11 subjects.

Threshold	Accuracy (%)			
	Purely stimulated	10 % MVC	20 % MVC	30 % MVC
110 %	91.00	2.73	30.91	93.00
120 %	94.00	1.82	24.55	90.00
130 %	95.00	0.00	17.27	85.00
140 %	95.00	0.00	11.82	77.00
150 %	95.00	0.00	9.09	73.00

Moreover, Table 9.2 presents the subject-specific accuracy (%) for the 120 % threshold. Detailed results for each subject's other four tested thresholds can be found in the Appendix A.

Subjects 7 and 8 encountered issues during the acquisition of the 30 % MVC contractions and the purely stimulated contractions, respectively. As a result, data from these specific cases were excluded from the analysis. However, the remaining data from these subjects were consistent with the results from the other subjects and were therefore included in the overall analysis.

Table 9.2: Accuracy of voluntary effort recognition for closed-loop. Accuracy (%) for different MVC levels vs purely stimulated contractions of *biceps brachii*. The imposed threshold is equal to the 120 % of the MMG - RMS value found during the purely stimulated contraction in the calibration phase.

Subject	Accuracy (%)			
	Purely stimulated	10 % MVC	20 % MVC	30 % MVC
1	100.00	0.00	10.00	90.00
2	100.00	0.00	100.00	100.00
3	90.00	20.00	90.00	100.00
4	100.00	0.00	60.00	100.00
5	100.00	0.00	0.00	100.00
6	60.00	0.00	0.00	100.00
7	100.00	0.00	0.00	\
8	\	0.00	0.00	90.00
9	90.00	0.00	10.00	80.00
10	100.00	0.00	0.00	60.00
11	100.00	0.00	0.00	80.00
TOT	94.00	1.82	24.55	90.00

9.1.2 Results of *vastus medialis* and *rectus femoris*

The same analysis made of *biceps brachii* has been made on the *quadriceps femoris* (*vastus medialis* and *rectus femoris*).

In Table 9.3 there is an overview of the accuracy (Equation 9.1) from data acquired by ten subjects. A comparison of the 110 %, 120 %, 130 %, 140 %, and 150 % in respect to a baseline value (identified as purely stimulated contractions) evaluated during the FES calibration.

In Table 9.4 the subject-specific accuracy results are reported for the 120 % threshold.

On the other hand, in Table 9.5 there is an overview of the performances in terms of accuracy, compared to the RMS of the MMG evaluated in real-time by the software during the purely stimulated contraction (calibration phase) and stimulated contraction with voluntary contribute at 30 % MVC.

Table 9.3: Accuracy (%) for different MVC levels vs purely stimulated contractions of *quadriceps femoris*. The imposed thresholds are given as percentages of the MMG - RMS value found during the purely stimulated contraction in the calibration phase. Data are evaluated over 11 subjects.

Threshold	Accuracy (%)			
	Purely stimulated	10 % MVC	20 % MVC	30 % MVC
110 %	87.00	21.00	36.00	53.00
120 %	97.00	17.00	33.00	47.00
130 %	100.00	14.00	28.00	36.00
140 %	100.00	12.00	22.00	33.00
150 %	100.00	9.00	19.00	30.00

Table 9.4: Accuracy of voluntary effort recognition for closed-loop. Accuracy (%) for different MVC levels vs purely stimulated contractions of *quadriceps femoris*. The imposed threshold is equal to the 120 % of the MMG - RMS value found during the purely stimulated contraction in the calibration phase.

Subject	Accuracy (%)			
	Purely stimulated	10 % MVC	20 % MVC	30 % MVC
1	100.00	50.00	60.00	80.00
2	100.00	0.00	0.00	0.00
3	100.00	0.00	60.00	70.00
4	90.00	10.00	0.00	100.00
5	100.00	0.00	30.00	50.00
6	100.00	0.00	0.00	0.00
7	100.00	80.00	90.00	70.00
8	100.00	30.00	90.00	100.00
9	90.00	0.00	0.00	0.00
10	90.00	0.00	0.00	0.00
TOT	97.00	17.00	33.00	47.00

The mean increase (%) is evaluated as in Equation 9.2.

$$\text{Mean increase (\%)} = 100 \times \frac{\text{RMS}_{30\% \text{ MVC}} - \text{RMS}_{\text{Purely stimulated}}}{\text{RMS}_{\text{Purely stimulated}}} \quad (9.2)$$

Table 9.5: RMS of the MMG signal acquired from *quadriceps femoris* for the purely stimulated and 30 % MVC conditions, mean increase in RMS signal, and accuracy for each subject. Accuracy is the percentage of correct classifications for the 30 % condition.

Subject n.	RMS of MMG signal (g)		Mean increase (%)	Accuracy (%)
	Purely stimulated	30 % MVC		
1	0.02379	0.03596	33.84	80.00
2	0.01625	0.01225	-32.68	0.00
3	0.01935	0.02641	26.74	70.00
4	0.01658	0.03438	51.77	100.00
5	0.02191	0.03290	33.41	50.00
6	0.03030	0.01763	-71.82	0.00
7	0.00547	0.00678	19.37	70.00
8	0.01547	0.03093	49.98	100.00
9	0.02198	0.01272	-72.84	0.00
10	0.03243	0.02213	-46.52	0.00

9.1.3 Second Protocol

The second protocol aimed to simulate the condition of a sick patient. Specifically, a movement resistor was utilized, achieved with an elastic band that opposed the movement.

An overview of the injected energy through the various FES session phases is reported in Table 9.6.

The protocol phases are:

- *Phase 1*: increase of the energy from the one found during the calibration phase without the elastic band (lower stimulation energy limit), to the one that provides the full movement with the elastic band (upper stimulation energy limit);
- *Phase 2*: energy reached for the full movement with the elastic band (max energy);
- *Phase 3*: max energy (phase 2) minus 1 mA without voluntary contribution;
- *Phase 4*: max energy (phase 2) minus 1 mA with voluntary contribution;

The results in terms of accuracy (%) are shown in Table 9.7. The subject-specific accuracy for detecting involuntary contractions during purely stimulated contractions is presented in the second column, while the results for voluntary contractions are shown in the third column. The last column displays the average detection

Table 9.6: Second protocol: injected energy. For each subject, there is an overview of the energy injected through the various phases of the protocol. 'C' is current, 'PW' is the pulse width. The protocol phases are 1. increase of the current, 2. max current for no voluntary contractions, 3-4. max current minus 1 mA.

Subj. n.	AROM (°)	Phase 1		Phase 2		Phase 3 - 4	
		C(mA)	PW (µs)	C(mA)	PW (µs)	C(mA)	PW (µs)
1	57	18 - 21	170	22	170	21	170
2	57	19 - 21	160	22	160	21	160
3	40	18 - 19	160	20	160	19	160
4	53	22 - 23	190	24	190	23	190
5	45	14 - 16	150	17	150	16	150
6	50	12 - 13	130	14	130	13	130
7	49	27 - 30	200-240	31	240	30	240
8	44	20 - 21	170	22	170	21	170
9	46	20 - 21	170	22	170	21	170
10	43	18 - 21	170	22	170	21	170

accuracy between involuntary and voluntary contractions.

Table 9.7: Second protocol accuracy in voluntary effort detection: accuracy for different subjects in purely stimulated, voluntary, and the mean between the previous conditions.

Subject n.	Accuracy (%)		
	Purely stimulated	Voluntary	Total
1	100.00	83.33	91.67
2	71.43	100.00	85.72
3	83.33	100.00	91.67
4	100.00	83.33	91.67
5	80.00	100.00	90.00
6	83.33	83.33	83.33
7	83.33	71.43	77.38
8	100.00	71.43	85.72
9	100.00	100.00	100.00
10	71.43	100.00	85.72
TOT	87.29	89.29	88.29

The roll angle reached during each phase is displayed in Table 9.8. Results are obtained as the mean value of each repetition performed in that phase.

Furthermore, Table 9.9 exploits the differences in the MMG value during the

Table 9.8: Second protocol, reached angle. For each subject, the average values are reached through the various repetitions. The protocol phases are 1. increase of the current, 2. max current for no voluntary contractions, 3. max current - 1 mA without voluntary contribution, and 4. max current - 1 mA with voluntary contribution.

Subj n.	AROM (°)	Mean roll angle reached (°)			
		Phase 1	Phase 2	Phase 3	Phase 4
1	57	28,82	49,23	25,41	55,39
2	57	16,39	42,54	20,67	45,75
3	40	16,52	36,93	16,77	40,05
4	53	25,25	40,71	27,29	42,31
5	45	21,82	36,05	23,94	48,38
6	50	11,48	37,19	21,73	44,53
7	49	13,72	40,65	15,20	47,29
8	44	21,13	33,06	11,26	41,54
9	46	18,61	38,02	21,08	42,81
10	43	14,82	41,51	15,60	49,70

voluntary and purely stimulated contractions. In particular, for each subject, the RMS value obtained in the calibration phase and the threshold (evaluated as the 120% of this value) are reported. Then, during the FES session, the mean RMS value obtained during purely stimulated (Phase 2) and voluntary contribution contractions (phase 4) is reported. The mean increase is evaluated as the difference between the mean value of the voluntary contribution contractions and the RMS of the calibration phase.

Table 9.9: Second protocol, MMG values obtained. MMG - RMS Value obtained during the calibration phase and during the FEs session for the purely stimulated and voluntary contractions. Mean increase percentage during voluntary contractions with respect to the value obtained in the calibration phase.

Subj. n.	MMG - RMS Value (g)				Mean Increase (%)
	Calibration	Th Value	Purely Stim	Voluntary	
1	0.01124	0.01349	0.00875	0.01840	63.66
2	0.00966	0.01159	0.00772	0.02405	148.96
3	0.00910	0.01092	0.00600	0.01281	40.80
4	0.01328	0.01594	0.00631	0.02485	87.07
5	0.01249	0.01499	0.00617	0.02645	111.70
6	0.01241	0.01489	0.00895	0.02157	73.82
7	0.00846	0.01015	0.00702	0.01025	21.21
8	0.01292	0.01551	0.00997	0.01574	21.79
9	0.01992	0.02390	0.01298	0.04730	137.45
10	0.01355	0.01626	0.00992	0.01888	39.36

9.2 Discussion of the results obtained in this experimental protocol

In this Section discussion of the results obtained during the two protocols, illustrated in the previous section (9.1).

9.2.1 First protocol

Discussion of results for *biceps brachii*

The experimental data (Table 9.1) found that it is possible to set a threshold to distinguish between voluntary and purely stimulated contractions. Indeed, robust results in terms of accuracy are obtained when the voluntary effort is at least 30 % of the MVC. Regardless of the specific threshold used, the average accuracy for distinguishing voluntary effort over the 10 subjects is always greater than 70 %. On the other hand, no strong correlation can be observed at the lower effort levels. For example, the 10 % of the MVC condition resulted in a voluntary contribution detection accuracy of less than 3 %, while the 20 % of the MVC condition achieved a maximum accuracy of only 31 %.

The results were analyzed by comparing the accuracy of purely stimulated contractions versus 30 % of the MVC contractions. As shown, the highest accuracy for purely stimulated contractions is achieved with threshold values of 130 %, 140 %, or 150 %, where an accuracy of 95 % is observed. Conversely, the highest accuracy for

the 30 % of the MVC trials is obtained at a threshold of 110 %, with a value of 93 %.

When selecting an appropriate threshold, it is important to consider robust performance in both cases. The 120 % threshold achieves this balance effectively. With this threshold, the accuracy loss for detecting 30 % of the MVC contractions is only 3 %, and the accuracy loss for detecting purely stimulated contractions is 1 %. Given the high recognition rates (around 90 %) for both cases, a maximum performance loss of 3 % is considered acceptable.

Moreover, when examining the subject-specific results presented in Table ??, the accuracy of detection for each subject using the 120 % threshold can be appreciated. Specifically, it is observed that during purely stimulated contractions, seven out of ten subjects achieve a detection accuracy of 100 %, two have an accuracy of 90 %, and one has an accuracy of 60 %. This indicates that the performance for most subjects aligns well with the average performance (94 %), while only one subject exhibits a significant accuracy loss of 34 %. Nonetheless, this subject's recognition rate remains above 50 %, which suggests that the overall recognition accuracy is still reasonably high.

Conversely, for detecting voluntary contributions at 30 % of the MVC, five out of ten subjects achieved an accuracy of 100 %, two achieved 90 %, two achieved 80 %, and one achieved 60 %. Considering that the average accuracy for detecting voluntary contributions is 90 %, seven out of ten subjects maintain this level of accuracy, two subjects experience a 10 % accuracy loss, and one subject has a 30 % accuracy loss. Overall, similar to the purely stimulated contractions, the results indicate that the 120 % threshold provides robust performance across individual subjects.

In addition, the case with 10 % of the MVC voluntary contribution resulted in an average recognition rate of 1.82 % for voluntary effort. This low average is due to the fact that only subject number 3 achieved an accuracy of 20 %, while the remaining ten subjects were unable to detect any voluntary contribution. Similarly, the 20 % of the MVC case yielded high accuracy for two subjects (numbers 2 and 3) and acceptable results for subject number 4 but was not effective for the other eight subjects. Therefore, neither of these cases provided satisfactory results for detecting voluntary contributions.

Therefore, the selected threshold for voluntary contribution recognition is set to 120 % of the RMS value of the MMG signal measured during the calibration phase, corresponding to the purely stimulated contractions. Any contraction that exhibits an RMS value of the MMG signal equal to or exceeding this threshold will

be considered as containing both stimulated and voluntary contributions. The software achieves a performance of 90 % in recognizing voluntary contributions when analyzing contractions with a 30 % of the MVC effort. Additionally, the accuracy for detecting non-voluntary contractions is 94 %.

Discussion of results for *vastus medialis* and *rectus femoris*

For the *quadriceps femoris* (stimulating *vastus medialis* and *rectus femoris*), a specific threshold for recognizing voluntary contribution in stimulated contractions has not been determined.

Specifically, the thresholds are computed as percentages of a baseline level that reflects purely stimulated contractions. The final injected energy defines this baseline during the calibration phase that induces full movement exclusively through stimulation. From this baseline the 110 %, 120 %, 130 %, 140 % and 150 % of this baseline value are used as thresholds.

As reported in Table 9.3, the average accuracy (%) across ten subjects is high when evaluating purely stimulated contractions, with values exceeding 85 %. However, the performance decreases when stimulated contractions with varying percentages of MVC are considered. Specifically, at 10 % of the MVC, the maximum achieved accuracy is 20 %. This value increases to 36 % at 20 % MVC, and further improves to 53 % at 30 % of the MVC contractions. However, the accuracy values found when a voluntary contribution is present are relatively low; indeed, a 53 % accuracy in recognition for 30 % of the MVC is not enough to believe that a system is reliable and robust.

Although the values are quite low, the same threshold used for the *biceps brachii* was applied to the data, as the 120 % threshold yields a high accuracy (97 %) for recognizing purely stimulated contractions. In contrast, the 110 % threshold results in lower accuracy of 87 % (of purely stimulated contractions recognition), while higher thresholds (130 %, 140 %, and 150 %) provide only a minor improvement in purely stimulated recognition (increasing accuracy by 3 %) but lead to a significant reduction in performance for recognizing voluntary contributions.

The results over each subject for the 120 % are reported in Table 9.4. While the subject-specific results with the other thresholds are reported in the Appendix A. In this Table, it is possible to notice that for all subjects, the accuracy of recognition of no voluntary contribution in purely stimulated contractions is at least equal to 90 %. Conversely, the accuracy of evaluation of the voluntary contribution with different percentages of % of the MVC is extremely variable between the different

subjects. Indeed, in the 30 % of the MVC case, there are two subjects with an accuracy of 100 %, other two subjects with an accuracy of 80 %, two with 70 %, one with 50 %, while the other four subjects have an accuracy of 0 %. This results in a very low average accuracy of 47 %, which is unacceptable.

In this thesis project, the contraction of the *quadriceps femoris* was not studied in earlier phases, as the focus was primarily on the *biceps brachii*. During the execution of this protocol, it became evident that stimulating the *quadriceps femoris* resulted in more pronounced muscle and skin oscillations compared to the *biceps brachii*. This is due to the *quadriceps femoris* being a much larger muscle group, consisting of the *vastus medialis* and *rectus femoris*. The effect of the electrical stimulation was visibly different from that observed with the *biceps brachii*. During the calibration phase, it was observed that lower currents activated only specific muscle fibers, which caused visible deformation of a precise portion of the thigh as muscle fibers shortened and increased their cross-sectional area. The pulses of stimulation current, combined with only partial muscle activation, led to visible muscle oscillations. These oscillations appeared in the MMG signals and fell within the MMG frequency band, making it difficult to develop a solution to eliminate them.

To analyze the relationship between the RMS value of the MMG during stimulated contractions and the low accuracy across different subjects, the comparison shown in Table 9.5 has been conducted.

Indeed, it can be seen that the mean percentage increase (evaluated as the increase from the purely stimulated contraction RMS and 30 % MVC) is negative in some subjects (n. 2-6-9-10). This means that the MMG values reached during the purely stimulated contractions are higher than the ones achieved during the ones with a voluntary contribution. Even though it seems that this result does not align with the previous studies and literature, some notes should be considered.

Firstly, the *quadriceps femoris* is a much stronger muscle since it sustains half of the body weight on a daily basis, so the % MVC that should have been taken into consideration for the discrimination of voluntary effort, could have been way higher than the ones tested.

Moreover, the skin and muscle fluctuation described earlier had an effect only when the portion of the excited muscle was smaller, while when the whole muscle was excited by the injected current, they decreased. This was visible in the calibration phase since the RMS value decreased with the increase of the injected energy, reaching the exactly opposite trend with respect to the *biceps brachii*.

So, the extremely low accuracy of 0 % over those four subjects can be explained by this decrease in the RMS value during voluntary effort because the whole muscle

was contracted, so this oscillation is not present.

On the other hand, some subjects reported after the stimulation that even though a weight was present, some contractions happened only due to the stimulus. Indeed, they could not realize if the movement was achieved only due to the stimulation or thanks to their voluntary contribution. While for the *biceps brachii* contractions, no movement was possible to perform with the chosen weight only by the stimulus.

Furthermore, the discrepancies between the accuracy of various subjects could be explained by the injected current and the muscle portion of excited fibers. Indeed, in Table 9.5 it is possible to see that subject 7 had an RMS of the MMG signal during purely stimulated contractions equal to 0.005,47 g and during voluntary contractions at 30 % of the MVC it increases of about 19.37 %. On the other hand, subject number 10 had an RMS value of 0.032,43 g, which is almost 10 times higher than the one of subject n.7. In addition, subject number 10 has a decrease in the RMS value when considering voluntary contraction. So, the effect of the oscillation during stimulated contractions can be appreciated in subject 10, while they were negligible in subject 7.

To conclude this section, further analysis should be conducted for the *quadriceps femoris* during voluntary and stimulated contractions in order to find a pattern for this voluntary contribution discrimination.

9.2.2 Second protocol

The results of the second protocol confirm the outcomes of the previous analysis over *biceps brachii* contractions, even though a movement resistance was included.

Firstly, Table 9.6 summarizes the injected energies for each subject for all the FES session phases. In phase 1, there is a gradual increase in the stimulation energy from the one found during the calibration phase without the elastic band to the one found during the calibration phase with the elastic band. By comparing with Table 8.5 that recaps the calibration energies for each subject, it is possible to notice that all subjects returned to the stimulation energy found during the calibration phase except for subject number five. Indeed, this subject has an injected current of 18 mA in the calibration phase, while in the FES session, it was equal to 17 mA. However, it is important to note that the energy increase between the two phases differs, so the energy level with the injected current of 17 mA was not tested during the calibration step. This indicates that the results are accurate because the subject was tested with 16 mA and 18 mA during calibration. The full movement was not achieved with 16 mA (similar to the FES session), but 17 mA is the correct stimulation intensity. If this level had been tested during the calibration

phase, it would have been the stopping point.

Moreover, since the energy increase differs between the two phases, the pulse width changes between the calibration and session phases. So, it is possible to say that the current increase is more relevant than a pulse width increase when trying to perform the full movement without any voluntary contribution.

Indeed, the results shown in Table 9.7 provide an average accuracy of detection of voluntary contribute or purely stimulated contractions of 88.29 %, confirming the performances obtained in the previous study.

Moreover, regarding each subject's performance, the accuracy of detection of no voluntary contribution in purely stimulated contractions is always over 70 %. The same consideration can be extracted from the results of the voluntary contribution detection.

In addition, the difference between the average of the two conditions (purely stimulated and voluntary contribution) differs from only 2 %, so both classes are recognized accurately.

Another important analysis can be achieved by looking at the angle reached for each subject through the various protocol steps (Table 9.8). The angle reached through each repetition corresponding to a specific phase has been averaged in this table. It is possible to notice that in phases 1 and 2, the angle reached does not respect the angle guidelines imposed by the AROM. This means that the current should be increased (as happens in phase 2), or a voluntary contribution should be added (phase 4) in order to perform the full movement. Indeed, in phases 2 and 4, all subjects reach the correct angle.

Furthermore, Table 9.9 illustrates the differences in the RMS values of the MMG between the FES calibration phase (using the final stimulation energy) and the FES session (comprising purely stimulated contractions and stimulated contractions with voluntary contribution). Specifically, the table shows that for each subject, there is a noticeable increase in the RMS value during the voluntary contribution phase compared to the calibration phase. This increase is quantified as the difference between the FES session's RMS value in phase 4 (voluntary contribution) and the RMS value from the calibration phase. The last column summarizes this increase, demonstrating that it varies from approximately 20 % to 150 % across subjects.

Moreover, it can be observed that the RMS value for purely stimulated contractions during the FES session is slightly lower than the RMS value observed during the calibration phase. This discrepancy might be attributed to the subjects' adaptation to the stimulation, which could involve both their initial apprehension and muscle response. Further research is needed to refine the threshold evaluation

methods for these stimulations.

In summary, examining both the angle and MMG data allows for extracting significant insights into the effects of stimulation. The angle data offers information about the movement during the stimulation, while the MMG data reveals any voluntary muscle contributions. Together, these data provide a more complete picture of the stimulation's effects, which cannot be discerned from a single parameter alone. This combined analysis is essential for refining stimulation strategies to optimize rehabilitative outcomes.

Chapter 10

Conclusion and future developments

10.1 Conclusion about the final closed-loop system developed

A closed-loop system to regulate the Functional Electrical Stimulation (FES) in response to the patient's muscle activity was proposed in this thesis study. The benefit of tailoring the stimulation according to the patient's direct feedback is the potential to utilise a closed-loop system-driven FES. This way, each subject will be stimulated using the stimulation parameters appropriate to him/her, negating the need to apply a predetermined pattern of stimulation on all the patients.

Finding a sensor that can identify muscle contraction during electrical stimulation was the initial step in developing this system. The stimulation artifact generated during the FES led to the exclusion of the Surface ElectroMyoGram (sEMG) signal. Following a literature review, the MechanoMyoGram (MMG) signal was selected to investigate the mechanical characteristics of the muscle, specifically the mechanical vibration that can be regarded as a muscular contraction. The acceleration vector's norm can be computed to yield the MMG signal. It was decided to add the roll angle as an additional element to guarantee that the correct activation is identified. This is one of Euler's angles, and it may be found by starting with gyroscope data.

It was determined that the Apollux devices that comprehend an IMU should be employed to develop the acquisition system since an accelerometer and a gyroscope were required to gather the interest data.

The ability of the MMG signal to identify the same muscle activation as the sEMG signal was confirmed by a comparison between the two signals in the first section of the thesis. After it was established that the MMG signal could similarly detect the same contractions utilising the FES, experiments were run to attempt to differentiate between a movement that was purely voluntary and a movement that was made possible by stimulation only. The results of these studies, which involved seven people, showed that the voluntary contribution could be identified using the Root Mean Square (RMS) of the MMG signal.

The closed-loop was realized based on these factors. The developed system does, in fact, monitor the MMG and the roll angle. It operates in two phases: the first phase, called *FES calibration*, serves to obtain optimal stimulation parameters to stimulate the subject, and the rehabilitative phase, known as *FES session*, begins with predetermined parameters and stimulates the subject to restore motor function. During the calibration process, the energy stimulation rises until the data from the roll angle and the MMG's RMS indicate that the required movement has been achieved. Then, throughout the session, the roll angle and the RMS of the MMG are adjusted to ensure that the energy injected is sufficient to finish the movement. If these parameters show that the movement is excessive or incomplete, the energy stimulation will decrease or increase accordingly.

The proposed closed-loop system was evaluated using two distinct procedures:

- The first protocol's goal was to identify the threshold for voluntary contribution. In this test, the *biceps brachii* performs the *elbow flexion* and the *quadriceps femoris* the *knee extension*. Eleven healthy subjects take part in the *biceps brachii* trial and ten in the *quadriceps femoris* trial. Using weight as the 30% of the MVC, this protocol's results show that, in the instance of the *biceps brachii*, the voluntary contribution may be detected with an accuracy of 90%. Instead, a threshold cannot be obtained for the *quadriceps femoris*.
- The second approach uses an elastic band to imitate a sick patient. This trial aims to comprehend how the system behaves while interacting with patients with illness, particularly if it is able to distinguish between a full movement that was conducted only as a result of stimulation and a complete movement that was purposefully completed. Ten healthy people are examined only while doing the *elbow flexion* with the *biceps brachii*. With an accuracy of 88.29%, the results show that it is possible to identify a voluntary contribution or one that is only stimulated.

10.2 Future developments

This research opens up several potential directions for further investigation, in particular next focus points could be:

- Extending the software's usability to support multiple muscles simultaneously. While the developed software currently operates effectively in open-loop mode, rehabilitation purposes require concurrent activation of different muscle groups. Therefore, the stimulation should modulate the activity of several muscles simultaneously by synchronously acquiring and processing data from various devices.
- Results obtained from *quadriceps femoris* did not show any significant results in terms of performances. This muscle was not the primary focus of this thesis project, and several challenges were encountered. However, studies specifically targeting this muscle could lead to important advancements.
- The calculation of the reached angle has been validated only visually. Therefore, further validation of the angle measured during stimulation is needed. For example, IMU data could be compared with results obtained from the gold standard for motion analysis, such as the Vicon system.
- The movement performed during stimulation was calculated based on the orientation values of the gyroscope in three-dimensional space. Further synchronization of the acquisition devices could enable the evaluation of angle variations between two devices placed on the proximal and distal segments of the joint.
- Improving the evaluation of the threshold for the voluntary contribution discrimination. It has been observed that, for the majority of subjects, the data obtained during the calibration phase are slightly higher than those achieved during the FES session. This discrepancy could be due to muscle adaptation to the stimulus or to the subject's apprehension when performing the full movement for the first time.
- Focus on improving the increase in injected energy to better adapt it compared to using a lookup table. For example, this could be achieved by adjusting the energy proportionally to the progressive increase in the reached angle or to the incremental changes in certain parameters within the MMG data.

- Evaluating the differences between the healthy subjects who volunteered for this thesis and patients with illnesses could be beneficial. This comparison could help in more accurately determining the discrimination factor between voluntary and stimulated contractions, as well as understanding how the presence of a pathology affects the response to stimulation.
- Linking the simultaneous acquisition of stimulation patterns from the therapist to replace fixed stimulation inputs. Building on the ATC-FES system developed by *Rossi et al.*, a closed-loop system could be implemented for dynamic patient input.

Appendix A

Appendix

A.1 Subject specific closed-loop accuracy

Table A.1: Accuracy of voluntary effort recognition for closed-loop. Accuracy (%) for Different MVC levels vs purely stimulated contractions of *biceps brachii*. The imposed threshold is equal to the 110% of the MMG - RMS value found during the purely stimulated contraction in the calibration phase.

Subject	Accuracy (%)			
	Purely stimulated	10 % MVC	20 % MVC	30 % MVC
1	100.00	0.00	30.00	100.00
2	100.00	0.00	100.00	100.00
3	80.00	20.00	90.00	100.00
4	100.00	0.00	60.00	100.00
5	100.00	10.00	10.00	100.00
6	50.00	0.00	0.00	100.00
7	100.00	0.00	0.00	\
8	\	0.00	30.00	100.00
9	90.00	0.00	10.00	80.00
10	100.00	0.00	0.00	70.00
11	90.00	0.00	10.00	80.00
TOT	91.00	2.73	30.91	93.00

Table A.2: Accuracy of voluntary effort recognition for closed-loop. Accuracy (%) for Different MVC levels vs purely stimulated contractions of *biceps brachii*. The imposed threshold is equal to the 130 % of the MMG - RMS value found during the purely stimulated contraction in the calibration phase.

Subject	Accuracy (%)			
	Purely stimulated	10 % MVC	20 % MVC	30 % MVC
1	100.00	0.00	0.00	80.00
2	100.00	0.00	80.00	100.00
3	100.00	0.00	80.00	100.00
4	100.00	0.00	20.00	100.00
5	100.00	0.00	0.00	100.00
6	60.00	0.00	0.00	80.00
7	100.00	0.00	0.00	\
8	\	0.00	0.00	90.00
9	90.00	0.00	10.00	80.00
10	100.00	0.00	0.00	40.00
11	100.00	0.00	0.00	80.00
TOT	95.00	0.00	17.27	85.00

Table A.3: Accuracy of voluntary effort recognition for closed-loop. Accuracy (%) for Different MVC levels vs purely stimulated contractions of *biceps brachii*. The imposed threshold is equal to the 140 % of the MMG - RMS value found during the purely stimulated contraction in the calibration phase.

Subject	Accuracy (%)			
	Purely stimulated	10 % MVC	20 % MVC	30 % MVC
1	100.00	0.00	0.00	80.00
2	100.00	0.00	30.00	90.00
3	100.00	0.00	70.00	100.00
4	100.00	0.00	20.00	100.00
5	100.00	0.00	0.00	90.00
6	60.00	0.00	0.00	80.00
7	100.00	0.00	0.00	\
8	\	0.00	0.00	80.00
9	90.00	0.00	10.00	70.00
10	100.00	0.00	0.00	10.00
11	100.00	0.00	0.00	70.00
TOT	95.00	0.00	11.82	77.00

Table A.4: Accuracy of voluntary effort recognition for closed-loop. Accuracy (%) for Different MVC levels vs purely stimulated contractions of *biceps brachii*. The imposed threshold is equal to the 150 % of the MMG - RMS value found during the purely stimulated contraction in the calibration phase.

Subject	Accuracy (%)			
	Purely stimulated	10 % MVC	20 % MVC	30 % MVC
1	100.00	0.00	0.00	80.00
2	100.00	0.00	30.00	90.00
3	100.00	0.00	40.00	100.00
4	100.00	0.00	20.00	100.00
5	100.00	0.00	0.00	90.00
6	60.00	0.00	0.00	80.00
7	100.00	0.00	0.00	\
8	\	0.00	0.00	50.00
9	90.00	0.00	10.00	70.00
10	100.00	0.00	0.00	10.00
11	100.00	0.00	0.00	60.00
TOT	95.00	0.00	9.09	73.00

Table A.5: Accuracy of voluntary effort recognition for closed-loop. Accuracy (%) for Different MVC levels vs purely stimulated contractions of *quadriceps femoris*. The imposed threshold is equal to the 110 % of the MMG - RMS value found during the purely stimulated contraction in the calibration phase.

Subject	Accuracy (%)			
	Purely stimulated	10 % MVC	20 % MVC	30 % MVC
1	100.00	60.00	60.00	80.00
2	70.00	20.00	0.00	0.00
3	100.00	0.00	60.00	100.00
4	90.00	20.00	10.00	100.00
5	100.00	0.00	40.00	50.00
6	100.00	0.00	0.00	0.00
7	100.00	80.00	90.00	100.00
8	90.00	30.00	100.00	100.00
9	80.00	0.00	0.00	0.00
10	40.00	0.00	0.00	0.00
TOT	87.00	21.00	36.00	53.00

Table A.6: Accuracy of voluntary effort recognition for closed-loop. Accuracy (%) for Different MVC levels vs purely stimulated contractions of *quadriceps femoris*. The imposed threshold is equal to the 130 % of the MMG - RMS value found during the purely stimulated contraction in the calibration phase.

Subject	Accuracy (%)			
	Purely stimulated	10 % MVC	20 % MVC	30 % MVC
1	100.00	40.00	50.00	80.00
2	100.00	0.00	0.00	0.00
3	100.00	0.00	20.00	30.00
4	100.00	0.00	0.00	90.00
5	100.00	0.00	30.00	40.00
6	100.00	0.00	0.00	0.00
7	100.00	80.00	90.00	20.00
8	100.00	20.00	90.00	100.00
9	100.00	0.00	0.00	0.00
10	100.00	0.00	0.00	0.00
TOT	100.00	14.00	28.00	36.00

Table A.7: Accuracy of voluntary effort recognition for closed-loop. Accuracy (%) for Different MVC levels vs purely stimulated contractions of *quadriceps femoris*. The imposed threshold is equal to the 140 % of the MMG - RMS value found during the purely stimulated contraction in the calibration phase.

Subject	Accuracy (%)			
	Purely stimulated	10 % MVC	20 % MVC	30 % MVC
1	100.00	20.00	40.00	70.00
2	100.00	0.00	0.00	0.00
3	100.00	0.00	10.00	30.00
4	100.00	0.00	0.00	90.00
5	100.00	0.00	0.00	40.00
6	100.00	0.00	0.00	0.00
7	100.00	80.00	90.00	0.00
8	100.00	20.00	80.00	100.00
9	100.00	0.00	0.00	0.00
10	100.00	0.00	0.00	0.00
TOT	100.00	12.00	22.00	33.00

Table A.8: Accuracy of voluntary effort recognition for closed-loop. Accuracy (%) for Different MVC levels vs purely stimulated contractions of *quadriceps femoris*. The imposed threshold is equal to the 150 % of the MMG - RMS value found during the purely stimulated contraction in the calibration phase.

Subject	Accuracy (%)			
	Purely stimulated	10 % MVC	20 % MVC	30 % MVC
1	100.00	10.00	10.00	60.00
2	100.00	0.00	0.00	0.00
3	100.00	0.00	0.00	20.00
4	100.00	0.00	0.00	90.00
5	100.00	0.00	30.00	30.00
6	100.00	0.00	0.00	0.00
7	100.00	70.00	70.00	0.00
8	100.00	10.00	80.00	100.00
9	100.00	0.00	0.00	0.00
10	100.00	0.00	0.00	0.00
TOT	100.00	9.00	19.00	30.00

Bibliography

- [1] Adil Khalil Hussien, Abdulaziz Khalid Alshehri, Fayez Khalid Alanazi, Abdulaziz Mohammed Aljabal, Ahmed Ibrahim Alanazi, Anas Mohammed Alqayidi, and Ibrahim Hussein Alghamdi. «Characterization of Demographic, Clinical, and Laboratory Risk Factors for Stroke in a Tertiary Hospital in Riyadh, Saudi Arabia». In: *Cureus* (2024). DOI: 10.7759/cureus.58266 (cit. on p. 1).
- [2] A. Soto, F. Guillén-Grima, G. Morales, S. Muñoz, I. Aguinaga-Ontoso, and R. Fuentes-Aspe. «Prevalencia e incidencia del ictus en Europa: revisión sistemática y metaanálisis». Spanish. In: *An Sist Sanit Navar* 45.1 (Apr. 2022), e0979. DOI: 10.23938/ASSN.0979 (cit. on p. 1).
- [3] Claudia Marquez-Chin and Milos R. Popovic. «Functional electrical stimulation therapy for restoration of motor function after spinal cord injury and stroke: a review». In: *BioMedical Engineering OnLine* 19.1 (May 2020), p. 34. DOI: 10.1186/s12938-020-00773-4 (cit. on pp. 1, 2).
- [4] L. Mercier, T. Audet, R. Hébert, A. Rochette, and M. F. Dubois. «Impact of motor, cognitive, and perceptual disorders on ability to perform activities of daily living after stroke». In: *Stroke* 32.11 (2001), pp. 2602–2608. DOI: 10.1161/hs1101.098154 (cit. on p. 2).
- [5] S. Luo, H. Xu, Y. Zuo, et al. «A Review of Functional Electrical Stimulation Treatment in Spinal Cord Injury». In: *Neuromolecular Medicine* 22 (2020), pp. 447–463. DOI: 10.1007/s12017-019-08589-9. URL: <https://doi.org/10.1007/s12017-019-08589-9> (cit. on pp. 2, 3).
- [6] Robert Martin, Cristina Sadowsky, Karen Obst, Brad Meyer, and John McDonald. «Functional electrical stimulation in spinal cord injury:: from theory to practice». In: *Topics in Spinal Cord Injury Rehabilitation* 18.1 (2012), pp. 28–33. DOI: 10.1310/sci1801-28 (cit. on p. 3).
- [7] Gad Alon. «Functional Electrical Stimulation (FES): Clinical successes and failures to date». In: *Journal of Novel Physiotherapy and Rehabilitation* 2 (Nov. 2018), pp. 080–086. DOI: 10.29328/journal.jnpr.1001022 (cit. on pp. 3, 4).

- [8] G. Alon. «Functional Electrical Stimulation (FES): Transforming Clinical Trials to Neuro-Rehabilitation Clinical Practice- A Forward Perspective». In: *Journal of Novel Physiotherapies* 3 (2013). URL: <https://goo.gl/1MDz kf> (cit. on p. 4).
- [9] Polytechnic Hub: Technical Editor. *Difference between open loop control system and close loop control system*. <https://www.polytechnichub.com/2211-2/>. Image of scheme open-loop and closed-loop. Apr. 2017 (cit. on p. 5).
- [10] Cindy L. Stanfield. *FISIOLOGIA - Quarta Edizione*. EdiSES, 2012, p. 323. ISBN: 978-887-959-714-2 (cit. on pp. 5, 9).
- [11] Labster. *Theory Pages*. Accessed: July 16, 2024. URL: <https://theory.labster.com/skeletal-muscle-architecture/> (cit. on p. 6).
- [12] Carbone Emilio, Aicardi Giorgio, and Maggi. Roberto. *Fisiologia : dalle molecole ai sistemi integrati*. EdiSES, 2018, p. 872. ISBN: 978-887-959-979-5 (cit. on pp. 6–8).
- [13] A. F. Huxley. «Muscle structure and theories of contraction». English, Italian. In: *Progress in Biophysics and Biophysical Chemistry* 7 (1957), pp. 255–318 (cit. on p. 7).
- [14] Sally Kim. *BioRender*. Accessed: July 16, 2024. URL: <https://www.biorender.com/template/cross-bridge-cycle> (cit. on p. 7).
- [15] Indiana University. *Basic Human Physiology - Cross Bridge cycling*. Accessed: July 16, 2024. URL: <https://iu.pressbooks.pub/humanphys/chapter/cross-bridge-cycling/> (cit. on p. 9).
- [16] Huxi Wang, Siming Zuo, María Cerezo-Sánchez, Negin Ghahremani Arekhloo, Kianoush Nazarpour, and Hadi Heidari. «Wearable super-resolution muscle-machine interfacing.» In: *Frontiers in neuroscience* 16 (2022), p. 1020546. DOI: 10.3389/fnins.2022.1020546 (cit. on pp. 10, 11, 20).
- [17] Susanna Rampichini, Taian Martins Vieira, Paolo Castiglioni, and Giampiero Merati. «Complexity analysis of surface electromyography for assessing the myoelectric manifestation of muscle fatigue: A review». In: *Entropy* 22.5 (2020). DOI: 10.3390/e22050529 (cit. on pp. 12, 13).
- [18] Roberto Merletti, Alberto Botter, Andrea Troiano, Enrico Merlo, and Marco Alessandro Minetto. «Technology and instrumentation for detection and conditioning of the surface electromyographic signal: state of the art». In: *Clinical Biomechanics* 24.2 (2009), pp. 122–134. DOI: 10.1016/j.clinbiomech.2008.08.006 (cit. on pp. 12–15).

- [19] Negin Ghahremani Arekhloo, Hossein Parvizi, Siming Zuo, Huxi Wang, Kianoush Nazarpour, Justus Marquetand, and Hadi Heidari. «Alignment of magnetic sensing and clinical magnetomyography». In: *Frontiers in Neuroscience* 17 (May 2023), p. 1154572. DOI: 10.3389/fnins.2023.1154572 (cit. on p. 12).
- [20] A. van Boxtel, A. J. Boelhouwer, and A. R. Bos. «Optimal EMG signal bandwidth and interelectrode distance for the recording of acoustic, electrocutaneous, and photic blink reflexes». In: *Psychophysiology* 35.6 (Nov. 1998), pp. 690–697 (cit. on p. 12).
- [21] Marco Antonio Cavalcanti Garcia and Taian Martins Vieira. «Surface electromyography: Why, when and how to use it». In: *Revista Andaluza de Medicina del Deporte* 4.1 (2011), pp. 17–28 (cit. on p. 13).
- [22] Fabio Rossi, Paolo Motto Ros, Stefano Sapienza, Paolo Bonato, Emilio Bizzi, and Danilo Demarchi. «Wireless Low Energy System Architecture for Event-Driven Surface Electromyography». In: *Applications in Electronics Pervading Industry, Environment and Society. ApplePies 2018*. Vol. 573. Lecture Notes in Electrical Engineering. Cham: Springer, 2019. DOI: 10.1007/978-3-030-11973-7_21 (cit. on pp. 15, 16).
- [23] Marco Crepaldi, Marco Paleari, Alberto Bonanno, Alessandro Sanginario, Paolo Ariano, Duc Hoa Tran, and Danilo Demarchi. «A quasi-digital radio system for muscle force transmission based on event-driven IR-UWB». In: *2012 IEEE Biomedical Circuits and Systems Conference (BioCAS)* (2012), pp. 116–119. URL: <https://api.semanticscholar.org/CorpusID:43189875> (cit. on p. 15).
- [24] Gerald Oster and Jonathan S Jaffe. «Low frequency sounds from sustained contraction of human skeletal muscle». In: *Biophysical journal* 30.1 (Apr. 1980), pp. 119–127. DOI: 10.1016/S0006-3495(80)85080-6 (cit. on p. 17).
- [25] G. Gordon and A. H. S. Holbourn. «The sounds from single motor units in a contracting muscle». In: *Journal of Physiology* 107.4 (Sept. 1948), pp. 456–464 (cit. on p. 17).
- [26] Pascal Madeleine, Preeti Bajaj, Karen Sjøgaard, and Lars Arendt-Nielsen. «Mechanomyography and electromyography force relationships during concentric, isometric and eccentric contractions». In: *Journal of Electromyography and Kinesiology* 11.2 (2001), pp. 113–121. ISSN: 1050-6411. DOI: 10.1016/S1050-6411(00)00044-4. URL: [https://doi.org/10.1016/S1050-6411\(00\)00044-4](https://doi.org/10.1016/S1050-6411(00)00044-4) (cit. on pp. 17, 18).
- [27] Claudio Orizio. «Muscle sound: Bases for the introduction of a mechanomyographic signal in muscle studies». In: *Critical reviews in biomedical engineering* 21 (Feb. 1993), pp. 201–43 (cit. on pp. 17–20).

- [28] John V Frangioni, Tao-Sheng Kwan-Gett, Lynn E Dobrunz, and Thomas A McMahon. «The mechanism of low-frequency sound production in muscle». In: *Biophysical Journal* 51.5 (1987), pp. 775–783. DOI: 10.1016/S0006-3495(87)83404-5 (cit. on p. 17).
- [29] IA Stokes, MS Moffroid, S Rush, and LD Haugh. «Comparison of acoustic and electrical signals from erectores spinae muscles». In: *Muscle & Nerve* 11.4 (1988), pp. 331–336. DOI: 10.1002/mus.880110409 (cit. on p. 19).
- [30] M.J. Stokes and R.G. Cooper. «Muscle sounds during voluntary and stimulated contractions of the human adductor pollicis muscle». In: *Journal of Applied Physiology* 72.5 (1992), pp. 1908–1913. DOI: 10.1152/jappl.1992.72.5.1908 (cit. on p. 19).
- [31] M.J. Stokes and P.A. Dalton. «Acoustic myographic activity increases linearly up to maximal voluntary isometric force in the human quadriceps muscle». In: *Journal of Neurological Sciences* 101.2 (1991), pp. 163–167. DOI: 10.1016/0022-510x(91)90041-5 (cit. on p. 19).
- [32] MJ Stokes and PA Dalton. «Acoustic myography for investigating human skeletal muscle fatigue». In: *Journal of Applied Physiology* 71.4 (1991), pp. 1422–1426. DOI: 10.1152/jappl.1991.71.4.1422 (cit. on p. 19).
- [33] O Lammert, F Jorgensen, and N Einer-Jensen. «Accelerometermyography (AMG), I: method for measuring mechanical vibrations from isometrically contracted muscles». In: *Biomechanics V-A*. Ed. by PV Komi. Baltimore: University Park Press, 1976, pp. 152–164 (cit. on p. 19).
- [34] Claudio Orizio, Renza Perini, and Arsenio Veicsteinas. «Muscular sound and force relationship during isometric contraction in man». In: *European Journal of Applied Physiology and Occupational Physiology* 58.5 (1989), pp. 528–533. DOI: 10.1007/BF02330708 (cit. on p. 19).
- [35] B Maton, M Petitjean, and JC Cnockaert. «Phonomyogram and electromyogram relationships with isometric force reinvestigated in man». In: *European Journal of Applied Physiology and Occupational Physiology* 60.3 (1990), pp. 194–201. DOI: 10.1007/BF00839159 (cit. on p. 19).
- [36] Machiel J Zwarts and Matthias Keidel. «Relationship between electrical and vibratory output of muscle during voluntary contraction and fatigue». In: *Muscle & Nerve* (Aug. 1991). DOI: 10.1002/mus.880140810. URL: <https://doi.org/10.1002/mus.880140810> (cit. on p. 19).
- [37] S. Cerquiglioni, M. Marchetti, and R. Venturini. «Spettrofonomiografia di muscoli scheletrici umani». In: *Arch. Fisiol.* 66 (1968), p. 173 (cit. on p. 20).

- [38] Samuel Wilson and Ravi Vaidyanathan. «Upper-limb prosthetic control using wearable multichannel mechanomyography». In: *2017 International Conference on Rehabilitation Robotics (ICORR)*. 2017, pp. 1293–1298. DOI: 10.1109/ICORR.2017.8009427 (cit. on p. 20).
- [39] Brian A. Rhatigan, Kevin C. Mylrea, Elizabeth Lonsdale, and Leonard Z. Stern. «Investigation of Sounds Produced by Healthy and Diseased Human Muscular Contraction». In: *IEEE Transactions on Biomedical Engineering* 33.10 (1986), pp. 967–971. DOI: 10.1109/TBME.1986.325668 (cit. on p. 20).
- [40] Bertrand Diemont, Marisa Maranzana Figini, Claudio Orizio, Renza Perin, and Arsenio Veicsteinas. «Spectral analysis of muscular sound at low and high contraction level». In: *International Journal of Bio-Medical Computing* 23.3 (Dec. 1988), pp. 161–175. ISSN: 0020-7101. DOI: 10.1016/0020-7101(88)90011-6 (cit. on p. 20).
- [41] Matthias Keidel and Wolf-Dieter Keidel. «The computer-vibromyography as a biometric progress in studying muscle function». In: *Biomedical Engineering* 34.5 (May 1989), pp. 107–116. DOI: 10.1515/bmte.1989.34.5.107 (cit. on p. 20).
- [42] Tae Kyung Kim, Yoshihito Shimomura, Koichi Iwanaga, and Tetsuo Katsuura. «Comparison of an accelerometer and a condenser microphone for mechanomyographic signals during measurement of agonist and antagonist muscles in sustained isometric muscle contractions». In: *Journal of Physiological Anthropology* 27.3 (2008), pp. 121–131. DOI: 10.2114/jpa2.27.121 (cit. on p. 20).
- [43] Andrey O. Posatskiy and Tom Chau. «The effects of motion artifact on mechanomyography: A comparative study of microphones and accelerometers». In: *Journal of Electromyography and Kinesiology* 22.2 (2012), pp. 320–324. ISSN: 1050-6411. DOI: 10.1016/j.jelekin.2011.09.004. URL: <https://doi.org/10.1016/j.jelekin.2011.09.004> (cit. on p. 20).
- [44] Claudio Orizio, Monica Gobbo, Bertilla Diemont, Fulvio Esposito, and Andrea Veicsteinas. «The surface mechanomyogram as a tool to describe the influence of fatigue on biceps brachii motor unit activation strategy. Historical basis and novel evidence». In: *European Journal of Applied Physiology* 90 (2003), pp. 326–336. DOI: 10.1007/s00421-003-0924-1. URL: <https://doi.org/10.1007/s00421-003-0924-1> (cit. on p. 21).
- [45] Angkoon Phinyomark, Chusak Limsakul, and P. Phukpattaranont. «A Novel Feature Extraction for Robust EMG Pattern Recognition». In: *Journal of Computing* 1 (Dec. 2009), pp. 71–80. DOI: <https://doi.org/10.1016/j.eswa.2012.01.102> (cit. on p. 21).

- [46] Alex Y Hui, William J McCarty, Koichi Masuda, Gary S Firestein, and Robert L Sah. «A systems biology approach to synovial joint lubrication in health, injury, and disease». In: *Wiley Interdisciplinary Reviews: Systems Biology and Medicine* 4.1 (2012), pp. 15–37. DOI: 10.1002/wsbm.157 (cit. on p. 23).
- [47] Abu Ilius Faisal, Sumit Majumder, Tapas Mondal, David Cowan, Sasan Naseh, and M. Jamal Deen. «Monitoring Methods of Human Body Joints: State-of-the-Art and Research Challenges». In: *Sensors* 19.11 (2019). DOI: 10.3390/s19112629 (cit. on pp. 23, 24).
- [48] Cheng-Yen Chiang, Kuan-Hao Chen, Kuan-Chun Liu, Shih-Jie Hsu, and Chia-Tai Chan. «Data Collection and Analysis Using Wearable Sensors for Monitoring Knee Range of Motion after Total Knee Arthroplasty». In: *Sensors* 17.2 (2017), p. 418. DOI: 10.3390/s17020418 (cit. on p. 23).
- [49] AnatomyStuff. *Hand and Wrist Charts*. Accessed: July 16, 2024. URL: <https://www.anatomystuff.co.uk/> (cit. on p. 24).
- [50] Microsoft. *Kinect for Windows*. Accessed: July 16, 2024. URL: <https://developer.microsoft.com/en-us/windows/kinect/> (cit. on p. 25).
- [51] Sajad Almasi, Hossein Ahmadi, Fatemeh Asadi, Leila Shahmoradi, Gholamreza Arji, Mohammad Alizadeh, and Hoshang Kolivand. «Kinect-Based Rehabilitation Systems for Stroke Patients: A Scoping Review». In: *BioMed Research International* 2022 (Mar. 2022), p. 4339054. DOI: 10.1155/2022/4339054 (cit. on p. 25).
- [52] Nathaniel Goldfarb, Alek Lewis, Alex Tacescu, and Gregory S. Fischer. «Open source Vicon Toolkit for motion capture and Gait Analysis». In: *Computer Methods and Programs in Biomedicine* 212 (2021), p. 106414. DOI: 10.1016/j.cmpb.2021.106414 (cit. on p. 25).
- [53] Vicon. *Plug-in Gait Reference Guide*. Accessed: July 16, 2024. URL: <https://help.vicon.com/space/Nexus216/11607059/Plug-in+Gait+Reference+Guide> (cit. on p. 25).
- [54] Andrea Prestia, Fabio Rossi, Andrea Mongardi, Paolo Motto Ros, Massimo Ruo Roch, Maurizio Martina, and Danilo Demarchi. «Motion Analysis for Experimental Evaluation of an Event-Driven FES System». In: *IEEE Transactions on Biomedical Circuits and Systems* 16.1 (Feb. 2022), pp. 3–14. DOI: 10.1109/TBCAS.2021.3137027 (cit. on p. 25).
- [55] Haohua Zhang, Yang Song, Cheng Li, Yong Dou, Dacheng Wang, Yinyue Wu, Xiaoyi Chen, and Di Liu. «Validation of a Wearable System for Lower Extremity Assessment». In: *Orthopaedic Surgery* 15.11 (2023), pp. 2911–2917. DOI: 10.1111/os.13836 (cit. on p. 26).

- [56] Mohammad Al-Amri, Kevin Nicholas, Kate Button, Valerie Sparkes, Liba Sheeran, and Jennifer L. Davies. «Inertial Measurement Units for Clinical Movement Analysis: Reliability and Concurrent Validity». In: *Sensors* 18.3 (2018), p. 719. DOI: [10.3390/s18030719](https://doi.org/10.3390/s18030719). URL: <https://www.mdpi.com/1424-8220/18/3/719> (cit. on p. 26).
- [57] Ibrahim (Abe) M Elfadel Zakriya Mohammed and Mahmoud Rasras. «Monolithic multi degree of freedom (MDoF) capacitive MEMS accelerometers». In: *Micromachines* 9.11 (2018), p. 602. DOI: <https://doi.org/10.3390/mi9110602> (cit. on p. 27).
- [58] Vittorio MN Passaro, Antonello Cuccovillo, Lorenzo Vaiani, Martino De Carlo, and Carlo Edoardo Campanella. «Gyroscope technology and applications: A review in the industrial perspective». In: *Sensors* 17.10 (2017), p. 2284. DOI: [10.3390/s17102284](https://doi.org/10.3390/s17102284) (cit. on pp. 27, 28).
- [59] Ma Myint Myint Aye. «Analysis of Euler angles in a simple two-axis gimbal set». In: *World Academy of Science, Engineering and Technology* 81 (2011), pp. 389–394. DOI: [10.5281/zenodo.1330465](https://doi.org/10.5281/zenodo.1330465) (cit. on pp. 28, 29).
- [60] Arend Schwab. «How to Draw Euler Angles and Utilize Euler Parameters». In: Sept. 2006. DOI: [10.1115/DETC2006-99307](https://doi.org/10.1115/DETC2006-99307) (cit. on p. 29).
- [61] Oliver J. Woodman. *An Introduction to Inertial Navigation*. Technical Report. 2007. URL: <https://www.cl.cam.ac.uk/techreports/UCAM-CL-TR-696.pdf> (cit. on p. 30).
- [62] Gad Alon. «Functional Electrical Stimulation (FES): Clinical successes and failures to date». In: *Journal of Novel Physiotherapy and Rehabilitation* 2 (Nov. 2018), pp. 080–086. DOI: <https://doi.org/10.29328/journal.jnpr.1001022> (cit. on pp. 31, 32).
- [63] Compex. *Compex Wireless User Guide*. Accessed: July 16, 2024. URL: <https://s3.amazonaws.com/assets.compex.com/uk/support-documents/Compex-Wireless-EN-FR-DE-IT-ES-SV-NL-PT.pdf> (cit. on p. 32).
- [64] Bioness. *NESS L300*. Accessed: July 16, 2024. URL: <https://www.manualslib.com/manual/1534607/Bioness-L300-Go.html> (cit. on p. 32).
- [65] Yu Zhou, Jia Zeng, Kairu Li, Levi J. Hargrove, and Honghai Liu. «sEMG-Driven Functional Electrical Stimulation Tuning via Muscle Force». In: *IEEE Transactions on Industrial Electronics* 68.10 (2021), pp. 10068–10077. DOI: [10.1109/TIE.2020.3026280](https://doi.org/10.1109/TIE.2020.3026280) (cit. on p. 32).

- [66] Fabio Rossi, Paolo Motto Ros, Sofia Cecchini, Andrea Crema, Silvestro Micera, and Danilo Demarchi. «An Event-Driven Closed-Loop System for Real-Time FES Control». In: *2019 26th IEEE International Conference on Electronics, Circuits and Systems (ICECS)*. 2019, pp. 867–870. DOI: 10.1109/ICECS46596.2019.8965153 (cit. on pp. 32, 33, 35).
- [67] Fabio Rossi, Andrea Mongardi, Paolo Motto Ros, Massimo Ruo Roch, Maurizio Martina, and Danilo Demarchi. «Tutorial: A Versatile Bio-Inspired System for Processing and Transmission of Muscular Information». In: *IEEE Sensors Journal* 21.20 (2021), pp. 22285–22303. DOI: 10.1109/JSEN.2021.3103608 (cit. on pp. 33, 34, 48, 55).
- [68] HASOMED GmbH. *Operation Manual RahStim2, RehaMove2*. 2012 (cit. on p. 35).
- [69] Norman S. Litofsky, Cesar Marquez-Chin, Aaron Marquis, and Milos R. Popovic. «EEG-Triggered Functional Electrical Stimulation Therapy for Restoring Upper Limb Function in Chronic Stroke with Severe Hemiplegia». In: *Case Reports in Neurological Medicine* 2016 (Nov. 2016), p. 9146213. ISSN: 2090-6668. DOI: 10.1155/2016/9146213. URL: <https://doi.org/10.1155/2016/9146213> (cit. on p. 36).
- [70] Paola Contessa, John Letizi, Gianluca De Luca, and Joshua C. Kline. «Contribution from motor unit firing adaptations and muscle coactivation during fatigue». In: *Journal of Neurophysiology* 119.6 (2018), pp. 1815–1826. DOI: 10.1152/jn.00766.2017. URL: <https://doi.org/10.1152/jn.00766.2017> (cit. on p. 36).
- [71] Geoff M. Graham, Timothy A. Thrasher, and Milos R. Popovic. «The effect of random modulation of functional electrical stimulation parameters on muscle fatigue». In: *IEEE Transactions on Neural Systems and Rehabilitation Engineering* 14.1 (2006), pp. 38–45. DOI: 10.1109/TNSRE.2006.870490 (cit. on pp. 36, 37).
- [72] Christine K. Thomas, Lisa Griffin, Sharlene Godfrey, Edith Ribot-Ciscar, and Jane E. Butler. «Fatigue of paralyzed and control thenar muscles induced by variable or constant frequency stimulation». In: *Journal of Neurophysiology* 89 (2003), pp. 2055–2064. DOI: <https://doi.org/10.1152/jn.01002.2002> (cit. on p. 36).
- [73] D. Graupe, P. Suliga, C. Prudian, and K. H. Kohn. «Stochastically-modulated stimulation to slow down muscle fatigue at stimulated sites in paraplegics using functional electrical stimulation for leg extension». In: *Neurological Research* 22 (2000), pp. 703–704. DOI: 10.1080/01616412.2000.11740743 (cit. on p. 37).

- [74] Qin Zhang, Mitsuhiro Hayashibe, and Christine Azevedo-Coste. «Evoked Electromyography-Based Closed-Loop Torque Control in Functional Electrical Stimulation». In: *IEEE Transactions on Biomedical Engineering* 60.8 (2013), pp. 2299–2307. DOI: 10.1109/TBME.2013.2253777 (cit. on pp. 38, 39).
- [75] Qin Zhang, Mitsuhiro Hayashibe, Philippe Fraisse, and David Guiraud. «FES-induced torque prediction with evoked EMG sensing for muscle fatigue tracking». In: *IEEE/ASME Transactions on Mechatronics* 16.5 (2011), pp. 816–826. DOI: 10.1109/TMECH.2011.2160809 (cit. on p. 38).
- [76] Yurong Li, Jun Chen, and Yuan Yang. «A Method for Suppressing Electrical Stimulation Artifacts from Electromyography». In: *International Journal of Neural Systems* 29 (Nov. 2018). DOI: 10.1142/S0129065718500545 (cit. on p. 40).
- [77] Zhi-Yong Bi, Yu-Xuan Zhou, Cheng-Xu Xie, Hui-Ping Wang, Hao-Xing Wang, Bao-Liang Wang, Jie Huang, Xiang-Yin Lü, and Zhi-Gong Wang. «A hybrid method for real-time stimulation artefact removal during functional electrical stimulation with time-variant parameters». In: *Journal of Neural Engineering* 18.4 (Apr. 2021). DOI: 10.1088/1741-2552/abf68c (cit. on pp. 39–41).
- [78] Morufu Olusola Ibitoye, Eduardo Henrique Estigoni, Nur Azah Hamzaid, Ahmad Khairi Abdul Wahab, and Glen M. Davis. «The effectiveness of FES-evoked EMG potentials to assess muscle force and fatigue in individuals with spinal cord injury». In: *Sensors* 14.7 (July 2014), pp. 12598–12622. DOI: 10.3390/s140712598 (cit. on p. 39).
- [79] X. Li, W.Z. Rymer, G. Li, and et al. «The effects of notch filtering on electrically evoked myoelectric signals and associated motor unit index estimates». In: *Journal of NeuroEngineering and Rehabilitation* 8.64 (2011). DOI: 10.1186/1743-0003-8-64. URL: <https://doi.org/10.1186/1743-0003-8-64> (cit. on p. 40).
- [80] Shuang Qiu, Jing Feng, Rui Xu, Jiapeng Xu, Kun Wang, Feng He, and Hongzhi Qi. «A Stimulus Artifact Removal Technique for SEMG Signal Processing During Functional Electrical Stimulation». In: *IEEE Transactions on Biomedical Engineering* 62.8 (Aug. 2015), pp. 1959–1968. DOI: 10.1109/TBME.2015.2407834 (cit. on p. 41).
- [81] Rohan Pilkar, Mathew Yarossi, Arvind Ramanujam, Venkata Rajagopalan, Mustafa Burak Bayram, Michael Mitchell, Steve Canton, and Gordon Forrest. «Application of Empirical Mode Decomposition Combined With Notch Filtering for Interpretation of Surface Electromyograms During Functional Electrical Stimulation». In: *IEEE Transactions on Neural Systems and*

- Rehabilitation Engineering* 25.8 (Aug. 2017), pp. 1268–1277. DOI: 10.1109/TNSRE.2016.2624763 (cit. on p. 41).
- [82] David Andreu, Benoit Sijobert, Michel Toussaint, Charles Fattal, Christine Azevedo-Coste, and David Guiraud. «Wireless Electrical Stimulators and Sensors Network for Closed Loop Control in Rehabilitation». In: *Frontiers in Neuroscience* 14 (Feb. 2020), p. 117. DOI: 10.3389/fnins.2020.00117 (cit. on pp. 41–43).
- [83] Graham Mann, Paul Taylor, and Richard Lane. «Accelerometer-triggered electrical stimulation for reach and grasp in chronic stroke patients: a pilot study». In: *Neurorehabilitation and Neural Repair* 25.8 (Oct. 2011), pp. 774–780. DOI: 10.1177/1545968310397200 (cit. on pp. 43, 44).
- [84] Eric Krueger, Lidija Popović-Maneski, and Percy Nohama. «Mechanomyography-Based Wearable Monitor of Quasi-Isometric Muscle Fatigue for Motor Neural Prostheses». In: *Artificial Organs* 42.2 (Feb. 2018), pp. 208–218. DOI: 10.1111/aor.12973 (cit. on pp. 44–46).
- [85] Eric Krueger, Lidija Popović-Maneski, Guilherme Nogueira Nogueira Neto, et al. «Neuromuscular fatigue detection by mechanomyography in people with complete spinal cord injury». In: *Research in Biomedical Engineering* 36 (2020), pp. 203–212. DOI: 10.1007/s42600-020-00061-z. URL: <https://doi.org/10.1007/s42600-020-00061-z> (cit. on pp. 44–46).
- [86] Eric Krueger-Beck, Eduardo M Scheeren, Guilherme N Nogueira-Neto, Vera L Button, and Percy Nohama. «Mechanomyographic response during FES in healthy and paraplegic subjects». In: *Annual International Conference of the IEEE Engineering in Medicine and Biology Society*. 2010, pp. 626–629. DOI: 10.1109/IEMBS.2010.5627274 (cit. on p. 44).
- [87] Edan Al-Zahrani, Chandrasekaran Gunasekaran, Michael Callaghan, Patrick Gaydecki, Diego Benitez, and Jackie Oldham. «Within-day and between-days reliability of quadriceps isometric muscle fatigue using mechanomyography on healthy subjects». In: *Journal of Electromyography and Kinesiology* 19.4 (2009), pp. 695–703. ISSN: 1050-6411. DOI: 10.1016/j.jelekin.2007.12.007. URL: <https://doi.org/10.1016/j.jelekin.2007.12.007> (cit. on p. 45).
- [88] Maria Teresa Tarata. «Mechanomyography versus Electromyography, in monitoring the muscular fatigue». In: *BioMedical Engineering OnLine* 2.3 (2003). DOI: 10.1186/1475-925X-2-3. URL: <https://doi.org/10.1186/1475-925X-2-3> (cit. on p. 45).
- [89] STMicroelectronics. *LSM6DSO32X - iNEMO Inertial Module: Always-on 3D Accelerometer and 3D Gyroscope*. 2021. URL: <https://www.st.com/en/mems-and-sensors/lsm6dso32x.html> (cit. on pp. 48, 50).

- [90] HASOMED GmbH. *RehaMove - Motion Training with Functional Electrical Stimulation (FES)*. 2024. URL: <https://hasomed.de/en/products/rehamove/> (visited on 06/08/2024) (cit. on p. 51).
- [91] Hasomed GmbH. *RehaMove2 Operation Manual*. 2016. URL: https://static1.squarespace.com/static/5f16af2c5732983b810510ef/t/625445ebc1f33f681fa9ec3e/1649690115682/RehaMove2_User+Manual_2.4._ENG_CM_20170201.pdf (cit. on pp. 51, 52).
- [92] Hasomed GmbH. *RehaMove2 User Manual*. Consulting Manual. 2016. URL: https://static1.squarespace.com/static/5f16af2c5732983b810510ef/t/625445ebc1f33f681fa9ec3e/1649690115682/RehaMove2_User+Manual_2.4._ENG_CM_20170201.pdf (cit. on p. 51).
- [93] Bjoern Kuberski. *Science Mode 2: Description and Protocol*. 2012. URL: https://hasomed.de/wp-content/uploads/hasomed-fileadmin/RehaMove/ScienceMode/Science_Mode2_Description_Protocol_20121212.pdf (cit. on pp. 52, 53).
- [94] Kevin K. McCully, Peter Prins, Krishan Mistry, and Thad B. Willingham. «Muscle-specific endurance of the trapezius muscles using electrical twitch mechanomyography». In: *Shoulder & Elbow* 10.2 (2018), pp. 136–143. DOI: 10.1177/1758573217726269 (cit. on pp. 54, 62).
- [95] Hasomed. *RehaMove FES Templates*. Accessed: July 16, 2024. 2016. URL: https://enableme.com/wp-content/uploads/2016/07/RehaMove_FES_Templates.pdf (cit. on p. 54).
- [96] Nordic Semiconductor. *nRF52840*. Accessed: July 16, 2024. 2024. URL: <https://www.nordicsemi.com/Products/nRF52840> (cit. on p. 54).
- [97] Kivy Team. *Kivy: Cross-platform Python Framework for GUI apps Development*. Accessed: July 16, 2024. URL: <https://kivy.org/> (cit. on pp. 54, 57).
- [98] Mouser Electronics. *Nordic nRF52840 USB Dongle*. Accessed: July 16, 2024. 2024. URL: <https://www.mouser.it/new/nordic-semiconductor/nordic-nrf52840-usb-dongle/> (cit. on p. 55).
- [99] HOSPIMedica International. *RehaStim2*. Accessed: July 16, 2024. 2024. URL: <https://www.hospimedicaintl.com/20/292/0/0/rehastim2~-prd.html> (cit. on p. 55).
- [100] Global Tag. *Bluetooth Low Energy (BLE) Overview*. Accessed: July 16, 2024. 2024. URL: <https://www.global-tag.com/it/bluetooth-low-energy-ble-overview/> (cit. on p. 55).

- [101] Letizia Cantore. «Realization and Validation of a Wearable Prototype for sEMG-based Facial Expressions Recognition». Rel. Danilo Demarchi, Fabio Rossi, Andrea Mongardi. Licenza: Creative Commons Attribution Non-commercial No Derivatives. Laurea Magistrale Thesis. Corso di laurea magistrale in Ingegneria Biomedica: Politecnico di Torino, Mar. 2024. URL: <http://webthesis.biblio.polito.it/id/eprint/30529> (cit. on p. 66).
- [102] Python Software Foundation. *multiprocessing - Process-based parallelism*. Accessed: July 16, 2024. URL: <https://docs.python.org/3/library/multiprocessing.html> (cit. on p. 82).
- [103] Wunder. *Manuale del Dinamometro CR*. <https://industriale.wunder.it/it/dinamometri/159-dinamometro-cr.html>. Wunder. 2024 (cit. on p. 103).
- [104] Hae-Young Kim. «Analysis of Variance (ANOVA) Comparing Means of More than Two Groups». In: *Restorative Dentistry & Endodontics* 39.1 (2014). DOI: 10.5395/rde.2014.39.1.74 (cit. on p. 106).
- [105] William H. Kruskal and W. Allen Wallis. «Use of ranks in one-criterion variance analysis». In: *Journal of the American Statistical Association* 47.260 (1952) (cit. on p. 106).